2015

Development of calcium stable isotopes as a new tool to understand calcium cycling in terrestrial ecosystems

BOSTON UNIVERSITY

GRADUATE SCHOOL OF ARTS AND SCIENCES

Dissertation

DEVELOPMENT OF CALCIUM STABLE ISOTOPES AS A TOOL TO UNDERSTAND CALCIUM CYCLING IN TERRESTRIAL ECOSYSTEMS

by

Kenneth Andrew Takagi

B.A., University of Colorado-Boulder, 2003
M.S., Pennsylvania State University, 2009

Submitted in partial fulfillment of the

requirements for the degree of

Doctor of Philosophy

2015

Approved by

First Reader _____

Andrew C. Kurtz, Ph.D.
Associate Professor of Earth & Environment

Second Reader _____

Adrien Finzi, Ph.D.
Professor of Biology

Third Reader _____

Ethan Baxter, Ph.D.
Associate Professor of Earth & Environment

To my family

ACKNOWLEDGMENTS

I would like to express deep gratitude to my PhD advisor, Andrew Kurtz. He challenged me to be a better scientist, provided guidance and support when I felt overwhelmed, and instilled in me a deep appreciation for geochemistry. I would also like to acknowledge the financial support of Boston University, the National Science Foundation, the Geological Society of America, and the United States Geological Survey.

I would like to extend a special thanks to my external committee member Tom Bullen of the United States Geological Survey, who was always quick to answer the many questions I had regarding Ca isotopes. I'd also like to thank committee member Ethan Baxter, who as director of the Boston University Thermal Ionization Mass Spectrometry Facility provided machine time and financial support during my early methodological work on Ca isotopes. I'd like to thank committee members Adrien Finzi, for providing important insights into the ecological aspects of my research, and Guido Salvucci, for providing guidance on statistical methods and hydrology.

I'd like to acknowledge Scott Bailey, Amey Bailey and Chris Johnson for providing access to archived samples and for showing me around the Hubbard Brook Forest, and Gene Likens for welcoming us to work at Hubbard Brook and for having the foresight to create a sample archive. Without this archive, my 1st chapter would not have been possible. I also would like to acknowledge the insights and samples provided by Heather Buss and other members of the LCZO

group with regard to my 2nd chapter. Finally, I dedicate the 2nd chapter of this dissertation to the memory of Dr. Fred Scatena, whose extensive knowledge of the Luquillo Critical Zone and logistical support made this research project possible.

I'd like to thank Boston University laboratory managers Denise Honn, Thomas Ireland and Jeremy Inglis for assistance with laboratory work and instrumentation. Additional assistance with data collection and laboratory work came from Melissa Chisholm, Stephanie Kukolich, John Oberschelp and Nicolas Murphy.

Finally, I'd like to acknowledge all of my friends inside and outside the Earth and Environment department for supporting me and making my time in Boston so memorable. Last but not least, I wish to thank my family; my parents Gail and Mikiro, my stepfather Tom, my brother Jonah and my wife Zhaomi, for the unconditional love and support they provided throughout my time at Boston University. It is truly because of their encouragement, guidance, and faith in me that I made it through graduate school.

DEVELOPMENT OF CALCIUM STABLE ISOTOPES AS A TOOL TO UNDERSTAND CALCIUM CYCLING IN TERRESTRIAL ECOSYSTEMS

KENNETH ANDREW TAKAGI

Boston University Graduate School of Arts and Sciences, 2015

Major Professor: Andrew C. Kurtz, Associate Professor of Earth & Environment

ABSTRACT

Calcium stable isotope ratios are a relatively new tool that biogeochemists can use to investigate the biogeochemical cycle of calcium in terrestrial ecosystems, having seen widespread application only in the past 15 years. To advance the application of calcium isotopes in biogeoscience research, I conducted three investigations focused on interpreting calcium isotope ratios in streamwater and in the cation exchange pool of forest soils.

In the first study, we observe a shift toward lower $^{44}Ca/^{40}Ca$ ratios in streamwater draining a New Hampshire watershed after an experimental clearcutting event. Isotope ratio measurements of ecosystem calcium pools indicate that enhanced leaching of the soil exchangeable pool produced the observed shift in $^{44}Ca/^{40}Ca$ ratios. A trend towards decreased $^{44}Ca/^{40}Ca$ ratios in soils in the years following the harvesting indicates that calcium leached from the soil exchangeable reservoir was likely replaced by calcium released by the decay of belowground biomass, maintaining pre-harvest levels of exchangeable calcium even in the face of a significant ecosystem disturbance.

In a second study, we observed significant differences in the $^{44}Ca/^{40}Ca$ of the soil exchange pool between two neighboring tropical watersheds, although $^{44}Ca/^{40}Ca$ of calcium inputs (bedrock and atmospheric deposition) at the two sites were indistinguishable. Further, both sites had higher $^{44}Ca/^{40}Ca$ ratios compared with external inputs, a relatively rare observation globally. We propose that hurricane disturbance best explains the high $^{44}Ca/^{40}Ca$ at each site, and that the difference in $^{44}Ca/^{40}Ca$ between the two sites can be accounted for by the magnitude of disturbance at each site.

Finally, a synthesis of our new data with previously published results shows that globally, soil exchangeable $^{44}Ca/^{40}Ca$ ratios can be higher, lower or equal to external inputs. Modeling work indicates that in addition to isotopic fractionation, the balance in fluxes between vegetation and soil is critical in determining how soil exchangeable $^{44}Ca/^{40}Ca$ ratios vary relative to external inputs. When plant uptake and return to the soil are equal, soil and external inputs $^{44}Ca/^{40}Ca$ are equal, while high soil $^{44}Ca/^{40}Ca$ ratios develop when uptake exceeds return. Soil develops low $^{44}Ca/^{40}Ca$ when biomass obtains calcium from sources other than the exchangeable reservoir.

TABLE OF CONTENTS

LIST OF TABLES

LIST OF FIGURES

CHAPTER 1: ASSESSING THE IMPACT OF CLEAR-CUTTING ON THE FOREST CALCIUM CYCLE USING CA STABLE ISOTOPES

1.1 ABSTRACT

To identify the sources of elevated Ca concentrations in stream water and the processes that maintained soil Ca following a 1983 whole-tree harvesting of Watershed 5 in Hubbard Brook Experimental Forest, we measured stable Ca isotopes in archived streamwater and soil samples collected before, during and after the harvesting event. Streamwater $\delta^{44}Ca$ ($\delta^{44}Ca_{stream}$) was negatively correlated with discharge, consistent with control by hydrologic flowpaths. Soil exchangeable $\delta^{44}Ca$ ($\delta^{44}Ca_{ex}$) was consistently more negative than Ca sources, with the most negative values in shallow soils. $\delta^{44}Ca_{stream}$ decreased by approximately 0.3‰ as streamwater Ca concentrations increased as result of the harvest. An isotope mass balance model indicates that the soil exchangeable Ca pool was the likely source of this elevated streamwater Ca. Neither increased apatite weathering nor dissolution of soil Ca oxalate appear able to account for losses of soil Ca to streamwater. $\delta^{44}Ca$ in bulk forest floor Ca and in the exchange pool at all depths became progressively more negative with time following the harvest. This trend towards more negative soil $\delta^{44}Ca$ is best explained by the release of Ca from the decay of belowground biomass, particularly roots. We suggest that losses of soil Ca to streamwater export and to biomass regrowth in the years following the harvest were largely balanced by replenishment of Ca from the decay of below ground biomass, leading to small

changes to the overall size of the exchange pool as was observed in earlier studies.

1.2 INTRODUCTION

Increased hydrologic export of nutrient cations (ie. Ca^{2+}, K^{+}, Mg^{2+}) following whole tree harvesting is well documented (Johnson et al. 1988; Mann et al. 1988; Johnson et al. 1991b; Johnson et al. 1997), likely resulting from the cessation of nutrient uptake by plants as well as increased organic matter decomposition, changes in soil pH, and input and production of anions (Reuss and Johnson 1986; Johnson et al 1991a; Joslin et al 1992; Lawrence et al 1995; Likens et al 1996) . Loss of these nutrients negatively impacts forest vegetation, and results in decreased tolerance to cold, resistance to disease, fine root production, and in the ability to take up nitrogen (Joslin et al. 1992; Ellsworth and Liu 1994; Driscoll et al. 1996; McLaughlin and Wimmer 1999). Furthermore insufficient calcium can limit water use efficiency and ecosystem function in base-poor forests, as evidenced by elevated rates of transpiration following a whole-watershed Ca amendment (Green et al. 2013). Calcium availability is particularly critical in the northeastern United States, where some watersheds are experiencing a net loss of calcium as stream output flux of calcium exceeds the sum of calcium inputs from mineral weathering and atmospheric deposition (Bailey et al. 1996; Likens et al. 1996).

Predicting how terrestrial ecosystems will recover from harvesting requires an understanding of the dynamics of forest base cation cycling, including

mechanisms for retention and replenishment of the cation exchange complex. Stable Ca isotopes have the potential to provide a new means of investigating these processes. In contrast to Sr isotopes, which have been extensively used by biogeochemists as a proxy for Ca taking advantage of distinct differences in the $^{87}Sr/^{86}Sr$ ratios of mineral and atmospheric inputs (Miller et al. 1993; Bailey et al. 1996; Nezat et al. 2010), differences in the stable Ca isotope ratios ($^{44}Ca/^{40}Ca$) of those inputs are minimal except in very old geologic terrains (Schmitt et al. 2003; Cenki-Tok et al. 2009; Holmden and Bélanger 2010; Wiegand and Schwendenmann 2013). Differences in $\delta^{44}Ca$ in calcium pools in terrestrial ecosystems are thus primarily the result of internal fractionation mechanisms that occur during biogeochemical cycling of Ca. Recent work has demonstrated that uptake of Ca from soil by roots discriminates against the heavier isotopes of Ca, such that plant tissue is generally isotopically light (enriched in ^{40}Ca) relative to both soil and bedrock (Wiegand et al. 2005; Page et al. 2008; Farkaš et al. 2011). The soil cation exchange complex in forests worldwide exhibit $\delta^{44}Ca$ that can be similar to, more positive than, or more negative than $\delta^{44}Ca$ in bedrock (Wiegand et al. 2005; Cenki-Tok et al. 2009; Holmden and Bélanger 2010; Hindshaw et al. 2011), likely reflecting relative rates of Ca uptake and return by vegetation, and external Ca inputs to the exchange pool. Isotopic differences between forest Ca pools may provide a means to identify the sources of Ca lost to streamwater, and importantly, to track how Ca sources change as a result of land use disturbance.

A harvesting experiment conducted in Watershed 5 during 1983-4 at Hubbard Brook Experimental Forest (HBEF) provides an ideal location to investigate the potential of stable Ca isotopes to trace changes in Ca cycling driven by disturbance. Watershed 5 underwent a whole tree harvest between the fall of 1983 and spring of 1984 that removed 93% of all aboveground biomass (Fuller et al. 1987; Johnson et al. 1991b; Hornbeck et al. 1997). A four-fold increase in cation nutrient export via streamwater was observed immediately following the harvest, as well decreases in soil and streamwater pH (Johnson et al. 1991b; Bailey et al. 2003b). Following the initial spike in Ca concentrations, Ca concentrations in streamwater remained elevated relative to Watershed 6, the biogeochemical reference watershed for at least 30 years following disturbance (Bailey et al. 2003b). The source of this increased cation export is uncertain as Johnson et al. (1991b; 1997) observed no resolvable depletion of the exchangeable cation pool in Watershed 5 either 3 or 8 years post-harvest. Johnson et al (1991b) hypothesized that the increased leaching of Ca must be balanced by accelerated mineral weathering or increased decomposition of roots, stumps and slash. More recently, Bailey et al. (2003b) applied a sodium-based mass balance model to Watershed 5 to investigate sources of the increased cation export, and found that weathering alone couldn't explain sustained elevated streamwater Ca (Bailey et al. 2003b). To reconcile the lack of Ca depletion in the cation exchange pool with the 4-fold increase in streamwater Ca, dissolution of biologically-derived calcium oxalate and/or increased biologic

dissolution of easily weatherable minerals such as apatite have been proposed as the source of elevated Ca in streamwater (Bailey et al. 2003b; Hamburg et al. 2003). We present stable Ca isotope ratios in stream, soil and leaf litter samples collected in Watershed 5 and Watershed 6 spanning the time period before, during and after the whole-tree harvest to address the uncertainty in the source of elevated streamwater Ca and the mechanism for replenishment of soil Ca following the harvest.

1.3 MATERIAL AND METHODS

1.3.1 Setting

The Hubbard Brook Experimental Forest (HBEF) is located in the southern portion of the White Mountain National Forest (43°56'N, 71°45'W) (Figure 1.1). The climate is humid continental, with mean annual precipitation of approximately 1400mm, with approximately 30% falling as snow (Federer 1973; Bailey et al. 2003a). Mean monthly temperatures range from -9°C in January to 19°C in July (Federer 1973). The elevation of Watershed 5 ranges from 500 m at the outlet to 775m at the ridgetop and encompasses an area of 21ha, with an average slope of 16°. The elevation range of Watershed 6, directly west of Watershed 5, spans 550m to 815m, and encompasses an area of 15ha with an average slope of 15°. Sillimanite-grade schist and calc-silicate granulite of the Silurian Rangeley Formation underlie both Watershed 5 and Watershed 6, with plagioclase feldspar the dominant Ca bearing mineral phase (Lyons et al. 1997; Bailey et al. 2003b).

Due to Pleistocene glaciation, bedrock in these watersheds is generally overlain by a <3m till layer predominantly composed of porphyritic granodiorite and lesser amounts of schist (Likens and Davis 1975; Bailey et al. 2003b). Soils developed over the glacial till are predominantly Spodosols (Typic Haplorthods) (Huntington et al. 1988). Prior to the experimental harvest, Watershed 5 and Watershed 6 had similar dominant vegetation species: American beech (*Fagus grandifolia* Ehrh.), sugar maple (*Acer saccharum* Marsh.), and yellow birch (*Betula allegheniensis* Britt.) at lower elevations and red spruce (*Picea ruben* Sarg.), balsam fir (*Abies balsamea* [L.] Mill), and white birch (*Betula papyrifera* var. *cordifolia* [Marsh.] Regel) at higher elevations (Whittaker et al. 1974; Johnson et al. 1997). Following whole tree harvesting of Watershed 5, a series of successional species dominated, including buried seed species such as *Rubus* spp. and pin cherry (*Prunus pensylvanica* L.f.), as well as American beech (*Fagus grandifolia* Ehrh.), yellow birch (*Betula allegheniensis* Britt.) and sugar maple (*Acer saccharum* Marsh.) (Mou et al. 1993).

1.3.2 Whole tree harvesting of Watershed 5

Full details of the whole tree harvesting in Watershed 5 can be found in a series of earlier papers describing the experiment (Ryan et al. 1992; Johnson 1995; Martin et al. 2000). Briefly, harvesting of above ground biomass occurred between October 18, 1983 and May 21, 1984, and removed an estimated 93% of all aboveground biomass and left no riparian buffer strips intact. All stems >2.5cm diameter at breast height were harvested by mechanical feller-bunchers

and moved off the watershed using a rubber-tire skidder. After harvesting, between 65% and 70% of the watershed surface was disturbed to some degree, with 25% of the watershed area having exposed mineral soil, primarily due to mechanical mixing of the forest floor with deeper mineral soil horizons (Ryan et al. 1992; Martin et al. 2000). Sediment yield in stream was elevated in the three years following the harvest, reaching a peak of 208 $kg*ha^{-1}$ in 1987 (Martin et al. 2000). As observed in other harvesting experiments, cation and nitrate concentrations in Watershed 5 streamwater increased dramatically following the harvest. Results from repeated watershed-scale soil sampling campaigns showed that the concentrations of exchangeable nutrient cations (Ca, Mg and K) decreased in the organic and E horizons, but were balanced by increases in the B horizons (Johnson et al. 1991b; Johnson et al. 1997). The researchers concluded that there was no net change in the magnitude of the soil exchangeable Ca pool within the statistical resolution of the sample design, which should have been capable of resolving any change larger than ~10-25% (Johnson et al. 1997).

1.3.4 Sampling

Subsamples of archived streamwater and precipitation samples were obtained from the HBEF Physical Sample Archive located at the Robert S. Pierce Ecosystem Laboratory in North Woodstock, NH. Streamwater and precipitation collection protocols are detailed in Buso et al (2000). Briefly, streamwater is sampled on a weekly basis 5 to 10m above each of the permanent watershed

gauging stations, typically within 10-20 minutes of one another, using acid-washed, low-density polyethylene (LDPE) bottles. Precipitation is also sampled weekly from within each of the watersheds using high-density polyethylene funnels connected to acid-washed, LDPE bottles. Elemental concentrations were measured at the Cary Institute for Ecosystem Studies, and samples were then stored unfiltered, unacidified, and unrefrigerated in the Physical Sample Archive at Hubbard Brook. Sample preservation was evaluated by re-measuring elemental concentrations on archived samples at Boston University (See Results section).

Streamwater samples for this study were selected to capture pre-harvest baseline conditions, the time period during the harvest, and the post-harvest recovery period. In addition, we selected samples to allow evaluation of the variability in streamwater $\delta^{44}Ca$ driven by seasonality and discharge. In total, we analyzed 40 streamwater collection dates in Watershed 5 and 32 streamwater collection dates in Watershed 6. Where possible, we selected dates for which paired samples were available for both Watershed 5 and Watershed 6 (20 pairs total). For dates on which streamwater samples didn't exist in the archive for both Watershed 5 and Watershed 6, we were in most cases able to find samples collected within 1 week of each other.

In addition to streamwater samples, we obtained subsamples of Watershed 5 soils originally collected during repeated sampling campaigns designed to assess changes to soil nutrient pools in response to the harvest

(Johnson et al. 1991a; 1991b; Johnson et al. 1997). For each sampling campaign, the researchers systematically collected representative soil profiles from locations within randomly selected 25x25m grid cells that covered the entire watershed. Samples were taken at discrete intervals (Oie horizon, Oa horizon, 0-10cm mineral soil, 10-20cm mineral soil, 20+ mineral soil and C horizon mineral soil). We subsampled one grid cell (grid cell #262), located approximately half way up the catchment along the western edge, that was originally sampled during 3 separate sampling campaigns (1983, 1986 and 1991). With the exception of the Oa soil horizon from 1991, the complete profile from each year was present in the archive and there was enough sample to allow us to subsample soil for our analyses. We note that due to the destructive nature of soil sampling, the soil profiles collected within grid cell 262 in 1983, 1986 and 1991 were not collected from the same soil pit each time, but rather from different locations within the 25x 25m grid cell. Finally, to characterize the $\delta^{44}Ca$ of Ca sources we measured a sample of unweathered glacial till collected from a depth of 125-130cm below the surface in Watershed 5, a sample of Rangley formation metapelitic schist that underlies approximately 98.4% of the watershed, and one precipitation sample from Watershed 6, collected on April 22, 1982, approximately 14 months before the whole tree harvesting began.

1.3.5 Elemental Concentration

Elemental concentrations in streamwater and precipitation were historically measured within 3 months of sample collection using flame atomic

absorption spectrophotometry (FAAS) either at Cornell University or the Cary Institute of Ecosystem Studies analytical laboratory (Buso et al. 2000). Water subsamples were filtered with 0.45µm nitrocellulose filters and remeasured for this project using a Jobin-Yvon Ulitma-C inductively coupled emission spectrophotometer (ICP-ES) at Boston University. Bedrock and glacial till were acid digested to determine bulk chemistry and of soil parent materials. Approximately 50mg of powder were digested in a HF–HCl mixture by alternating the sample between hot plate and sonicator over approximately one week. Digested samples were treated with ultrapure concentrated nitric acid and Optima ultrapure hydrogen peroxide to oxidize any remaining organics including graphite. The sample were then dried down and brought back up in 2% HNO_3 for analysis on the ICP-ES at Boston University. A separate aliquot was used for isolation of Ca for isotopic analysis, described below.

A sequential extraction procedure was conducted on soil samples and glacial till to isolate the exchangeable cation pool and a more recalcitrant organic and mineral-bound soil cation pool that includes calcium oxalate (hereafter referred to as the acid extraction). Exchangeable cations were extracted from soils following a procedure modified from Johnson et al. (1991). Between 0.5 and 5g of soil were extracted with a 10:1 ratio (10ml of 1*M* Puratronic grade NH_4Cl per gram of soil) in an acid-washed test tube. Test tubes where shaken on a mechanical shaker for 24hrs. then centrifuged and supernatant filtered using 0.45um nitrocellulose filter. One aliquot of the filtered supernatant was then

diluted in 2% nitric acid for analysis of major element concentrations, while a separate aliquot was saved for isotopic analysis. Soil samples were subsequently treated with 0.5N HCl in a 2:1 ratio of acid to soil following a procedure modified from Lilieholm et al.(1992) and Dauer and Perakis (2013). After shaking the sample for 5 hours, the sample was centrifuged and the supernatant filtered using 0.45µm nitrocellulose filter. Again an aliquot was diluted for analysis of major elements, and one preserved for isotopic analysis. A third aliquot of the supernatant from the acid extraction was reserved for determination of oxalate concentration using a Dionex ICS-1000 ion chromatograph with ion suppression at Wheaton College.

Forest floor samples (Oie soil horizons), comprised of slightly to moderately decomposed organic soil material, were treated with a sequential digestion procedure. First, the exchangeable cations were extracted following procedure described above. The residue from this extraction was digested in a mixture of ultrapure concentrated nitric acid and Optima ultrapure hydrogen peroxide using a Milestone microwave digestion system. This digestion should dissolve organic-bound Ca, including Ca-oxalate. Additionally, a separate bulk Oie sample was digested in one step using the nitric acid-hydrogen peroxide procedure described above. Aliquots were diluted in 2% HNO_3 for analysis of cation concentrations on the ICP-ES at Boston University and for isolation of Ca for isotopic analysis.

1.3.6 Calcium isotope mass spectrometry

Calcium isotope measurements were carried out in the Boston University Thermal Ionization Mass Spectrometry (TIMS) Facility, using a Thermo Finnigan Triton® TIMS. We utilized a ^{42}Ca-^{48}Ca double spike to correct for fractionation during column chemistry and mass spectrometry (Russell and Papanastassiou 1978; Russell et al. 1978). We used an iterative double spike subtraction routine that removes the double spike and corrects for mass dependent fractionation using an exponential mass fractionation law (Compston and Oversby 1969; Heuser et al. 2002; Fantle and Bullen 2009). The double spike subtraction routine was implemented as a spreadsheet in the MS Excel software program.

The double spike and sample solutions were mixed to achieve a 85:15 sample to spike ratio (by mass of Ca) to minimize error propagation during the iterative double spike subtraction (Rudge et al. 2009). Typically, between 1 and 3µg of sample Ca was mixed with an appropriate amount of double spiked Ca prior to column chemistry. Column chemistry consisted of passing the spiked sample through AG50-X8 cation resin in an 8cm long and 0.6cm diameter Teflon column with a 30ml reservoir. Ultrapure, distilled 1N, 1.5N and 4N HNO_3 were used as reagents, with the 1N HNO_3 used as the final eluent. After the double spiked sample passed through the column, it was dried down, brought back up in 100µl concentrated nitric and 50µl ultrapure hydrogen peroxide solution, dried down again, and twice more brought up in 100µl concentrated nitric acid and dried down to oxidize any remaining organics. Finally, the sample was brought

up in approximately 2µl 2N HNO_3 for loading onto an outgassed zone refined rhenium filament. After loading the sample onto the filament, 0.5µl of 5% H_3PO_4 was added to increase the ionization efficiency. Samples were run using the double filament method, with the ionization filament heated until the pyrometer reached 1410°C first (typically 2600-3000mA), and then the evaporation filament current ramped to between 1600mA and 1900mA over the course of 1 hour, with constant monitoring to insure that the ^{40}Ca beam did not increase above 10V, which increases the likelihood of faraday cup "poisoning" (Holmden and Bélanger 2010). Each sample was run for at least 100 cycles, to insure robust statistics. Two standards, National Institute of Standards and Technology (NIST) Standard Reference Material (SRM) 915A calcium standard and a North Atlantic Seawater Standard (NASS), were typically measured during each session to quantify the external precision of our measurements. Ca isotope ratios are expressed as the permil deviation of the corrected $^{44}Ca/^{40}Ca$ sample ratio relative to the seawater value (Hippler et al. 2003). Two standard error internal precision for a single analysis (consisting of 15 blocks of 10 cycles) was better than 0.10‰, and typically < 0.06‰ (2SE). Most unknown samples were run 2 or more times, with repeated runs of the same sample generally agreeing within 0.10‰ or less. Long term external precision was quantified based on two times the standard deviation of repeated measurement of our two standards: NIST SRM 915A and NASS seawater. For NIST SRM 915A we obtained a mean of -1.91‰ ±0.14‰ (2SD, n = 14), and for seawater 0.03‰ ±0.12‰ (2SD, n = 14) (SD: standard deviation).

Unlike Holmden and Bélanger (2010), no long-term drift was evident in our Ca standards database, and therefore no drift corrections were made to standards or samples. We therefore report analytical uncertainty on a single measurement of an unknown as ±0.14‰ (the larger of the 2SD for our two standards).

1.4 RESULTS

1.4.1 Comparison of Ca concentrations in archived streamwater measured at the time of collection and present day

A comparison of historical (measured shortly after the time of collection) and contemporary (measured at Boston University) concentrations of Ca, Mg and K in streamwater indicate good agreement (e.g. R^2: 0.96, slope: 0.98, y-intercept: 0.06, p-value: <0.0001, mean absolute error: 0.13 ppm across a factor of 5 range in Ca concentration; Table 1.1, Figure 1.2). A rough calculation suggests that sample preservation artifacts (from precipitation dissolution of Ca-bearing phases) large enough to produce analytically resolvable changes in $\delta^{44}Ca$ (>0.14‰) would likely require changes in dissolved Ca concentrations of >15%, which would be easily measureable and are not observed. Based on these observations we are confident that the Ca isotope ratios measured at present reflect the ratios of dissolved Ca at the time of sample collection.

1.4.2 Soil Ca concentrations

Exchangeable Ca data, even on this limited sample set, demonstrate most of the features described by Johnson et al. (1997) based on their analysis of

multiple profiles collected throughout the watershed. Soil exchangeable Ca concentrations are highest in shallow horizons, and decrease with time after the experimental harvesting (Figure 1.3a-c). The observed decrease in Oa horizon exchangeable Ca is at least in part balanced by increases in deeper 0-10 and 10-20cm mineral soil exchangeable Ca In 1983 (pre-harvest), grid cell 262 Oa horizon contained 1900µg $Ca*g^{-1}$ soil, the highest measured exchangeable Ca in our dataset (Figure 1.3a, Table 1.2). Exchangeable Ca decreases rapidly with depth, with only 67µg $Ca*g^{-1}$ soil in the 0-10cm mineral soil and decreasing further to 13µg $Ca*g^{-1}$ within the C horizon. This 1983 Ca concentration profile is similar to the average of over 60 soil profiles collected during the 1983 soil sampling campaign by Johnson et al. (1991).

Exchangeable Ca in 1986 (post-harvest) grid 262 Oa soil is 19% lower than 1983, while in the 0-10cm mineral soil, Ca is significantly higher (121% increase) in 1986 relative to 1983. The 1991 grid 262 Oa horizon sample was unfortunately not preserved in the archive, but at 0-10cm exchangeable Ca is dramatically higher yet in 1991 relative to 1986. The overall pattern therefore seems to be decreasing exchangeable Ca in the Oa, and increasing exchangeable Ca in the shallow (0-10cm) mineral soil in the years following the harvest.

Although not measured in previous studies, we also examined Ca concentrations in forest floor (Oie) horizons collected from these profiles (Table 1.2). In contrast to the decrease in Oa horizon Ca concentrations between 1983

and 1991, we observed increasing Ca concentrations with time in the Oie horizon. The increase was observed in bulk Oie samples and in the residual fraction (sequential extraction #2). Ca concentrations in Oie horizon bulk digestions increased from 3366µg*g^{-1} in 1983 to 5334µg*g^{-1} in 1986 to 9060µg*g^{-1} in 1991. Time-dependent concentration increases are similarly observed for other nutrients (P, Mg, K) in grid 262 Oie samples. For the one Oie exchangeable fraction measured, the 1983 exchangeable Ca fraction in the Oie horizon comprises 57% of the total exchangeable Ca present.

Acid extractions of Ca were not performed on these soils in the earlier study, but were done here as soil Ca-oxalate has repeatedly been cited as a potential source of increased Ca export following harvesting (Bailey et al. 2003b; Hamburg et al. 2003). Ca-oxalate should be readily dissolved by the acid extraction used here, but this extraction does not target Ca-oxalate exclusively. In fact a similar acid extraction has been used at Hubbard Brook and elsewhere to target apatite-sourced Ca (Blum et al. 2002; Nezat et al. 2007). The acid extraction produced a markedly different Ca concentration profile with depth when compared to the exchangeable Ca extraction (Figure 1.3b). Acid extractable Ca concentration in the pre-harvest 1983 grid cell 262 profile was high in the near surface Oa horizon (419µg*g^{-1} soil), but rapidly decreased to a minimum of 20µg*g^{-1} in the 0-10cm mineral soil depth (Table 1.2). Ca then increases with depth, reaching a maximum of 767µg*g^{-1} in the glacial till. This extraction produced a Ca/P molar ratio of 1.6, which is identical to the Ca/P

molar ratio in apatite suggesting that high concentrations of acid extractable Ca at depth reflect apatite dissolution rather than release of Ca bound by oxalate. Changes in depth profiles of acid extractable Ca pre- and post-harvest mimicked the pattern seem in exchangeable Ca. The 1986 profile produced lower Ca in the Oa horizon (419µg $Ca*g^{-1}$ and 121µg $Ca*g^{-1}$ in 1983 and 1986, respectively) and higher Ca in the 0-10 and 10-20cm mineral soil horizons.

Depth patterns in acid extractable oxalate ion are quite distinct from acid-extractable Ca (Figure 1.3c). Dissolution of Ca-oxalate should produce molar Ca:oxalate ratios of 1, but in the near-surface maximum in acid extractable Ca, this ratio is 4.3, suggesting substantial contributions of Ca from non-Ca oxalate sources perhaps including residual exchangeable Ca not collected during the NH_4Cl extraction, or release of Ca bound to other organics. At depth, where acid extractable oxalate (and Fe, Al) concentrations are high, Ca concentrations are low (molar Ca:oxalate 0.18 to 0.23), suggesting that most of the oxalate extracted here was held in soil phases other than Ca oxalate, perhaps by sorption to secondary Fe-Al sesquioxides. These observations make the acid extractable Ca data somewhat difficult to interpret. We measured $\delta^{44}Ca$ only from the depths where acid extractable Ca concentrations are high: near surface horizons, where this Ca may in part reflect Ca oxalate produced by vegetation and fungi (Graustein et al. 1977; Cromack Jr et al. 1979; Gadd 1999; Gadd 2007), and from the C-horizon, where the Ca is likely from apatite dissolution.

1.4.3 $\delta^{44}Ca$ of Ca sources

$\delta^{44}Ca$ of Ca inputs to the ecosystem fall in a narrow range close to -1‰ (vs. seawater; Table 1.1 and 2.2). $\delta^{44}Ca$ in the Rangely fm. metapelitic mica schist bedrock was -1.25‰, while the bulk digestion of glacial till had a $\delta^{44}Ca$ value of -1.09‰. The (HCl) acid extractable Ca component of till had a $\delta^{44}Ca$ of -0.9‰. While the acid-extractable component represents only ~10% of bulk till Ca, this component, which we infer to be predominantly composed of apatite, may be a significant source of Ca actively cycled Ca (Blum et al., 2002). Exchangeable Ca from till was significantly more negative (-1.52‰) than bulk or acid-extractable Ca, but this component represents a trivial fraction (~0.1%) of bulk till Ca. A single precipitation sample (collected at a rain gauge adjacent to Watershed 6 on 4/27/1982) has a $\delta^{44}Ca$ similar to till values, -1.01‰.

1.4.4 $\delta^{44}Ca$ of soil Ca

The $\delta^{44}Ca$ of each of the measured soil pools are consistently more negative than all of the Ca sources described above. In 1983 soil exchangeable $\delta^{44}Ca$ was lowest in the Oie (-2.11‰), and increased with depth (Oa horizon and 0-10cm -1.76‰ and -1.80‰, respectively), reaching a maximum value of -1.4‰ in the 20+cm mineral soil (Table 1.2 and Figure 1.4). The $\delta^{44}Ca$ of the soil exchangeable pool in the 1986 profile exhibited a similar trend with depth, though all $\delta^{44}Ca$ values were more negative than their 1983 equivalent, -2.38 in the Oie horizon and -1.96‰ in the Oa and 0-10cm horizons. Exchangeable $\delta^{44}Ca$ values in the 1991 profile were also consistently more negative than 1986 (-2.58 in the

Oie and -2.18‰ in 0-10cm). $\delta^{44}Ca$ values from Oie sequential extraction residual fractions were approximately 0.2‰ lower than the exchangeable fraction values (-2.27‰, -2.59‰ and -2.80‰ in 1983, 1986, and 1991, respectively). Bulk acid digestion of fine roots (<2mm in diameter) taken from the 1983 Oie sample yielded a $\delta^{44}Ca$ of -2.38‰ and is the most isotopically negative component measured from the 1983 soil profile.

Acid extractable Ca in Oa horizons, which as discussed above may reflect at least in part Ca-oxalate, are also isotopically negative, generally more so than exchangeable Ca from the same samples, and similar to exchangeable Ca in overlying Oie horizons of the collection year. As with exchangeable Ca, shallow (Oa and 0-10cm) acid-extractable Ca becomes more negative with time.

1.4.5 Calcium isotopes in streamwater

29 streamwater samples from Watershed 5 were analyzed for $\delta^{44}Ca$. 13 samples were from pre-harvest, 3 samples were from during the harvest, and 13 samples were from the post-harvest period (Figure 1.5). Prior to the whole-tree harvest, Watershed 5 streamwater $\delta^{44}Ca$ averaged -1.17‰ with the lowest values of -1.31‰ occurring on February 3, 1983 and the highest value of -1.00‰ occurring on September 22, 1983. Pre-harvest streamwater $\delta^{44}Ca$ exhibited a nonlinear negative relationship with stream discharge, with high stream discharge carrying low $\delta^{44}Ca$ (Figure 1.6).

Figure 1.5 indicates that a shift toward lower $\delta^{44}Ca$ occurs during the harvest period. Average post-harvest $\delta^{44}Ca$ was -1.47‰ (n = 15), and

streamwater $\delta^{44}Ca$ remained below pre-harvest values until approximately spring of 1987, when streamwater $\delta^{44}Ca$ values increased to values that are similar to pre-harvest values as streamwater Ca concentrations decreased. The two lowest $\delta^{44}Ca$ values occurred on dates with the highest discharge of any samples analyzed (Figure 1.6). Post-harvest streamwater $\delta^{44}Ca$ also exhibited a negative relationship with discharge, but $\delta^{44}Ca$ were offset by approximately -0.3‰ relatively to pre- harvest $\delta^{44}Ca$ values for similar discharge values.

Twenty streamwater samples from Watershed 6 were analyzed for $\delta^{44}Ca$. $\delta^{44}Ca$ values of pre-harvest streamwater samples collected in Watershed 6 and Watershed 5 on the same day were highly correlated (R^2: 0.80, p-value = 0.00012), but Watershed 6 $\delta^{44}Ca$ values are more negative than corresponding pre-harvest Watershed 5 samples by an average of 0.12‰. The same day correlation between the two watersheds becomes much weaker following the harvest. Watershed 6 streamwater $\delta^{44}Ca$, like Watershed 5, exhibits a non-linear negative relationship with discharge (Figure 1.6), but there is no change in the relationship between pre- and post-harvest periods as was observed in Watershed 5.

1.5 DISCUSSION

1.5.1 Hydrologic control on Streamwater $\delta^{44}Ca$

Variability of calcium isotope ratios with changes in stream discharge has generally been observed in the few worldwide streams and rivers where this has

been studied (Schmitt et al. 2003; Cenki-Tok et al. 2009; Holmden and Bélanger 2010). Cenki-Tok et al. (2009) observed that streamwater $\delta^{44}Ca$ shifted toward shallow soil $\delta^{44}Ca$ values at high stream discharge, while at low discharge streamwater had a $\delta^{44}C$ value similar to bedrock. The researchers suggested that during low discharge, water entering the stream was predominantly transported via deeper soil and bedrock flow pathways, and the isotopic signature of the streamwater was controlled by dissolution of primary minerals. At high discharge water moved through shallower soil flow pathways before entering the stream.

In Watershed 5 and Watershed 6, the observed relationship between discharge and streamwater may be explained similarly through hydrologic flowpath control. Based on our analysis of till and bedrock, we expect primary weathering to yield Ca with $\delta^{44}Ca$ between -0.9‰ and -1.1‰. These values agree closely with our measurements of baseflow streamwater (Figure 1.6) suggesting that baseflow streamwater largely carries Ca liberated from the weathering of primary minerals in till and/or bedrock, delivered to the stream via relatively deep flowpaths.

During spring snowmelt and other high discharge events, the $\delta^{44}Ca$ of streamwater shifts toward more negative values, likely reflecting activation of shallow (or even surface) flowpaths and export of Ca from the shallow cation exchange (bio-available Ca) complex. Research conducted in Hubbard Brook Watershed 3 indicated that transient water tables and groundwater flow though

shallow soil pathways occurs during rainfall events, and these shallow soil pathways can influence downstream water chemistry (Zimmer et al. 2013; Bailey et al. 2014). A good example of this effect is seen in the data from spring 1987. The March 31, 1987 sample was collected during a rain-on-snow event that produced approximately 10cm of rain and almost completely melted a ~30-45cm deep snowpack on the south-facing slopes. This is the highest-discharge sample in our dataset (320 $L*sec^{-1}$ at time of sample collection) and had the lowest streamwater $\delta^{44}Ca$ value measured in this study (-1.76‰). Five days later, when discharge was substantially lower (52 $L*sec^{-1}$ at time of sample collection), Watershed 5 streamwater $\delta^{44}Ca$ had increased by 0.35‰ to -1.36‰. Similarly, Hurricane Gloria passed over HBEF on September 25, 1985. This storm produced the second highest instantaneous discharge in our sample set (185.1 $L*sec^{-1}$), and a very negative $\delta^{44}Ca$ (-1.70‰). Approximately 3 weeks before, on September 8, 1985, when instantaneous stream discharge was very low (4.3 $L*sec^{-1}$), the Watershed 5 streamwater $\delta^{44}Ca$ value was -1.40‰, the second highest measured streamwater $\delta^{44}Ca$ post-harvest. Clearly, changes in hydrologic flowpaths, particularly activation of shallow flow pathways that interact with the isotopically light shallow soil Ca pools, affect streamwater stable Ca isotopes.

Although pre-harvest streamwater Ca isotope compositions in Watershed 5 and 6 streamwaters are highly correlated, there are important differences that may ultimately be related to hydrologic control. Watershed 5 $\delta^{44}Ca$ averages

0.12‰ higher than Watershed 6 over 13 same-day sample pairs. Similarly, Ca concentrations were consistently higher in Watershed 5 than in Watershed 6 (by an average of 28%) in these 13 same-day sample pairs. Watershed 5 is 40% larger than Watershed 6, which likely drives differences in subsurface flowpaths, water transit times, locations of groundwater seeps, length and tortuosity of the stream channel or slightly greater groundwater contribution in Watershed 5 relative to 6 (McGuire et al. 2005; Tetzlaff et al. 2009; Zimmer et al. 2013; Bailey et al. 2014).

1.5.2 Effect of the Watershed 5 whole tree harvest on streamwater Ca

The Watershed 5 experimental harvesting, which resulted in a dramatic increase in Ca export, also produced a pronounced shift toward lower $\delta^{44}Ca$ in streamwater compared to pre-harvest values (Figure 1.5). This requires that additional Ca for export must have come from a source with more negative $\delta^{44}Ca$. Bailey et al (2003) argued that enhanced chemical weathering of primary silicate minerals is an unlikely Ca source, based on the absence of an increased Na mass balance, as would be expected as a result of weathering of silicates such as plagioclase. Blum et al. (2002) demonstrated the importance of apatite- rather than silicate-bound Ca in forest ecosystems, and Hamburg et al. (2003) suggested that dissolution of apatite may be an important Ca source for regrowing forests. However, chemical weathering (of silicates or apatite) cannot account for increased export of isotopically light Ca unless the Ca liberated by weathering was first actively cycled through vegetation, which seems improbable

in a freshly clearcut watershed. Instead the increase in Ca export more likely reflects loss from a pre-existing pool of biologically cycled, isotopically light Ca. Such pools include soil exchangeable Ca, the acid extractable Ca component of shallow soil, or Ca bound in forest floor (Oie) organics.

To better constrain the source of increased Ca export following clear-cutting, we utilize a two component mixing model in which we treat the observed post-harvest Ca export flux (F_t) from Watershed 5 as the sum of two Ca sources, a "baseline" Ca export flux that would have been observed in the absence of an experimental harvest (F_1) and an excess Ca flux resulting from the harvest (F_2). F_1 for a given post-harvest sample is calculated based on the instantaneous discharge measured at the time of sample collection and the relationship between pre-harvest (January 1977-November 1983) instantaneous discharge and Ca export (R^2:0.99, slope: 2.52, y-int:0.95). The magnitude of F_2, the excess Ca export flux from Watershed 5, is calculated by subtracting F_1 from F_t (measured Ca concentration times measured instantaneous discharge). The fractional contribution of the excess component to Ca export (F_2/F_t) increased after the harvest, reaching a maximum of 0.76 on November 13, 1984 then steadily decreased to below 0.10 by the spring of 1987 (Table 1.3).

The isotope ratio of the excess Ca source ($\delta^{44}Ca_2$) for a post-harvest sample can be approximated by extending the mass balance to include Ca isotopes:

$$F_t\delta^{44}Ca_t = F_1\delta^{44}Ca_1 + F_2\delta^{44}Ca_2 \qquad (1)$$

The isotope ratio of the "baseline" Ca source, $\delta^{44}Ca_1$, varies between -1.1 and -1.3‰, based on the observed pre- harvest δ^{44}Ca-discharge relationship for Watershed 5, fitted using a power law (Figure 1.6; a: -1.13, b: 0.034). Solving this equation for $\delta^{44}Ca_2$, we can calculate the isotope ratio of the excess Ca component for each post-harvest measurement of Watershed 5 streamwater δ^{44}Ca (Figure 1.7). Excluding samples where F_2 is very small (see discussion below), post-harvest Watershed 5 samples yield $\delta^{44}Ca_2$ values between -1.5‰ and -2.75‰ (Table 1.3), values consistent with those measured in biologically fractionated soil pools. The range of calculated $\delta^{44}Ca_2$ values for the peak of excess Ca export (where F_2 is > 50% of total Ca export) is limited to -1.5 to -2.0‰, consistent with the range in exchangeable δ^{44}Ca and suggesting that the soil exchange complex may be the dominant source of Ca lost to streamwater.

The isotope ratio of this excess component ($\delta^{44}Ca_2$) appears to decrease with time, from -1.58‰ on November 13, 1984 at peak excess Ca export, to -2.75‰ on 9/21/86 (Figure 1.7) suggesting that the source of excess Ca was becoming more isotopically light in the years following the harvest. This trends is consistent with the trend towards lighter soil δ^{44}Ca values seen with time in soil Ca pools (Figure 1.4). We used a Monte Carlo sensitivity analysis that incorporates measurement uncertainty Watershed 5 discharge, streamwater Ca concentration and streamwater δ^{44}Ca to assess the uncertainty in modeled $\delta^{44}Ca_2$ values (Figure 1.7) and to evaluate whether the calculated trend toward lighter values of $\delta^{44}Ca_2$ is significant. Uncertainty in modeled $\delta^{44}Ca_2$ increases

rapidly as F_2 approaches zero, which is important because this component diminishes toward the end of our time series. Our analysis indicates a statistically significant decrease in $\delta^{44}Ca_2$ between 9/17/1984 and 9/21/1986 (mean slope: -0.00132, 95% CI: -0.00133, -0.00131), after which F_2 contributes less than 10% of total Ca export flux, and uncertainties in $\delta^{44}Ca_2$ become too large to evaluate temporal trends.

The total mass of excess Ca that was exported from Watershed 5 as a result of the harvest is calculated by integrating the daily excess export value (F_2) over the period between 1984 and 1988. This produces an estimate of 915mol*ha^{-1} of excess Ca export, with roughly 80% of that occurring within the first two years. Using values from Likens (1998), This total excess export is equivalent to only 13% of the Ca stored in the pre-harvest depth integrated Watershed 5 exchange pool, which supports our inference based on isotopic evidence that the exchange complex is the dominant source of excess Ca export. Some calculated values of $\delta^{44}Ca_2$, particularly toward the end of our model simulation, are more negative than contemporaneous values of exchangeable δ^{44}Ca. This may reflect a contribution of more recalcitrant organically bound Ca in roots, decaying organic material, and perhaps Ca-oxalate, as the most negative pools of Ca measured in W5 across all dates were fine roots and Oie extraction residual fractions.

1.5.3 Effect of the Watershed 5 whole tree harvest on Ca cycling

Johnson et al. (1991b, 1997) showed that the Watershed 5 harvest resulted in decreased exchangeable Ca and increased exchangeable Al in in Oa horizons, but that increases in exchangeable Ca in deeper horizons resulted in very little net change in the magnitude of the soil exchangeable Ca pool. To reconcile the inferred increased export of exchangeable Ca in the absence of an appreciable decrease in the size of the Ca exchangeable pool, we draw upon our $\delta^{44}Ca$ measurements of soil exchangeable, acid extractable, and forest floor (Oie) Ca, all of which became consistently more isotopically negative from 1983 to 1986 to 1991 (Figure 1.4). The observation that the isotope ratios of each of these pools change at all in the years following the harvest with little change in pool size requires that these pools are actively turning over on this timescale. The trend towards lighter Ca in each of these pools puts constraints on processes affecting the forest Ca cycle in the years following the harvest.

As a result of the biological fractionation of Ca isotopes, biomass is isotopically light relative to Ca sources, and roots generally have the most negative $\delta^{44}Ca$ values of any portion of biomass, upwards of 1‰ more negative than leaf litter (Page et al. 2008; von Blanckenburg et al. 2009; Holmden and Bélanger 2010; Hindshaw et al. 2012). We speculate that loss of Ca from the soil exchange pool may have been in part balanced by elevated decomposition and mineralization of isotopically light Ca bound in below ground biomass, particularly roots, which were the most negative $\delta^{44}Ca$ component measured from the 1983

soil profile. Replenishment of soil Ca from this light reservoir might account for the trend towards lighter $\delta^{44}Ca$ in soil Ca pools

Between 1984 and 1988, the aggrading Watershed 5 forest accumulated some 2500mol Ca/ha in aboveground biomass (Mou et al., 1993), while exporting an excess 915 $mol*ha^{-1}$ Ca largely from the soil exchange pool to streamwater, all without appreciably depleting the exchange pool. Inputs of new Ca from external sources including atmospheric deposition and weathering over this interval are estimated at only 375 $mol*ha^{-1}$ (Likens et al. 1998), requiring an additional source of Ca. Likens et al. (1998) argued that remineralization of Ca from decomposing logging debris and decaying roots following harvest is a major source of Ca to soil, sufficient to account for Ca uptake by re-growth of the forest. Fahey et al. (1988) calculated a pre-harvest Watershed 5 mass of ~2600 $mol*ha^{-1}$ Ca stored in lateral roots, with 45-63% of root biomass lost to decomposition in the first 5 years following the Watershed 5 harvest (Fahey et al., 1993). The decomposition of lateral roots and logging debris (released 2500mol $Ca*ha^{-1}$ in the first three years post-harvest, Likens et al., 1998), would have been a more than adequate source of Ca to replace the excess Ca lost to streamwater and vegetation regrowth between 1984 and 1988. Continued decomposition of belowground biomass, releasing isotopically light organically bound Ca, could likely account for trend towards increasingly more negative $\delta^{44}Ca$ in the soil exchange pool. Importantly, the $\delta^{44}Ca$ of Oie (forest floor) residual Ca evolves in parallel with overall soil exchangeable Ca, becoming lighter by 0.5‰ between

1983 and 1991. This change in forest floor litter likely tracks aboveground biomass, which was itself evolving to more negative $\delta^{44}Ca$ as the forest regrew. These observations suggest that isotopically light Ca from root and other biomass decomposition continued to play an important role both in replenishing the soil exchange pool and in supplying Ca for the rebuilding forest for many years following whole-tree harvesting.

1.6 CONCLUSIONS

This is the first study to apply Ca isotopes to investigate the response of the calcium cycle to land use disturbance. It further demonstrates the utility of Ca isotopes for studies of the terrestrial Ca cycle providing a complement to mass balance studies and other Ca cycle tracers such as Ca/Sr and $^{87}Sr/^{86}Sr$. The unique long-term sample archive from Hubbard Brook Experimental Forest allows us to use stable Ca isotopes to provide a new perspective in addressing outstanding questions regarding the source of streamwater Ca and changes in forest Ca cycling following a decades-old experimental whole-tree harvest conducted at Hubbard Brook. The most important observations in this new dataset are 1) a shift towards more negative $\delta^{44}Ca$ of streamwater coinciding with increased streamwater Ca concentrations following harvesting, 2) a decrease with time in the $\delta^{44}Ca$ of soil exchangeable Ca, acid-extractable (“Ca-oxalate”) Ca, and of forest floor litter. Earlier studies have called on a variety of mechanisms to explain enhanced Ca export in the absence of a resolvable decrease in exchangeable Ca concentrations. Our isotopic mass balance

approach strongly suggests that enhanced Ca export was in fact sourced from isotopically light soil pools, dominated by the soil cation exchange complex. Additionally, our stable Ca isotopes indicate that increased dissolution of apatite was not the primary source of Ca replenishing the soil exchangeable pool, and mass balance considerations suggest there is not enough Ca oxalate in the soil to account for the increased streamwater Ca export. The shift towards more negative δ^{44}Ca in the exchange pool requires that Ca lost from the exchange pool was replenished by an isotopically light source, which we infer to have been decomposition of root biomass. The parallel trend in the δ^{44}Ca of forest floor litter indicates that that the rebuilding forest ultimately sourced its Ca from the decomposition root biomass, perhaps cycled through the soil exchange pool. Better understanding the dynamics of the terrestrial Ca cycle to forest disturbance is important to managing forest resources and predicting the response of forest ecosystems to future changes in climate, and recovery of forests from acid rain deposition. Ca isotopes should prove a useful addition to the biogeochemist's toolbox in addressing these questions.

1.7 REFERENCES

Bailey AS, Hornbeck JW, Campbell JL, Eagar C (2003a) Hydrometeorological database for Hubbard Brook Experimental Forest: 1955-2000. U.S. Department of Agriculture, Forest Service, Northeastern Forest Experiment Station Gen. Tech. Rep. NE-305, Newtown Square, PA

Bailey SW, Brousseau PA, McGuire KJ, Ross DS (2014) Influence of landscape position and transient water table on soil development and carbon distribution in a steep, headwater catchment. Geoderma 226–227:279–289. doi: 10.1016/j.geoderma.2014.02.017

Bailey SW, Buso DC, Likens GE (2003b) Implications of Sodium Mass Balance for Interpreting the Calcium Cycle of a Forested Ecosystem. Ecology 84:471–484.

Bailey SW, Hornbeck JW, Driscoll CT, Gaudette HE (1996) Calcium Inputs and Transport in A Base-Poor Forest Ecosystem as Interpreted by Sr Isotopes. Water Resources Research 32:707–719. doi: 10.1029/95WR03642

Blum JD, Klaue A, Nezat CA, et al (2002) Mycorrhizal weathering of apatite as an important calcium source in base-poor forest ecosystems. Nature 417:729–731. doi: 10.1038/nature00793

Buso DC, Likens GE, Eaton JS (2000) Chemistry of precipitation, streamwater, and lakewater from the Hubbard Brook Ecosystem Study: a record of sampling protocols and analytical procedures. U.S. Department of Agriculture, Forest Service, Northeastern Research Station, Newtown Square, PA

Cenki-Tok B, Chabaux F, Lemarchand D, et al (2009) The impact of water–rock interaction and vegetation on calcium isotope fractionation in soil- and stream waters of a small, forested catchment (the Strengbach case). Geochimica et Cosmochimica Acta 73:2215–2228. doi: 10.1016/j.gca.2009.01.023

Compston W, Oversby VM (1969) Lead Isotopic Analysis Using a Double Spike. Journal of Geophysical Research 74:4338–4348. doi: 10.1029/JB074i017p04338

Cromack Jr K, Sollins P, Graustein WC, et al (1979) Calcium oxalate accumulation and soil weathering in mats of the hypogeous fungus Hysterangium crassum. Soil Biology and Biochemistry 11:463–468. doi: 10.1016/0038-0717(79)90003-8

Dauer JM, Perakis SS (2013) Contribution of Calcium Oxalate to Soil-Exchangeable Calcium: Soil Science 178:671–678. doi: 10.1097/SS.0000000000000029

Driscoll CT, Cirmo CP, Fahey TJ, et al (1996) The Experimental Watershed Liming Study: Comparison of Lake and Watershed Neutralization Strategies. Biogeochemistry 32:143–174.

Ellsworth DS, Liu X (1994) Photosynthesis and canopy nutrition of four sugar maple forests on acid soils in northern Vermont. Canadian Journal of Forest Research 24:2118–2127. doi: 10.1139/x94-272

Fantle M, Bullen T (2009) Essentials of iron, chromium, and calcium isotope analysis of natural materials by thermal ionization mass spectrometry. Chemical Geology 258:50–64. doi: 10.1016/j.chemgeo.2008.06.018

Farkaš J, Déjeant A, Novák M, Jacobsen SB (2011) Calcium isotope constraints on the uptake and sources of Ca2+ in a base-poor forest: A new concept of combining stable (δ44/42Ca) and radiogenic (εCa) signals. Geochimica et Cosmochimica Acta 75:7031–7046. doi: 10.1016/j.gca.2011.09.021

Federer CA (1973) Annual cycles of soil and water temperatures at Hubbard Brook. U.S. Department of Agriculture, Forest Service, Northeastern Forest Experiment Station Research Note NE-167, Upper Darby, PA

Fuller RD, Driscoll CT, Lawrence GB, Nodvin SC (1987) Processes regulating sulphate flux after whole-tree harvesting. Nature 325:707–710. doi: 10.1038/325707a0

Gadd GM (1999) Fungal Production of Citric and Oxalic Acid: Importance in Metal Speciation, Physiology and Biogeochemical Processes. In: Advances in Microbial Physiology. Academic Press, pp 47–92

Gadd GM (2007) Geomycology: biogeochemical transformations of rocks, minerals, metals and radionuclides by fungi, bioweathering and bioremediation. Mycological Research 111:3–49. doi: 10.1016/j.mycres.2006.12.001

Graustein WC, Cromack K, Sollins P (1977) Calcium Oxalate: Occurrence in Soils and Effect on Nutrient and Geochemical Cycles. Science 198:1252–1254. doi: 10.1126/science.198.4323.1252

Green MB, Bailey AS, Bailey SW, et al (2013) Decreased water flowing from a forest amended with calcium silicate. Proceedings of the National Academy of Sciences 110:5999–6003. doi: 10.1073/pnas.1302445110

Hamburg SP, Yanai RD, Arthur MA, et al (2003) Biotic Control of Calcium Cycling in Northern Hardwood Forests: Acid Rain and Aging Forests. Ecosystems 6:399–406.

Heuser A, Eisenhauer A, Gussone N, et al (2002) Measurement of calcium isotopes (δ44Ca) using a multicollector TIMS technique. International Journal of Mass Spectrometry 220:385–397. doi: 10.1016/S1387-3806(02)00838-2

Hindshaw RS, Reynolds BC, Wiederhold JG, et al (2012) Calcium isotope fractionation in alpine plants. Biogeochemistry. doi: 10.1007/s10533-012-9732-1

Hindshaw RS, Reynolds BC, Wiederhold JG, et al (2011) Calcium isotopes in a proglacial weathering environment: Damma glacier, Switzerland. Geochimica et Cosmochimica Acta 75:106–118. doi: 10.1016/j.gca.2010.09.038

Hippler D, Schmitt A-D, Gussone N, et al (2003) Calcium Isotopic Composition of Various Reference Materials and Seawater. Geostandards Newsletter 27:13–19. doi: 10.1111/j.1751-908X.2003.tb00709.x

Holmden C, Bélanger N (2010) Ca isotope cycling in a forested ecosystem. Geochimica et Cosmochimica Acta 74:995–1015. doi: 10.1016/j.gca.2009.10.020

Hornbeck J., Bailey S., Buso D., Shanley J. (1997) Streamwater chemistry and nutrient budgets for forested watersheds in New England: variability and management implications. Forest Ecology and Management 93:73–89. doi: 10.1016/S0378-1127(96)03937-0

Huntington TG, Ryan DF, Hamburg SP (1988) Estimating Soil Nitrogen and Carbon Pools in a Northern Hardwood Forest Ecosystem. Soil Science Society of America Journal 52:1162–1167. doi: 10.2136/sssaj1988.03615995005200040049x

Johnson CE (1995) Soil nitrogen status 8 years after whole-tree clear-cutting. Canadian Journal of Forest Research 25:1346–1355. doi: 10.1139/x95-147

Johnson CE, Johnson AH, Huntington TG, Siccama TG (1991a) Whole-Tree Clear-Cutting Effects on Soil Horizons and Organic-Matter Pools. Soil Science Society of America Journal 55:497–502. doi: 10.2136/sssaj1991.03615995005500020034x

Johnson CE, Johnson AH, Siccama TG (1991b) Whole-Tree Clear-Cutting Effects on Exchangeable Cations and Soil Acidity. Soil Science Society of America Journal 55:502–508. doi: 10.2136/sssaj1991.03615995005500020035x

Johnson CE, Romanowicz RB, Siccama TG (1997) Conservation of exchangeable cations after clear-cutting of a northern hardwood forest. Canadian Journal of Forest Research 27:859–868. doi: 10.1139/x96-192

Johnson DW, Kelly JM, Swank WT, et al (1988) The Effects of Leaching and Whole-tree Harvesting on Cation Budgets of Several Forests. Journal of Environmental Quality 17:418–424. doi: 10.2134/jeq1988.00472425001700030012x

Joslin JD, Kelly JM, Van Miegroet H (1992) Soil Chemistry and Nutrition of North American Spruce-Fir Stands: Evidence for Recent Change. Journal of Environmental Quality 21:12–30. doi: 10.2134/jeq1992.00472425002100010002x

Lawrence GB, David MB, Shortle WC (1995) A new mechanism for calcium loss in forest-floor soils. Nature 378:162–165. doi: 10.1038/378162a0

Likens GE, Davis AM (1975) Post-glacial history of Mirror Lake and its watershed in New Hampshire, USA: An initial report. Verh Int Ver Theor Angew Limnol 982–993.

Likens GE, Driscoll CT, Buso DC (1996) Long-Term Effects of Acid Rain: Response and Recovery of a Forest Ecosystem. Science 272:244–246. doi: 10.1126/science.272.5259.244

Likens GE, Driscoll CT, Buso DC, et al (1998) The Biogeochemistry of Calcium at Hubbard Brook. Biogeochemistry 41:89–173.

Lilieholm BC, Dudley LM, Jurinak JJ (1992) Oxalate Determination in Soils Using Ion Chromatography. Soil Science Society of America Journal 56:324. doi: 10.2136/sssaj1992.03615995005600010053x

Lyons JB, Bothner WA, Moench RH, Thompson JB (1997) Bedrock geologic map of New Hampshire. 1:250,000. United State Geological Survey, Denver, Colorado USA.

Mann LK, Johnson DW, West DC, et al (1988) Effects of Whole-Tree and Stem-Only Clearcutting on Postharvest Hydrologic Losses, Nutrient Capital, and Regrowth. Forest Science 34:412–428.

Martin CW, Hornbeck JW, Likens GE, Buso DC (2000) Impacts of intensive harvesting on hydrology and nutrient dynamics of northern hardwood forests. Canadian Journal of Fisheries and Aquatic Sciences 57:19–29. doi: 10.1139/f00-106

McGuire KJ, McDonnell JJ, Weiler M, et al (2005) The role of topography on catchment-scale water residence time. Water Resources Research 41:W05002. doi: 10.1029/2004WR003657

McLaughlin SB, Wimmer R (1999) Tansley Review No. 104 Calcium Physiology and Terrestrial Ecosystem Processes. New Phytologist 142:373–417.

Miller EK, Blum JD, Friedland AJ (1993) Determination of soil exchangeable-cation loss and weathering rates using Sr isotopes. Nature 362:438–441. doi: 10.1038/362438a0

Mou P, Fahey TJ, Hughes JW (1993) Effects of Soil Disturbance on Vegetation Recovery and Nutrient Accumulation Following Whole-Tree Harvest of a Northern Hardwood Ecosystem. Journal of Applied Ecology 30:661–675. doi: 10.2307/2404245

Nezat CA, Blum JD, Driscoll CT (2010) Patterns of Ca/Sr and 87Sr/86Sr variation before and after a whole watershed CaSiO3 addition at the Hubbard Brook Experimental Forest, USA. Geochimica et Cosmochimica Acta 74:3129–3142. doi: 10.1016/j.gca.2010.03.013

Nezat CA, Blum JD, Yanai RD, Hamburg SP (2007) A sequential extraction to determine the distribution of apatite in granitoid soil mineral pools with application to weathering at the Hubbard Brook Experimental Forest, NH, USA. Applied Geochemistry 22:2406–2421. doi: 10.1016/j.apgeochem.2007.06.012

Page BD, Bullen TD, Mitchell MJ (2008) Influences of calcium availability and tree species on Ca isotope fractionation in soil and vegetation. Biogeochemistry 88:1–13. doi: 10.1007/s10533-008-9188-5

Reuss JO, Johnson DW (1986) Acid depostion and acidification of soils and waters. viii + 119pp.

Rudge JF, Reynolds BC, Bourdon B (2009) The double spike toolbox. Chemical Geology 265:420–431. doi: 10.1016/j.chemgeo.2009.05.010

Russell WA, Papanastassiou DA (1978) Calcium isotope fractionation in ion-exchange chromatography. Analytical Chemistry 50:1151–1154. doi: 10.1021/ac50030a036

Russell WA, Papanastassiou DA, Tombrello TA (1978) Ca isotope fractionation on the Earth and other solar system materials. Geochimica et Cosmochimica Acta 42:1075–1090. doi: 10.1016/0016-7037(78)90105-9

Ryan DF, Huntington TG, Martin CW (1992) Redistribution of soil nitrogen, carbon and organic matter by mechanical disturbance during whole-tree harvesting in northern hardwoods. Forest Ecology and Management 49:87–99.

Schmitt A-D, Chabaux F, Stille P (2003) The calcium riverine and hydrothermal isotopic fluxes and the oceanic calcium mass balance☆. Earth and Planetary Science Letters 213:503–518. doi: 10.1016/S0012-821X(03)00341-8

Tetzlaff D, Seibert J, McGuire KJ, et al (2009) How does landscape structure influence catchment transit time across different geomorphic provinces? Hydrological Processes 23:945–953. doi: 10.1002/hyp.7240

Von Blanckenburg F, von Wiren N, Guelke M, et al (2009) Fractionation of Metal Stable Isotopes by Higher Plants. Elements 5:375–380. doi: 10.2113/gselements.5.6.375

Whittaker RH, Bormann FH, Likens GE, Siccama TG (1974) The Hubbard Brook Ecosystem Study: Forest Biomass and Production. Ecological Monographs 44:233–254. doi: 10.2307/1942313

Wiegand BA, Chadwick OA, Vitousek PM, Wooden JL (2005) Ca cycling and isotopic fluxes in forested ecosystems in Hawaii. Geophysical Research Letters 32:L11404. doi: 10.1029/2005GL022746

Wiegand BA, Schwendenmann L (2013) Determination of Sr and Ca sources in small tropical catchments (La Selva, Costa Rica) – A comparison of Sr and Ca isotopes. Journal of Hydrology 488:110–117. doi: 10.1016/j.jhydrol.2013.02.044

Zimmer MA, Bailey SW, McGuire KJ, Bullen TD (2013) Fine scale variations of surface water chemistry in an ephemeral to perennial drainage network. Hydrological Processes 27:3438–3451. doi: 10.1002/hyp.9449

1.8 SUPPLIMENTARY INFORMATION

1.8.1 Figures

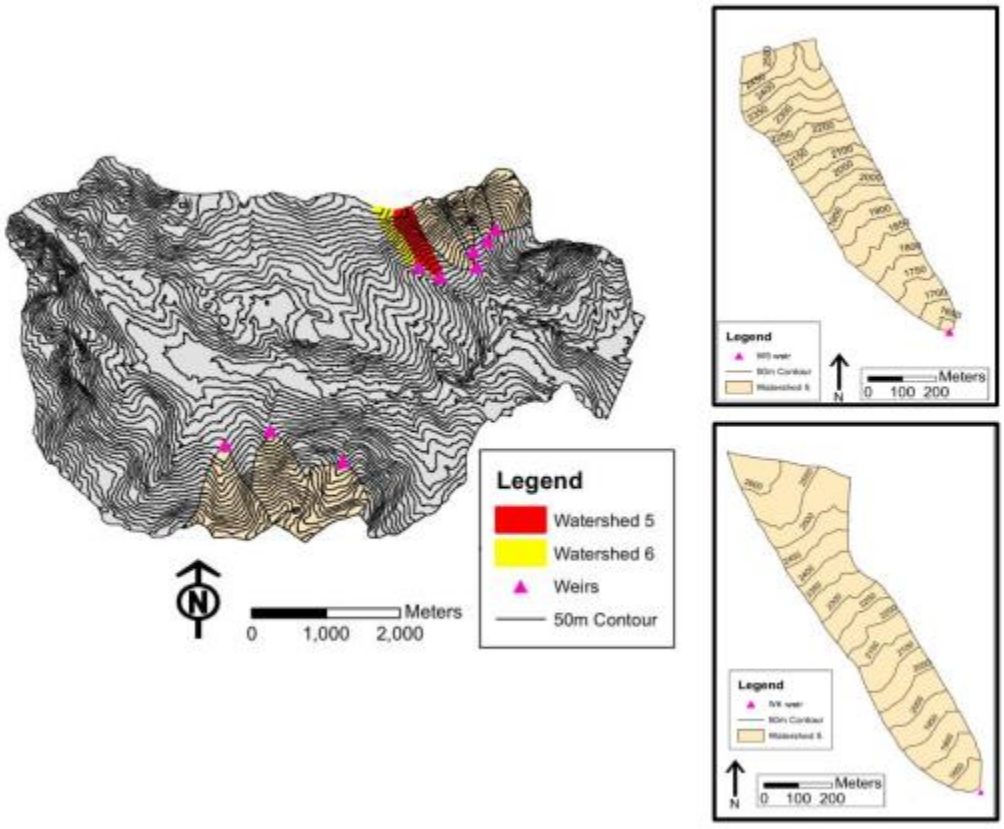

Figure 1.1. Site map of a) the entire HBEF watershed, including location of 9 research sub-watersheds, b) detail of Watershed 5 where the harvesting experiment took place in 1983-4, and c) detail of Watershed 6 the biogeochemical reference watershed, located immediately west of Watershed 5.

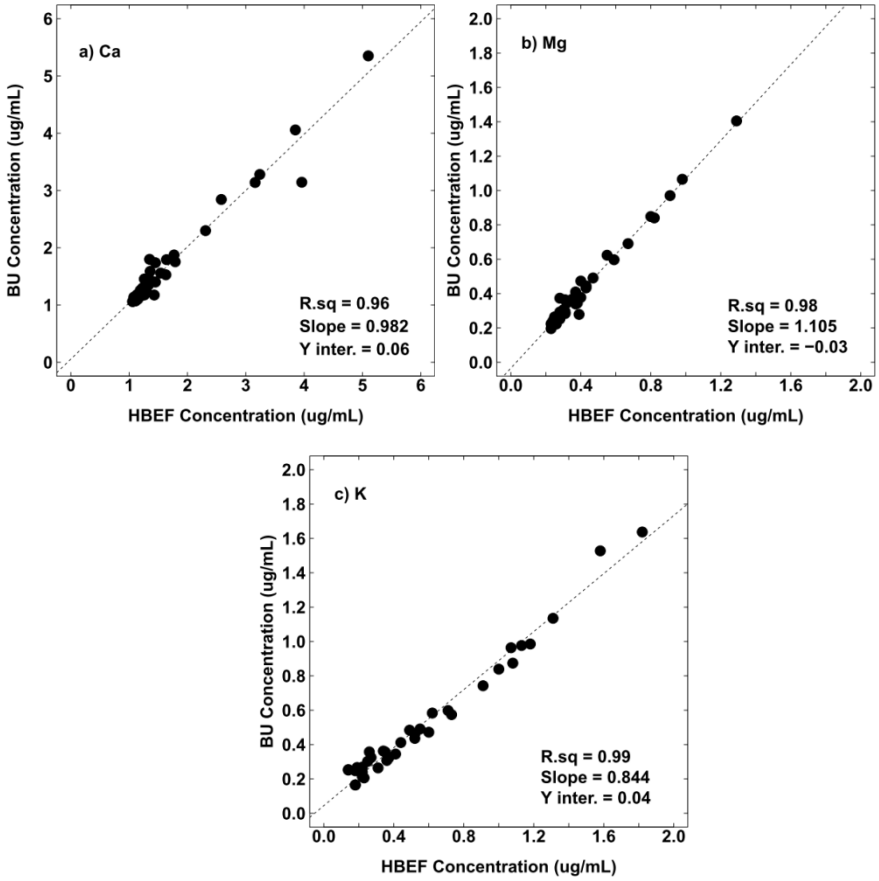

Figure 1.2. Comparison of a) Ca concentrations, b) Mg concentrations and c) K concentrations in archived streamwater measured at the time of collection (HBEF) and present day (BU).

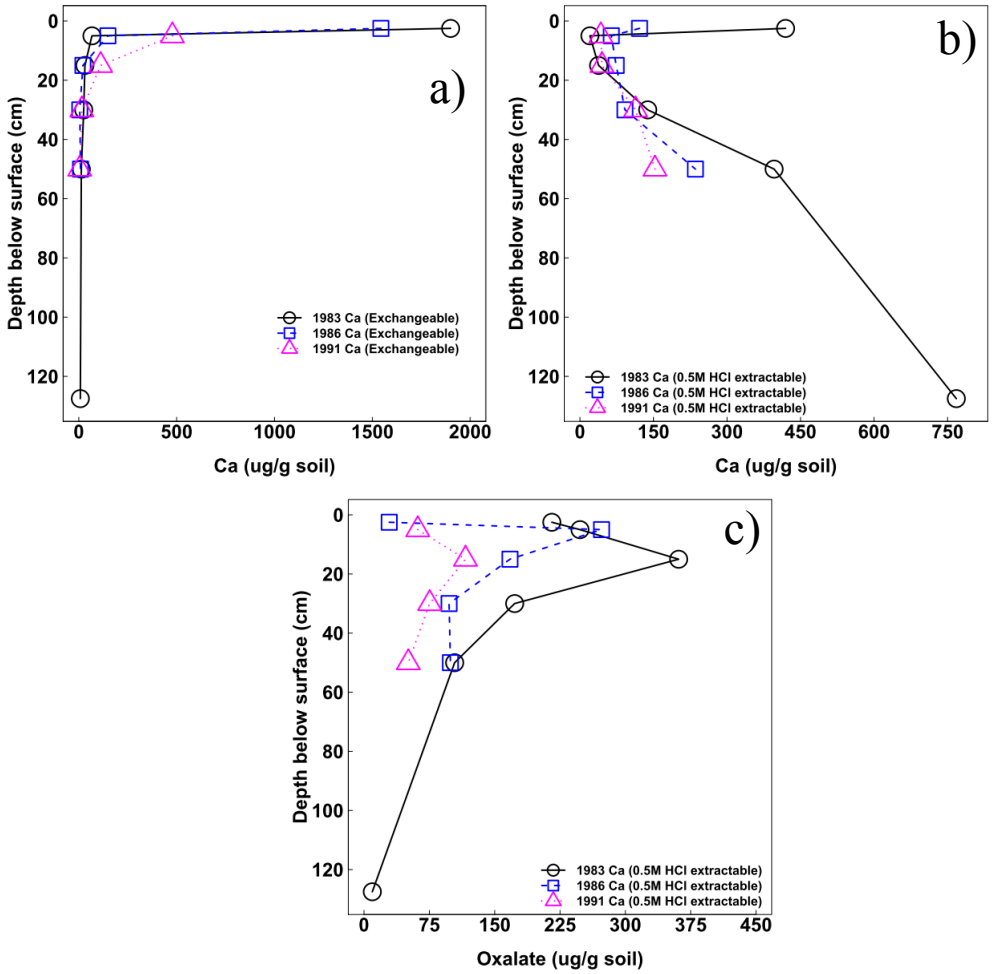

Figure 1.3. a) Depth profile of soil exchangeable Ca concentrations, b) depth profile of 0.5M HCl extractable Ca concentrations and c) depth profile of 0.5M HCl extractable oxalate concentrations from soil pits excavated within grid cell 262 located in Watershed 5.

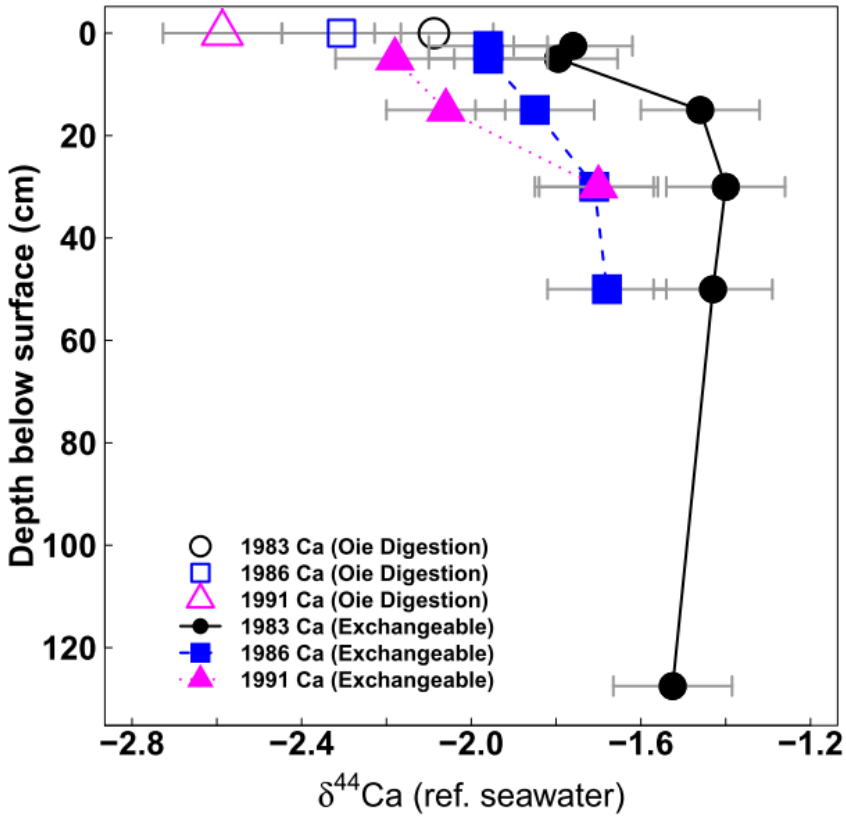

Figure 1.4. Depth profile of $\delta^{44}Ca$ values for forest floor (Oie) and soil exchangeable Ca and from soil pits excavated within grid cell 262 located in Watershed 5.

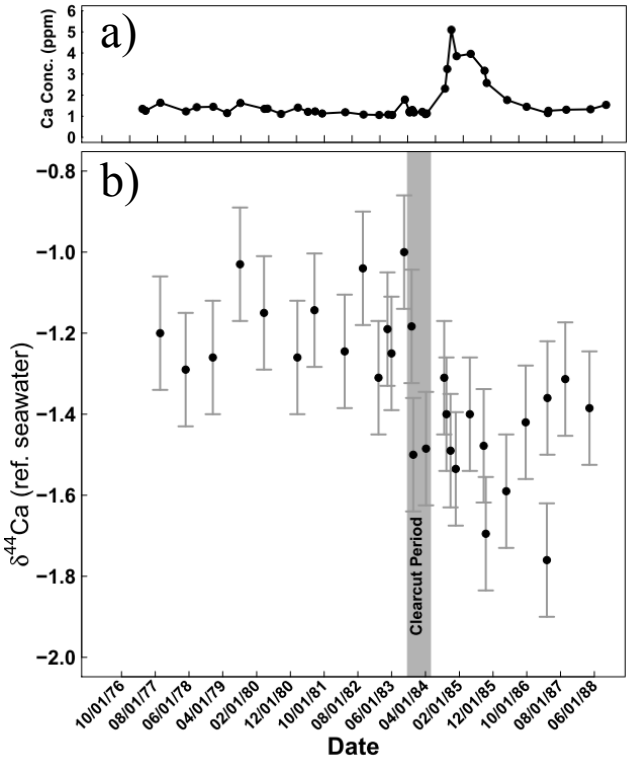

Figure 1.5. a) Time series of Watershed 5 streamwater Ca concentrations and b) Watershed 5 streamwater $\delta^{44}Ca$ values. The period when the harvest event took place is highlighted in grey.

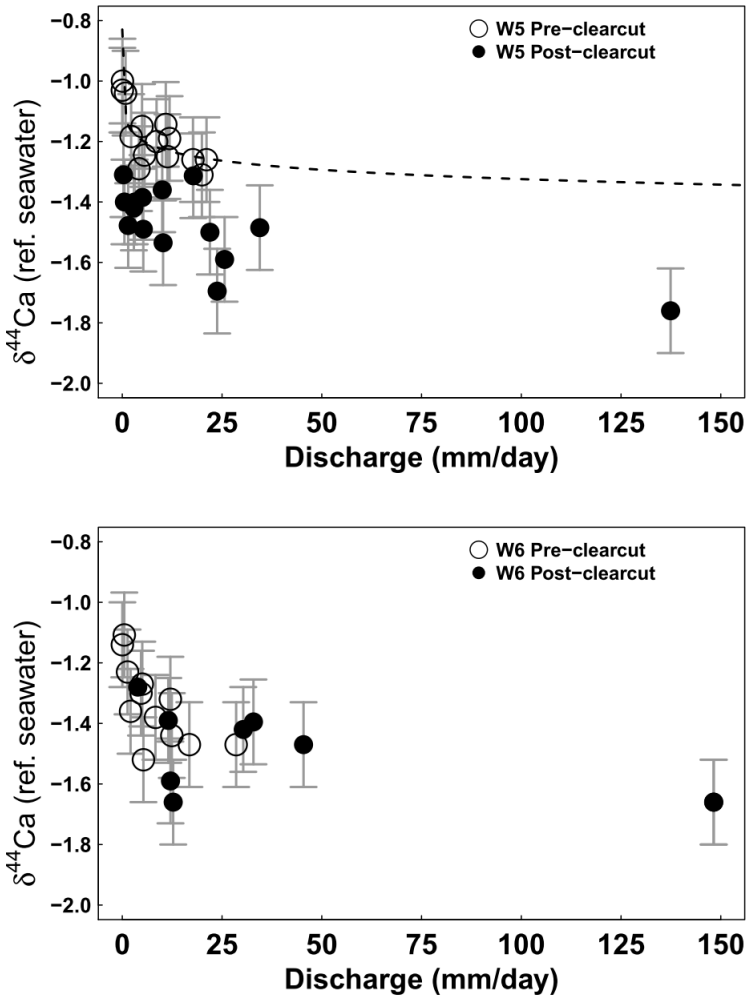

Figure 1.6. Relationship between specific discharge and streamwater $\delta^{44}Ca$ in Watershed 5 and 6 before and after the harvest. Dashed line represents power law model used in isotope mass balance model ($\delta^{44}Ca = -1.13*(Discharge)^{0.034}$) (see Section 2.5.2 for details).

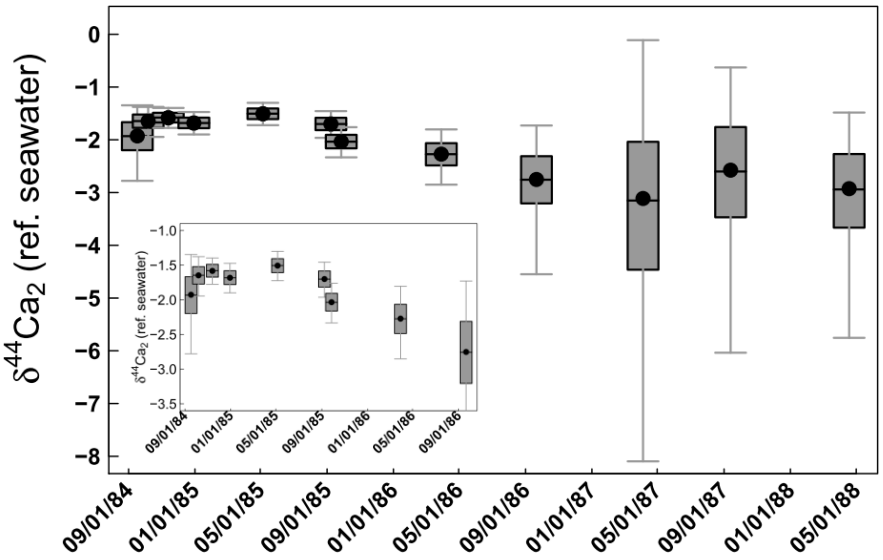

Figure 1.7. Model results for determination of $\delta^{44}Ca_2$, the stable Ca isotope ratio of the excess Ca streamwater export attributed to the harvest. Grey boxes represent the 1st to 3rd quartile range of 10,000 Monte Carlo simulations, the whiskers represent simulation values within 1.5 times the 1st-3rd interquartile range. Inset is a close-up of the first 9 post-harvest samples.

1.8.2 Tables

Table 1.1. Summary of instantaneous streamwater discharge, elemental concentrations (measured at Boston University, BU) and $\delta^{44}Ca$ in archived streamwater. For comparison, elemental concentration measured at the time of collection (Hubbard Brook Experimental Forest, HBEF) are included. n indicates number of replicate Ca stable isotope measurements made on the sample.

			BU Contemporary Analysis (ug/mL)								HBEF Historical Analysis (ug/mL)			
Date	Watershed	Instantaneous Discharge ($L*sec^{-1}$)	Ca	Mg	Na	K	Sr	$\delta^{44}Ca$ (‰ rel. SW)	n	2 s.d. (‰ rel. SW)	Ca	Mg	Na	K
9/14/1977	5	30.0	1.79	0.41	0.67	0.32	0.014	-1.20	1	-	1.64	0.37	0.56	0.27
5/2/1978	5	10.3	1.30	0.26	0.69	0.25	0.010	-1.29	1	-	1.23	0.25	0.6	0.18
1/2/1979	5	55.6	1.74	0.47	bdl	0.48	0.010	-1.26	1	-	1.45	0.4	0.64	0.49
9/4/1979	5	0.05	1.53	0.49	1.21	0.25	0.013	-1.03	2	0.03	1.63	0.47	1.29	0.14
4/7/1980	5	16.0	1.44	0.35	0.80	0.36	0.010	-1.15	1	-	1.35	0.32	0.75	0.26
2/2/1981	5	91.9	1.41	0.34	0.69	0.49	0.009	-1.26	2	-	1.41	0.37	0.81	0.55

nd: Not determined.
bdl: Below detection limit.

Table 1.1. Continued.

Date	Watershed	Instantaneous Discharge ($L*sec^{-1}$)	BU Contemporary Analysis (ug/mL)					$\delta^{44}Ca$ (‰ rel. SW)	n	2 s.d. (‰ rel. SW)	HBEF Historical Analysis (ug/mL)			
			Ca	Mg	Na	K	Sr				Ca	Mg	Na	K
7/6/1981	5	38.5	1.20	0.25	0.72	bdl	0.010	-1.14	3	0.18	1.23	0.25	0.68	0.08
4/4/1982	5	14.4	1.26	0.29	0.62	0.17	0.006	-1.24	2	0.07	1.19	0.29	0.77	0.18
9/15/1982	5	6.21	1.14	0.31	0.71	0.47	0.006	-1.04	2	0.05	1.08	0.3	0.86	0.6
2/3/1983	5	94.4	1.06	0.22	0.51	0.30	0.007	-1.31	1	-	1.06	0.25	0.59	0.25
4/25/1983	5	33.2	1.10	0.24	0.55	0.21	0.005	-1.19	2	0.20	1.08	0.24	0.67	0.22
5/31/1983	5	25.5	1.06	0.20	0.61	bdl	0.008	-1.25	1	-	1.06	0.23	0.73	0.17
9/22/1983	5	0.09	1.76	0.60	0.99	0.32	0.012	-1.00	2	0.08	1.79	0.59	1.31	0.37
11/28/1983	5	5.61	1.22	0.28	0.73	0.36	0.009	-1.18	3	0.16	1.3	0.31	0.75	0.35
12/13/1983	5	75.1	1.18	0.22	0.48	0.46	0.008	-1.50	1	-	1.18	0.26	0.56	0.52
4/6/1984	5	69.1	1.11	0.26	0.48	0.60	0.004	-1.48	2	0.08	1.13	0.26	0.52	0.71
9/17/1984	5	0.82	2.30	0.69	1.21	0.84	0.015	-1.32	3	0.09	2.31	0.67	1.63	1
10/7/1984	5	1.39	3.28	0.97	1.23	0.99	0.023	-1.40	1	-	3.24	0.91	1.62	1.18
11/13/1984	5	14.0	5.35	1.41	1.15	2.26	0.037	-1.48	2	0.17	5.1	1.29	1.44	2.58
12/30/1984	5	22.2	4.06	1.07	0.89	1.64	0.026	-1.53	4	0.04	3.85	0.98	1.02	1.82
5/6/1985	5	6.89	3.14	0.85	1.00	1.14	0.021	-1.39	2	0.01	3.96	0.8	1.24	1.31
9/8/1985	5	4.34	3.14	0.84	0.89	0.98	0.021	-1.40	2	0.04	3.16	0.82	1.15	1.13
9/27/1985	5	185	2.84	0.62	bdl	1.53	0.018	-1.69	2	0.19	2.58	0.55	0.66	1.58
3/30/1986	5	63.9	1.87	0.45	0.52	0.74	0.010	-1.59	1	-	1.77	0.43	0.55	0.91
9/21/1986	5	8.42	1.40	0.38	0.70	0.35	0.007	-1.42	2	0.08	1.45	0.4	0.85	0.41
3/31/1987	5	320	1.15	0.27	bdl	0.96	0.006	-1.76	2	0.00	1.15	0.28	0.36	1.07
4/5/1987	5	52.0	1.18	0.30	0.48	0.57	0.005	-1.36	4	0.17	1.26	0.31	0.52	0.73
9/13/1987	5	15.9	1.36	0.37	0.67	0.26	0.006	-1.31	3	0.13	1.31	0.35	0.84	0.31
4/18/1988	5	21.1	1.35	0.34	0.62	0.44	0.006	-1.39	2	0.16	1.33	0.38	0.72	0.52

Table 1.1. Continued.

Date	Watershed	Instantaneous Discharge ($L*sec^{-1}$)	BU Contemporary Analysis (ug/mL)					$\delta^{44}Ca$ (‰ rel. SW)	n	2 s.d. (‰ rel. SW)	HBEF Historical Analysis (ug/mL)			
			Ca	Mg	Na	K	Sr				Ca	Mg	Na	K
9/14/1977	6	17.9	1.52	0.34	0.59	0.33	0.011	-1.38	1	-	1.44	0.33	0.64	0.28
5/8/1978	6	5.9	1.17	0.24	0.69	0.26	0.009	-1.52	1	-	0.94	0.2	0.52	0.16
9/4/1979	6	0.03	1.50	0.45	1.51	bdl	0.012	-1.14	1	-	1.18	0.32	1.28	0.06
4/7/1980	6	7.84	1.43	0.34	0.74	0.35	0.010	-1.30	1	-	1.25	0.31	0.71	0.29
2/2/1981	6	57.0	1.37	0.36	0.65	0.56	0.009	-1.47	1	-	1.28	0.37	0.75	0.65
7/6/1981	6	22.4	1.08	0.23	0.67	bdl	0.009	-1.32	1	-	1.02	0.23	0.65	0.08
4/4/1982	6	7.89	1.14	0.28	0.72	0.25	0.009	-1.27	2	0.09	1.05	0.28	0.74	0.19
9/15/1982	6	4.83	1.06	0.32	0.99	0.40	0.009	-1.23	1	-	1.01	0.31	1.06	0.4
2/3/1983	6	71.7	bdl	bdl	bdl	bdl	bdl	-1.47	1	-	0.85	0.22	0.54	0.28
5/31/1983	6	16.4	0.88	0.18	0.56	0.27	0.007	-1.44	1	-	0.85	0.21	0.68	0.18
9/22/1983	6	1.21	0.94	0.30	1.01	0.28	0.008	-1.11	1	-	0.96	0.31	1.2	0.27
11/28/1983	6	3.30	0.97	0.23	0.66	0.24	0.008	-1.36	2		0.98	0.25	0.71	0.18
12/13/1983	6	69.6	0.82	0.15	0.42	0.26	0.006	-1.42	1	-	0.84	0.19	0.5	0.25
4/6/1984	6	54.9	0.72	0.17	bdl	0.30	0.006	-1.47	2	0.20	0.77	0.18	0.48	0.71
12/30/1984	6	15.9	0.95	0.24	0.53	0.32	0.008	-1.39	2	0.02	0.92	0.24	0.62	0.3
9/27/1985	6	85.3	1.07	0.24	bdl	0.41	0.009	-1.66	1	-	1.02	0.23	0.43	0.43
3/30/1986	6	35.4	0.87	0.20	0.49	0.25	0.007	-1.40	2	0.02	0.81	0.2	0.54	0.18
3/31/1987	6	224	0.94	0.22	bdl	0.61	0.007	-1.66	1	-	0.91	0.23	0.44	0.73
4/5/1987	6	25.1	0.91	0.23	0.64	0.25	0.007	-1.59	1	-	0.87	0.21	0.51	0.27
4/18/1988	6	9.6	0.80	0.19	bdl	0.30	0.006	-1.28	1	-	0.95	0.29	0.75	0.19
Precipitation														
4/22/1982	6	nd	nd	nd	nd	nd	nd	-1.01	2	0.32	0.25	0.05	0.11	0.03

Table 1.2. Elemental concentrations and $\delta^{44}Ca$ of bulked digestions and extraction of bedrock and soil samples. n indicates number of replicate Ca stable isotope measurements made on the sample.

Sample Type or Depth (cm)	Year	Treatment	(µg/g sample) Ca	Mg	Na	K	Sr	Si	Al	Fe	P	Ba	Oxalate	$\delta^{44}Ca$ (‰ rel. SW)	n	2 s.d. (‰ rel. SW)
Rangley Fm. Schist	-	HF/HNO_3bulk digestion	4824	30568	11398	32155	85	nd	87471	51656	130	640	nd	-1.25	1	-
Till	-	HF/HNO_3bulk digestion	7299	3263	6391	12656	117	nd	72671	17448	283	504	nd	-1.09	1	-
Till	-	HCl extraction	768	18	8	bdl	1	359	1338	537	363	3	10	-0.85	1	-
Till	-	NH_4Cl exchange	8	1	4	27	2	nd	63	nd	nd	20	nd	-1.52	2	0.012
Oie fine roots	1983	HNO_3/H_2O_2 bulk digestion	7172	579	bdl	bdl	41	138	bdl	512	1304	116	nd	-2.38	1	-
Oie	1983	HNO_3/H_2O_2 digestion (extraction residual)	1006	138	bdl	436	6	bdl	1283	1772	494	32	nd	-2.27	1	-
Oie	1986	HNO_3/H_2O_2 digestion (extraction residual)	1401	322	bdl	594	8	bdl	2740	4161	579	38	nd	-2.59	1	-
Oie	1991	HNO_3/H_2O_2 digestion (extraction residual)	3915	518	bdl	690	15	34	2454	3497	813	66	nd	-2.80	1	-
Oie	1983	HNO_3/H_2O_2 bulk digestion	3366	346	55	694	18	bdl	nd	1226	691	62	nd	-2.09	1	-
Oie	1986	HNO_3/H_2O_2 bulk digestion	5334	759	83	814	26	3	nd	4026	820	83	nd	-2.31	1	-
Oie	1991	HNO_3/H_2O_2 bulk digestion	9060	1520	65	1306	35	17	nd	3073	1171	99	nd	-2.59	1	-

nd: Not determined.
bdl: Below detection limit.

Table 1.2. Continued.

Sample Type or Depth (cm)	Year	Treatment	(µg/g sample) Ca	Mg	Na	K	Sr	Si	Al	Fe	P	Ba	Oxalate	$\delta^{44}Ca$ (‰ rel. SW)	n	2 s.d. (‰ rel. SW)
Oie	1983	NH_4Cl exchange	2774	268	nd	436	14	nd	nd	nd	389	44	nd	-2.11	1	-
Oa	1983	NH_4Cl exchange	1900	104	43	297	13	nd	72	nd	nd	42	nd	-1.76	1	-
0-10	1983	NH_4Cl exchange	67	9	3	22	1	nd	102	nd	nd	4	nd	-1.80	2	0.012
10-20	1983	NH_4Cl exchange	31	7	5	15	1	nd	348	nd	nd	4	nd	-1.46	2	0.083
20+	1983	NH_4Cl exchange	25	2	4	9	0	nd	235	nd	nd	4	nd	-1.40	1	-
C	1983	NH_4Cl exchange	13	1	3	9	0	nd	96	nd	nd	7	nd	-1.43	1	-
Oie	1986	NH_4Cl exchange	nd	nd	nd	nd	nd	nd	nd	nd	nd	nd	nd	-2.38	1	-
Oa	1986	NH_4Cl exchange	1543	145	nd	171	9	nd	196	48	124	26	nd	-1.96	1	-
0-10	1986	NH_4Cl exchange	149	13	nd	nd	1	3	348	74	nd	3	nd	-1.96	1	-
10-20	1986	NH_4Cl exchange	21	2	nd	nd	0	8	222	9	nd	3	nd	-1.85	1	-
20+	1986	NH_4Cl exchange	5	nd	nd	nd	nd	7	126	2	nd	4	nd	nd	-	-
C	1986	NH_4Cl exchange	9	1	nd	16	0	11	127	2	nd	6	nd	-1.68	1	-
Oie	1991	NH_4Cl exchange	nd	nd	nd	nd	nd	nd	nd	nd	nd	nd	nd	-2.58	1	-
Oa	1991	NH_4Cl exchange	*Sample not present in archive.*													
0-10	1991	NH_4Cl exchange	478	39	nd	nd	2	nd	327	123	nd	11	nd	-2.18	1	-
10-20	1991	NH_4Cl exchange	111	6	15	35	1	13	312	26	nd	5	nd	-2.06	1	-
20+	1991	NH_4Cl exchange	15	1	nd	19	0	11	144	3	nd	5	nd	-1.70	1	-
C	1991	NH_4Cl exchange	4	nd	nd	17	0	11	77	1	nd	5	nd	nd	-	-

Table 1.2. Continued.

Sample Type or Depth (cm)	Year	Treatment	(µg/g sample) Ca	Mg	Na	K	Sr	Si	Al	Fe	P	Ba	Oxalate	$\delta^{44}Ca$ (‰ rel. SW)	n	2 s.d. (‰ rel. SW)
Oa	1983	HCl extraction	419	18	bdl	bdl	3	62	614	219	87	16	216	-2.07	1	-
0-10	1983	HCl extraction	20	10	bdl	bdl	bdl	55	728	2338	bdl	2	248	nd	-	-
10-20	1983	HCl extraction	38	10	bdl	bdl	bdl	293	4227	2216	bdl	3	361	nd	-	-
20+	1983	HCl extraction	138	6	bdl	bdl	0	1204	6950	320	63	5	173	nd	-	-
C	1983	HCl extraction	396	10	bdl	bdl	0	1763	6637	685	220	6	104	nd	-	-
Oa	1986	HCl extraction	121	8	bdl	bdl	1	3	159	114	21	3	29	-2.18	1	-
0-10	1986	HCl extraction	64	10	bdl	bdl	0	180	1767	1286	12	2	273	nd	-	-
10-20	1986	HCl extraction	74	bdl	bdl	bdl	0	662	4247	149	27	1	168	nd	-	-
20+	1986	HCl extraction	92	3	bdl	bdl	0	825	3572	252	46	1	98	nd	-	-
C	1986	HCl extraction	235	4	bdl	bdl	0	1030	3750	361	126	2	99	nd	-	-
Oa	1983	HCl extraction	419	18	bdl	bdl	3	62	614	219	87	16	216	-2.07	1	-
0-10	1983	HCl extraction	20	10	bdl	bdl	bdl	55	728	2338	bdl	2	248	nd	-	-
Oa	1991	HCl extraction	*Sample not present in archive.*													
0-10	1991	HCl extraction	42	6	bdl	bdl	0	31	489	757	14	2	62	-2.41	1	-
10-20	1991	HCl extraction	45	2	bdl	bdl	0	655	3402	302	20	1	116	nd	-	-
20+	1991	HCl extraction	113	3	bdl	bdl	0	837	3640	278	69	1	75	nd	-	-
C	1991	HCl extraction	153	4	bdl	bdl	0	831	2991	435	109	2	51	nd	-	-

Table 1.3. Mixing model parameters and calculated $\delta^{44}Ca$ of "excess" Ca source to streamwater ($\delta^{44}Ca_2$). 1st and 3rd Quartiles for the modeled $\delta^{44}Ca_2$ values are derived from 10000 Monte Carlo simulations that incorporate uncertainty in model parameters. See section 1.4.2 for additional model details.

Date	$\delta^{44}Ca_t$ (‰ vs SW)	Ca (µg/g)	Instantaneous Discharge ($L*sec^{-1}$)	fraction Ca from "baseline" component 1	$\delta^{44}Ca_1$ (‰ vs SW)	fraction Ca from "excess" component 2	$\delta^{44}Ca_2$ (‰ vs SW)	1st Quartile (‰ vs SW)	3st Quartile (‰ vs SW)
9/17/1984	-1.31	2.30	0.82	0.74	-1.09	0.26	-1.93	-2.197	-1.666
10/7/1984	-1.40	3.28	1.39	0.46	-1.11	0.54	-1.65	-1.773	-1.521
11/13/1984	-1.49	5.35	14.0	0.24	-1.19	0.76	-1.58	-1.672	-1.488
12/30/1984	-1.54	4.06	22.2	0.31	-1.21	0.69	-1.68	-1.78	-1.58
5/6/1985	-1.40	3.14	6.89	0.31	-1.16	0.69	-1.51	-1.608	-1.406
9/8/1985	-1.48	3.14	4.34	0.40	-1.15	0.60	-1.70	-1.817	-1.583
9/27/1985	-1.70	2.84	185.1	0.45	-1.29	0.55	-2.03	-2.162	-1.906
3/30/1986	-1.59	1.87	63.9	0.67	-1.25	0.33	-2.27	-2.486	-2.064
9/21/1986	-1.42	1.40	8.42	0.84	-1.17	0.16	-2.75	-3.206	-2.311
3/31/1987	-1.76	1.15	320	1.02	-1.31	-0.02	22.64	-19.46	16.41
4/5/1987	-1.36	1.18	52.0	0.94	-1.24	0.06	-3.11	-4.463	-2.038
9/13/1987	-1.31	1.36	15.9	0.91	-1.20	0.09	-2.58	-3.469	-1.758
4/18/1988	-1.39	1.35	21.1	0.90	-1.21	0.10	-2.93	-3.666	-2.27

CHAPTER 2: CONTROLS ON CA ISOTOPE RATIOS IN TROPICAL SOILS AT THE LUQUILLO CRITICAL ZONE OBSERVATORY

2.1 ABSTRACT

Globally, soil exchangeable stable calcium isotope ratios ($\delta^{44}Ca_{Ex}$) exhibit greater variability than the variability in $\delta^{44}Ca$ of atmospheric deposition and silicate bedrock, the dominant external inputs of Ca into terrestrial ecosystems. To investigate processes contributing to the variability in $\delta^{44}Ca_{Ex}$, we measured $\delta^{44}Ca$ in soil, vegetation, bedrock, streamwater and atmospheric deposition and $^{87}Sr/^{86}Sr$ in soil and vegetation in two tropical watersheds that are part of the Luquillo Critical Zone Observatory in Puerto Rico. $\delta^{44}Ca$ measurements of silicate bedrock at both sites (volcaniclastic and quartz diorite) are indistinguishable from one another and precipitation $\delta^{44}Ca$ agrees well with measurements made worldwide. Soil exchangeable $\delta^{44}Ca$ is heavier than Ca sources at both sites. We observe a significant difference in $\delta^{44}Ca_{Ex}$ between sites, which is reflected in the streamwater $\delta^{44}Ca$ during high discharge events. $^{87}Sr/^{86}Sr$ data rule out differences in external inputs as a driver of the between-site differences $\delta^{44}Ca_{Ex}$. Isotopic separation factors ($\delta^{44}Ca$ in soil vs. $\delta^{44}Ca$ in vegetation) of the dominant vegetation type at each site is distinct, indicating differences in the magnitude of isotopic separation during plant uptake of Ca. However, modeling work indicates that differences in the isotopic separation factor alone can't produce the observed between-site differences in $\delta^{44}Ca_{Ex}$ without an accompanying imbalance in the uptake and return flux of Ca between

the soil exchangeable and biomass reservoir. Ecosystem disturbance and subsequent biomass regrowth related to hurricanes have been well documented at the Luquillo Critical Zone Observatory, driving imbalances in the uptake and return fluxes of Ca. Model results indicate that ecosystem disturbance, when accompanied by isotopic fractionation associated with biological uptake of Ca, can produce $\delta^{44}Ca_{Ex}$ significantly different than external inputs, even decades after the disturbance.

2.2 INTRODUCTION

Calcium is an essential plant nutrient that when limiting to plants can negatively impact water use efficiency, tolerance to cold, resistance to disease and ability to take up nitrogen (Joslin et al. 1992; Ellsworth and Liu 1994; Driscoll et al. 1996; McLaughlin and Wimmer 1999). As such, the impact of anthropogenic disturbances such as acid rain and harvesting of biomass on the Ca cycle in temperate forests has been the subject of significant amounts of research (Lawrence et al. 1987; Dahlgren and Driscoll 1994; Likens et al. 1994). However, the Ca cycle in tropical ecosystems can differ fundamentally from Ca cycling in temperate forests, particularly in locations that experience high rates of mineral weathering. Although tropical soils generally contain adequate Ca in shallow soil to sustain forest productivity (Jordan et al. 1972), unlike in temperate forests where unweathered Ca-bearing primary minerals can be directly accessed by roots, the high weathering rates typical of tropical ecosystems can

deplete mineral sources of Ca (White et al. 1998; Blum et al. 2002; Pett-Ridge et al. 2009), However, recent research has shown that high erosion rates may partial offset this (Porder et al. 2015). As such, vegetation grown on old tropical soils may depend heavily on atmospherically-derived Ca and the recycling of Ca in the forest floor due to the high carbon costs associated with mining for Ca via deep roots (Silver et al. 1994; Chadwick et al. 1999; Poszwa et al. 2002; Wiegand et al. 2005). For example, in a study of an Amazon basin ecosystem, Stark and Jordan (1978) found that roots were able to take up ^{45}Ca directly from isotopically labeled leaf litter and that less than 1% ^{45}Ca applied to the surface leached through the rootmat into the soil below. Clearly, the retention of Ca in the near surface is an important mechanism for maintaining sufficient pools of nutrient to meet vegetation requirements in ecosystems existing on highly weathered soils.

Stable Ca isotopes are a relatively new tool to investigate the internal cycling of Ca in terrestrial ecosystems (Page et al. 2008; Cenki-Tok et al. 2009; Bélanger and Holmden 2010; Farkaš et al. 2011; Heijden et al. 2014). It is well documented that the primary fractionation mechanism for stable calcium isotopes in terrestrial ecosystems occurs as Ca is taken up from the soil pool by the plant roots. Vegetation discriminates against the heavier isotopes of Ca, producing biomass that is isotopically light (enriched in ^{40}Ca) compared to both soil and bedrock (Wiegand et al. 2005; Page et al. 2008; Farkaš et al. 2011). Similarly, there is a Rayleigh-like fractionation process that occurs as Ca moves along the

transpiration stream within vegetation, as the lighter isotopes of Ca are preferentially retained in roots and stems relative to leaves (Page et al. 2008; Bélanger and Holmden 2010; Cobert et al. 2011; Hindshaw et al. 2012; Schmitt et al. 2013). To date, much of the research utilizing stable Ca isotopes to investigate Ca cycling and improve our understanding of stable Ca isotope fractionation mechanisms have been carried out in temperate and boreal forests (Perakis et al. 2006; Tipper et al. 2008; Page et al. 2008; Cenki-Tok et al. 2009; Hindshaw et al. 2011; Farkaš et al. 2011; Bagard et al. 2013), with few studies carried out in tropical forests (Wiegand et al. 2005; Wiegand and Schwendenmann 2013). Interestingly, these earlier studies demonstrated stable calcium isotopes in the shallow soil exchangeable pool (an important source of Ca to vegetation) can exhibit a wide range of values across sites, even though inputs of Ca to terrestrial systems tend to be restricted to a fairly narrow range of values (Schmitt and Stille 2005). This observation suggests stable calcium isotope ratios in the soil exchangeable pool may reflect different processes operating on seasonal to decadal timescales, and may provide useful information regarding the calcium cycle (Holmden and Bélanger 2010; Fantle and Tipper 2014).

Given the wide range of measured soil exchangeable stable Ca isotope values across different sites, a mechanistic understanding of how different processes alter the stable Ca isotope signature of terrestrial ecosystems is required. Having recognized this need and the lack of stable Ca isotopes

measurements in tropical ecosystems to date, we quantify the stable Ca isotopes ratios of dominant Ca pools (vegetation, soil, bedrock) and well as inputs (bedrock, precipitation) in two highly weathered tropical watersheds within the Luquillo Experimental Forest: Bisley 1 which is a Tabonuco dominated forest underlain by volcaniclastic bedrock, and Rio Icacos which is a Colorado dominated forest underlain by quartz diorite. While these two watersheds are located only 6km apart and share similar climate, they exhibit contrasting dominant vegetation species, lithologies, soil nutrient stocks, and possibly degree of disturbance related to hurricanes (Lodge et al. 1991; Boose et al. 1994; Sullivan et al. 1999; Porder et al. 2015). The objectives of this study were to evaluate whether atmospheric inputs strongly influence the soil exchangeable $\delta^{44}Ca$ of tropical ecosystems as is the case for $^{87}Sr/^{86}Sr$ (Kennedy et al. 1998; Pett-Ridge et al. 2009), or alternatively to determine how differences in species composition, lithology and disturbance history affects the isotopic signature of calcium cycling in tropical forests.

2.3 MATERIAL AND METHODS

2.3.1 Site Description

Bisley 1 and Rio Icacos watersheds are located within the Luquillo Experimental Forest (LEF) in Puerto Rico, which has long been studied as a site in the U.S. Long Term Ecological Research Program (Brown et al. 1983), as a

USGS Water, Energy, and Biogeochemical Budgets Program site (Larsen et al. 1993), and now as a Critical Zone Observatory (Luquillo Critical Zone Observatory, LCZO) (Figure 2.1). Temperatures vary both with season and with elevation, ranging from 23.5°C (Jan) to 27°C (Sept) at low elevations and 17°C to 20°C at high elevations. Rainfall within the forest is orographic, so varies with elevation, from 3530mm/yr at low elevation to 4850mm/yr at high elevation. Although the seasonality is small relative to temperate sites, May through November define a wet season (>300mm/month) and January to March comprise a relatively dry season (<200mm/month; Schellekens et al., 2004). Bisley 1 is located within the Rio Mamayes drainage basin, underlain by andesitic volcaniclastic rocks and classified as a “Tabonuco forest”, named for the dominant Tabonuco tree (*Dacryodes excelsa*), which form a 20-25m upper canopy with a moderately dense understory of palms and woody plants and a ground cover of herbs and shrubs. Bisley 1 covers an area of 6.7ha, elevation ranges from 260m at the outlet to 410m at the highest elevation with greater than 50% of slopes greater than 45°, and soil are classified as clayey, highly weathered ultisols (Scatena 1989). The Rio Icacos basin is a 322 ha basin with elevations spanning 640-800 m. The basin is underlain by Eocene age porphyry hornblende quartz-diorite and is classified as a “Colorado forest”, so named for the dominant canopy Palo Colorado tree (*Cyrilla racimiflora*), with a canopy about 15m high. Soil samples were collected on a ridge above the Quebrada Guaba

tributary, a ~12 ha watershed within the Rio Icacos basin. Mean annual rainfall is 4200mm/yr, somewhat higher than Bisley I (3500mm/yr).

The lithologic contrast between Bisley 1 and Rio Icacos is expressed in major differences in geomorphology, hydrology, and rates of critical zone processes. In fact, a primary research objective of the LCZO has been to elucidate the differences in critical zone processes resulting from the contrasting lithology underlying the LEF. Granodiorite watersheds have higher landslide frequency, higher rates of chemical and physical weathering, sandy eutropeptic soils, sand-bedded stream channels that sometimes disappear into meter-scale macropores, and well-defined floodplains (McDowell et al. 1992; Larsen et al. 1993; Ahmad et al. 1993; White and Blum 1995; Brown et al. 1995; White et al. 1998; Larsen et al. 1999). Saprolite thicknesses of 8 meters are observed on granodioritic ridgetops (White and Blum 1995). Volcaniclastic watersheds have steep, boulder-lined channels, smaller landslides, lower suspended sediment fluxes, fewer macropores, and clayey tropohumultic soils (McDowell et al. 1992; Silver et al. 1994; Schellekens et al. 2004). Saprolite thicknesses can be greater than 15 meters on ridgetops in volcaniclastic areas (H. Buss, unpublished data).

2.3.2 Soil sampling and chemical analysis

At each site, a soil pit was excavated to a depth of approximately 1m along topographic ridges to minimize differences in soil chemistry related to landscape position. Soils were sampled by horizon and shipped to Boston University for chemical analysis. Samples were first oven-dried at 60˚C then

passed through a 2mm sieve to remove roots and rock fragments. Following methods adopted from Nezat et. al. (2007), a representative 0.5-5.0g subsample of each soil sample was first examined with a microscope to ensure no large un-decomposed organic matter was present, then a 1 M NH_4Cl solution was added to the subsample in a 10:1 ratio (10ml of 1 M NH_4Cl : 1g soil) and shaken for 24 hours on an end-over-end shaker. Subsamples were centrifuged and the supernatant was separated and passed through 0.45µm filter paper. Aliquots of the soil extractions were dried down and brought up in 2% HNO_3 for concentration analysis on a Jobin Yvon Ultrace JY-138 inductively coupled plasma emission spectrometer (ICP-ES). An aliquot of each soil extraction was retained for stable Ca isotopic analysis by thermal ionization mass spectrometry. Sr isotopic analyses were made later on a separate set of extractions of subsamples of the same soils following identical procedures.

2.3.3 Bedrock sampling and chemical analysis

For each watershed a sample of exposed bedrock (Fajardo Formation quartz diorite and andesitic volcaniclastic in Rio Icacos and Bisley 1, respectively) was sampled and shipped to Boston University for chemical analysis. Bedrock samples were acid digested for determination of bulk chemistry and stable Ca isotope ratios of soil parent material. Approximately 50mg of powdered bedrock were digested in a HF–HCl mixture by alternating sample between hot plate and sonicator over approximately one week. Digested samples were centrifuged and the supernatant collected and treated with

ultrapure concentrated nitric acid and Optima ultrapure hydrogen peroxide to oxidize any remaining organics including graphite. The samples were then dried down and brought up in 2% HNO_3 for analysis on the ICP-ES at Boston University. A separate aliquot was retained for isolation of Ca for isotopic analysis.

2.3.4 Streamwater sampling and chemical analysis

In order to assess the range in stable Ca isotopes draining each watershed, we analyzed stream water samples from both watersheds representing baseflow and peak stormflow discharge conditions (Table 2.2). Both watersheds exhibit strong variability in chemistry as a function of discharge reflecting flowpath control (Kurtz et al. 2011; Goldsmith et al. 2013). Rio Icacos samples were collected at the USGS stream gauge (50075000) during an earlier sampling campaign (Kurtz et al. 2011). Bisley samples were collected for related CZO research and provided to us by Steve Goldsmith and Stephen Porder (Brown University). Stream water concentrations were analyzed on a Jobin Yvon Ultrace JY-138 inductively coupled plasma emission spectrometer (ICP-ES) at Boston University. The peak stormflow sample for Bisley 1 was collected (June 6th, 2011, 9:45) on a day when daily discharge at the downstream Rio Mameyes USGS stream gauge (50065500) was 2.2m^3*sec^{-1}, which is in the 84th percentile for daily discharge values for the period between 1967 and 2015, while the baseflow sample was collected when daily discharge at Rio Mameyes was 0.8m^3*sec^{-1} (35% percentile). For Rio Icacos, the peak storm flow sample was

collected (November 13th, 2006, 13:30) on a day when the daily discharge was 1.8m^3*sec^{-1}, which is in the 97th percentile for daily discharge values between 1967 and 2015, while the baseflow sample was collected on a day daily discharge was 0.4m^3*sec^{-1}, representing the 5th percentile of daily discharge.

2.3.5 Vegetation sampling and chemical analysis

Samples of leaves, roots, bark, and stemwood from a Tabonuco tree in Bisley 1, a Palo Colorado tree in Rio Icacos and a Cercropia tree from both watersheds were collected within 10m of each soil pit and returned to Boston University for chemical analysis. The vegetation samples were first oven-dried at 60˚C and then passed through a Wiley Mill to prepare samples for chemical analysis. A representative 0.5g subsample of each vegetation sample was digested in a mixture of 1 mL of H_2O_2 and 9 mL of concentrated HNO_3 using a Milestone microwave. An aliquot of the digestion was dried down and brought up in 2% HNO_3 for concentration analysis on a Jobin Yvon Ultrace JY-138 inductively coupled plasma emission spectrometer (ICP-ES) and another aliquot retained for stable Ca isotopic analysis using a thermal ionization mass spectrometer.

2.3.6 Mass spectrometry

Calcium isotope measurements were carried out in the Boston University Thermal Ionization Mass Spectrometry (TIMS) Facility, using a Thermo Finnigan Triton® TIMS. We utilized a ^{42}Ca-^{48}Ca double spike to correct for any

fractionation that may occur during column chemistry or mass spectrometry (Russell and Papanastassiou 1978; Russell et al. 1978). We used an iterative double spike subtraction routine that removes the double spike and corrects for mass dependent fractionation using an exponential mass fractionation law (Compston and Oversby 1969; Heuser et al. 2002; Fantle and Bullen 2009). The double spike subtraction routine was implemented as a spreadsheet in the MS Excel software program.

The double spike and sample solutions were mixed to achieve an 85:15 sample to spike ratio (by mass of Ca) to minimize error propagation during the iterative double spike subtraction (Rudge et al. 2009). Typically, between 1 and 3µg of sample Ca was mixed with an appropriate amount of double spiked Ca solution prior to column chemistry. Column chemistry consisted of passing the spiked sample through AG50-X8 cation resin in a 5cm long and 0.7cm diameter Teflon column with a 30ml reservoir. Ultrapure, distilled 1N, 1.5N and 4N HNO_3 were used as reagents, with the 1N HNO_3 used as the final eluent. After the double spiked sample passed through the column, it was dried down, brought back up in 100µl concentrated nitric and 50µl ultrapure hydrogen peroxide solution, dried down again, and twice more brought up in 100µl concentrated nitric acid and dried down to oxidize any remaining organics. Finally, the sample was brought up in approximately 2µl 2N HNO_3 for loading onto outgassed zone refined rhenium filament. After loading the sample onto the filament, 0.5µl of 5% H_3PO_4 was added to increase the ionization efficiency. Samples were run using

the double filament technique, with the ionization filament heated to 1410°C, and evaporation filament heated to between 1600° and 1900°C over the course of 1 hour, with constant monitoring to insure that the ^{40}Ca beam does not increase above 10V, which increases the likelihood of faraday cup “poisoning” (Bélanger and Holmden 2010). Each sample was run for at least 100 cycles to insure robust statistics. Two standards, National Institute of Standards and Technology (NIST) Standard Reference Material (SRM) 915A calcium carbonate standard and North Atlantic Seawater Standard (NASS), were typically measured during each session to quantify the external precision of our measurements. Internal precision for a single analysis was determined by calculating the 2SE (SE: standard error) of all cycles. Internal precision for a single analysis was better than 0.10‰, and typically < 0.06‰ (2SE). Most unknown samples were run 2 or more times, with our average reproducibility of our unknown samples being 0.10‰ 2SD (SD: standard deviation). External precision was determined by calculating the 2SD for repeated measurement of our two standards: NIST SRM 915A and NASS seawater. For NIST SRM 915A we obtained a mean of -1.91‰ ±0.14‰ (2SD, n = 14), and for seawater 0.03‰ ±0.12‰ (2SD, n = 14). Unlike Holmden and Bélanger (2010), no long-term drift was evident in our Ca standards database, and therefore no drift corrections were made to standards or samples. We report analytical uncertainty on a single measurement of an unknown as 0.14‰ (the larger of the 2SD for our two standards). We report

stable Ca isotope ratios ($^{44}Ca/^{40}Ca$) in delta notation ($\delta^{44}Ca$) relative to our long-term average value for seawater.

Strontium isotopes were also measured on the BU TIMS Facility Triton. Sr was separated by column chemistry utilizing Eichrom Sr-Spec resin and run on single Re filaments with Ta_2O_5 as an emitter. $^{87}Sr/^{86}Sr$ ratios were corrected for mass fractionation using an exponential fractionation law and $^{86}Sr/^{88}Sr$ of 0.1194. Analyses of SRM 987 measured in this study were within the long-term BU TIMS facility average for $^{87}Sr/^{86}Sr$ of 0.71034 ± 0.00026. Sr blanks for NH4Cl extractions, acid-digestions, and water samples were negligible

2.3.7 Stable Ca isotope mass balance model

We developed an isotope mass balance model of the Ca cycle that focuses on the cycling of Ca between vegetation and the upper 60cm of the soil exchangeable reservoir (Figure 2.2). The model consists of 2 boxes (reservoirs) representing the mass of actively cycled soil Ca integrated over the root zone (M_S) and the mass of Ca in biomass (M_V) (mol Ca*ha^{-1}) and 7 fluxes (mol Ca*ha^{-1}*yr^{-1}) representing the movement of Ca into, out of, and between reservoirs. Two external fluxes enter the soil exchangeable reservoir, representing atmospheric deposition (F_A) and bedrock weathering-derived (F_W) sources of Ca to the system. One external flux (F_{NU}) enters the vegetation pool directly, bypassing the soil exchange pool. This flux represents direct uptake of new Ca by roots from sources other than the soil exchangeable reservoir, contributing to “nutrient uplift”. Internal biomass cycling of Ca is represented by an uptake flux from the

soil exchange pool (F_U), and the return of Ca from biomass to the soil exchangeable reservoir (F_R) via decomposition. Ca is exported from the system by one of two fluxes, via leaching from the soil exchange pool (F_Z) to groundwater or streamwater, and as export of Ca from the vegetation pool (F_{POM}), for example by stream export of particulate organic matter. Additional model details describing steady state and non-steady state equations is provided in Appendix A2.

We take advantage of extensive data collected from previous research conducted in Bisley 1 to parameterize the model (Walker 1991; Heartsill-Scalley et al. 2007; Heartsill Scalley et al. 2010). The model requires initial values for the amount of Ca in each reservoir (M_S and M_V), initial δ^{44}Ca values of the Ca pools (δ_S and δ_V), the separation factor (Δ_U), as well as δ^{44}Ca values of the Ca fluxes (F) entering or exiting each reservoir and information on how they vary (if at all) over the length of the simulation. For model simulations presented here, we assume the system is at steady state prior to any disturbance. Initially, the litterfall and uptake flux (F_R and F_U respectively) is assumed to be 10% of the biomass reservoir, based on previous studies of litterfall rates pre-hurricane Hugo (Lodge et al. 1991). Due to some of the highest bedrock weathering rates measured globally, Ca bearing mineral have been effectively weathered out of the upper 60cm of the soil profile and replaced with non-Ca bearing secondary clay minerals such as kaolinite and goethite (White et al. 1998; Buss et al. 2008; Dosseto et al. 2012). As such, we assume F_W presently contributes a negligible

amount of Ca to the upper 60cm of the soil profile and F_A is constant in time and equal to the long term atmospheric deposition rate (Heartsill Scalley et al. 2010). Leaching rates (F_Z) are challenging to measure and thus generally poorly constrained in many ecohydrology models. However, a number of studies have noted a significant "quick flow" component to storm hydrographs, which can comprise 40-84% of the stormflow exiting Bisley and is thought to be rainfall that has limited interaction with the mineral soil (Schellekens 2000; Schellekens et al. 2004; Kurtz et al. 2011). Nonetheless, to maintain initial steady-state conditions, we chose to have F_Z initially be equal to external sources (atmospheric deposition and weathering), although we acknowledge significant uncertainty in the actual value of F_Z. Finally, given our initial steady-state assumption, we assume that the pre-hurricane Hugo value of $\delta^{44}Ca$ in the exchange pool (δ_S) will equal the $\delta^{44}Ca$ of external inputs (F_A and F_W both set to -1‰) and δ_V is equal to $\delta_S + \Delta_U$. We varied Δ_U between -2.0 and 0 across model runs to test the effect of this parameter on the time evolution of $\delta^{44}Ca$ values. Parameters used and literature sources for parameter estimates are summarized in Table 2.5.

2.4 RESULTS

2.4.1 Ca Concentrations in bedrock, soil exchangeable and streamwater in Bisley 1 and Rio Icacos

Here we report elemental and isotopic data for one bedrock sample collected at each site. Detailed analysis on variability in bedrock elemental

concentrations and isotopic data for the quartz diorite and volcaniclastics bedrock have been presented elsewhere (Buss et al. 2013; Porder et al. 2015), but our samples generally agree with these earlier analyses. Ca concentrations in bulk digestion of bedrock indicate that the volcaniclastic bedrock underlying Bisley 1 had higher Ca concentrations (7.4 CaO wt. %) compared with the Rio Blanco quartz diorite underlying the Icacos basin (3.7 CaO wt. %) (Table 2.1). This difference was also apparent in the soil exchangeable Ca extractions (Table 2.3, Figure 2.3a). The Bisley 1 soil profile has higher Ca concentrations than Rio Icacos throughout the soil profile which may be in part driven by the large amount of clay in Bisley soil relative to quartz-rich soil in Rio Icacos and geomorphology driven by differential erosion rates between the two forests (White et al. 1998; Porder et al. 2015). In the 0-10cm depth Bisley contained 180µg Ca/g soil, while Rio Icacos contained 80µg Ca/g soil, and in the 10cm depth, Bisley soil contains 110µg Ca/g soil, while Rio Icacos contains 30µg Ca/g soil. For the remaining depths down to 1m, soil exchangeable Ca in Bisley was approximately twice that of Icacos. These values agree with total Ca stocks in volcaniclastic and quartz diorite derived soils calculated by Porder et al. (2015), who found that Tabonuco forests contain approximately twice the amount of exchangeable Ca compared with Palo Colorado forests. Based on published bulk density values for soils in Bisley and Rio Icacos (Silver et al. 1994; McDowell et al. 2012) and our Ca concentration data, we estimate that the upper 30cm comprise approximately 77% and 80% of total soil solum Ca for Bisley 1 and Rio Icacos, respectively.

Two streamwater samples from each watershed were analyzed for Ca concentration (Table 2.2). Low flow samples had higher Ca concentrations compared with high flow samples. This was expected as a strong discharge-dilution relationship has been observed in both watersheds. As with bedrock and the soil exchangeable extractions, the Bisley 1 streamwater Ca concentrations were higher than the Rio Icacos streamwater samples (Table 2.2). The Ca concentration for the stormflow sample from Bisley 1 was 0.71ppm, while the low flow sample was 5.33ppm. For Rio Icacos, the Ca concentration for the stormflow sample was 0.71ppm, while the low flow sample was 2.8ppm.

2.4.2 Vegetation Ca concentrations in Bisley and Icacos

For the two species sampled that were present in both Bisley 1 and Rio Icacos (Sierra Palm and Cercropia), the Ca concentration in all biomass compartments (ie. roots, stems and leaves) were higher in Bisley relative to Rio Icacos, mirroring the bedrock and soil concentrations contrast described above (Figure 2.3b). This observation has also been observed in previous studies (Weaver and Murphy 1990; Lodge et al. 1991). For the respective dominant vegetation species, Tabonuco trees had higher Ca concentrations in all biomass compartments compared with Palo Colorado trees. However, for all species regardless of watershed, Ca concentration increased along the transpiration stream, with roots having the lowest Ca concentrations and leaves having the highest Ca concentrations.

2.4.3 $\delta^{44}Ca$ of bedrock and precipitation

$\delta^{44}Ca$ in bulk digestions of the two bedrock types were within external precision of one another (Table 2.1). Rio Blanco quartz diorite had a $\delta^{44}Ca$ value of -0.95‰ (relative to seawater), while Bisley volcaniclastics has a $\delta^{44}Ca$ value -0.98‰. The $\delta^{44}Ca$ values of the two Rio Icacos precipitation samples were within external precision of one another, with a mean $\delta^{44}Ca$ value of -1.15‰, slightly more negative than the two bedrock values. Our measured $\delta^{44}Ca$ values of bedrock and precipitation are similar to values measured elsewhere, supporting the assertion of Fantle and Tipper (2014) that these sources have $\delta^{44}Ca$ values that vary minimally worldwide.

2.4.4 $\delta^{44}Ca$ and $^{87}Sr/^{86}Sr$ of soil exchangeable pool

While the upper 60cm of soil exchangeable $\delta^{44}Ca$ values for each site exhibited limited internal variability, the soil exchangeable $\delta^{44}Ca$ differed significantly between sites (Table 2.3, Figure 2.4). The Bisley soil profile exhibited soil exchangeable $\delta^{44}Ca$ values that ranging between +0.03‰ in 10-25cm depth interval to -0.28‰ in Oa2 horizon (5-10cm) with a Ca mass weighted average $\delta^{44}Ca$ of -0.09‰. $\delta^{44}Ca$ of soil exchangeable Ca in the Rio Icacos soil profile was significantly lighter than comparable depths in Bisley, with values that varied between -0.64‰ and -0.83‰, and a Ca mass weighted average $\delta^{44}Ca$ of -0.72‰, 0.63‰ lighter than Bisley. Relative to external inputs, the Ca mass weighted average $\delta^{44}Ca$ of exchangeable soil from both sites were significantly more positive that the $\delta^{44}Ca$ of both bedrock and precipitation.

$^{87}Sr/^{86}Sr$ ratios were similar between the watersheds, encompassing a fairly narrow range between 0.7093 and 0.7099. The depth trends exhibited similar behavior. At Rio Icacos, $^{87}Sr/^{86}Sr$ was lowest in the shallowest depths (0.70932 and 0.70934 in the 0-5cm and 5-10cm depths), and became more radiogenic with depth (0.70986 and 0.71050 in the 68-78cm and 78-104cm depths). Similarly Bisley 1, the smaller values occurred in the shallowest depths (0.70952 and 0.70965 in the 0-5cm and 5-10cm depths) and becoming somewhat more radiogenic in the B horizon (0.70993 and 0.70988 in the 38-55cm and 55-68cm depths). All soil exchangeable $^{87}Sr/^{86}Sr$ ratios were substantially more radiogenic than bedrock at Icacos and Bisley (0.7041, Jolly et al. 1998; Pett-Ridge et al. 2009; Porder et al. 2015), closer to the average $^{87}Sr/^{86}Sr$ measured for wet deposition at Icacos (0.7103; Pett-Ridge et al., 2009).

2.4.5 $\delta^{44}Ca$ and $^{87}Sr/^{86}Sr$ of vegetation

Dominant vegetation at each watershed (Palo Colorado in Rio Icacos and Tabonuco at Bisley) (Table 2.4, Figure 2.5) exhibited lower $\delta^{44}Ca$ values in roots (-1.68‰ and -1.52‰ for Palo Colorado and Tabonuco, respectively) compared to leaves (-1.27‰ and -1.00‰ for Palo Colorado and Tabonuco, respectively). The Tabonuco sample exhibited a slightly larger differences in $\delta^{44}Ca$ values between leaves and roots ($\Delta_{leaves\text{-}roots}$) compared with the Palo Colorado ($\Delta_{leaves\text{-}roots}$ for Tabonuco = 0.91‰, while the $\Delta_{leaves\text{-}roots}$ for Palo Colorado = 0.55‰). However, we observed a larger difference between the $\delta^{44}Ca$ values of Tabonuco roots and the Ca mass weighted average soil exchangeable $\delta^{44}Ca$ value of Bisley 1

soil ($\Delta_{soil\text{-}roots}$ = 1.43‰) compared with $\delta^{44}Ca$ values of Palo Colorado roots and the mass-weighted average soil exchangeable $\delta^{44}Ca$ value of Rio Icacos soil ($\Delta_{soil\text{-}roots}$ = 0.96‰).

Cercropia samples collected from both sites also exhibited lower $\delta^{44}Ca$ values in roots relative to the leaves and $\Delta_{leaves\text{-}roots}$ values that agreed well with Tabonuco and Palo Colorado species ($\Delta_{leaves\text{-}roots}$ for Bisley Cercropia = 0.43‰, $\Delta_{leaves\text{-}roots}$ for Rio Icacos Cercropia = 0.42‰). Despite the differences in the $\delta^{44}Ca$ of soil exchangeable Ca concentrations in both watersheds, the Cercropia samples exhibited similar $\Delta_{soil\text{-}roots}$ ($\Delta_{soil\text{-}roots}$ = 1.48‰ and 1.49‰ for Cercropia in Bisley 1 and Rio Icacos, respectively).

Measurements of $^{87}Sr/^{86}Sr$ ratios of leaves and roots from the Tabonuco sample (0.70922 and 0.70933 for roots and leaves, respectively) and Cecropia (0.70922 and 0.70926 for roots and leaves, respectively) collected in Bisley 1 closely reflected the $^{87}Sr/^{86}Sr$ ratios of the soil exchangeable reservoir. The similarity between $^{87}Sr/^{86}Sr$ ratios in vegetation compartments and the soil exchangeable reservoir has also been observed in Rio Icacos and Bisley 1 (Pett-Ridge et al. 2009; Porder et al. 2015).

2.4.6 $\delta^{44}Ca$ of streamwater

We measured the $\delta^{44}Ca$ values of both the high and low discharge streamwater samples from Bisley 1 and Rio Icacos (Table 2.2). For both watersheds, the baseflow stream water $\delta^{44}Ca$ (-1.02‰ and -0.99‰ for Bisley and Rio Icacos, respectively) were not significantly different from each other or from

their respective bedrock $\delta^{44}Ca$ values. However, both high flow samples from Bisley 1 and Rio Icacos exhibited a significant shift toward more positive $\delta^{44}Ca$ values (-0.72‰ and -0.90‰ for Bisley and Rio Icacos, respectively) when compared with their respective low discharge samples. The Ca isotopic difference between high and low discharge was larger for Bisley 1 compared with Rio Icacos ($\Delta_{highQ\text{-}lowQ}$ = 0.30‰ and 0.09‰ in Bisley 1 and Rio Icacos streamflow, respectively).

2.5 DISCUSSION

2.5.1 Mechanism for heavy soil $\delta^{44}Ca$ in LEF sites

The observation that soil exchangeable $\delta^{44}Ca$ in both Luquillo forests are more positive than external inputs contrasts with the majority of stable Ca isotope studies carried out in terrestrial ecosystems. In the two previous studies with this characteristic (Wiegand et al. 2005; Holmden and Bélanger 2010), $^{87}Sr/^{86}Sr$ ratios indicate that soil exchangeable Sr is atmospherically dominated (Kennedy et al. 1998; Bélanger and Holmden 2010). As such, atmospherically derived sea salt Ca has been proposed as a mechanism for producing isotopically heavy soil exchangeable reservoir relative to external inputs (Bullen et al. 2004; Wiegand et al. 2005). However, additional mechanisms may produce isotopically heavy soils relative to inputs, particularly an imbalance in the uptake and return flux of Ca between the soil exchangeable and biomass reservoir (Holmden and Bélanger 2010; Fantle and Tipper 2014). Below, we discuss these two mechanisms in the

context of the Bisley 1 and Rio Icacos data, then discuss what might be producing the significant difference in the Ca stable isotope ratios of the soil exchangeable reservoir between the two sites.

2.5.2 Atmospheric inputs of Ca to LEF

Puerto Rico lies in the path of the easterly trade winds that deliver Saharan dust along with significant contributions of cations derived from seasalt aerosols into the Luquillo Experimental Forest (Muhs et al. 1990; Moreno et al. 2006; Murphy and Stallard 2012). Pett-Ridge et al. (2009) studied atmospheric inputs of Sr and Ca to the Icacos site using $^{87}Sr/^{86}Sr$ and Ca/Sr as tracers. Their data shows that Sr in wet deposition is dominated by seasalt (87%), with a secondary contribution from dissolved Sr from dust. They calculated that total atmospheric deposition (wet plus dry) is comprised of a greater proportion of dust (49%), which releases additional radiogenic (0.7197) Sr to soils as it dissolves. Pett-Ridge et al. (2009) argued that soil exchangeable Sr at the Icacos ridgetop site ($^{87}Sr/^{86}Sr$ ~0.7095) was dominated by atmospheric inputs (seasalt plus dust; 58% total) with additional contributions from bedrock Sr (42%), attributed to weathering of scattered bedrock corestones within otherwise deeply weathered saprolite. Our Icacos Sr data are consistent with this interpretation as are our Sr data from Bisley. Bisley soil exchangeable $^{87}Sr/^{86}Sr$ ratios (0.7093) are just slightly less radiogenic than Icacos, implying a perhaps a slightly larger contribution from bedrock-derived Sr than Icacos (44%), but overall similar proportions of atmosphere-derived Sr between the two sites. Our values agree

well with a larger data set of soil excchnageable $^{87}Sr/^{86}Sr$ ratios reported in Porder et al. (2015), which found that Tabonuco forests on vocaniclastic soils generally have less radiogenic $^{87}Sr/^{86}Sr$ ratios relative to Rio Icacos.

Inferring the provenance of Ca based on Sr isotopes requires consideration of Ca/Sr ratios of sources. Applying our measured bedrock Ca/Sr ratios for Icacos (545 molar) and Bisley (166), we calculate that Ca inputs to Icacos are divided roughly equally between atmospheric (seasalt plus dust; 47%) and bedrock (53%). For Bisley, the lower bedrock Ca/Sr ratio implies a higher proportion of atmospheric Ca (72%) relative to bedrock (28%).

Because the atmospheric source of Ca is important at both LEF sites, atmospheric deposition of Ca has the potential to shift soil $\delta^{44}Ca$ away from values typical of bedrock. Seasalt in particular should have high $\delta^{44}Ca$ (0‰) relative to bedrock, so it is worth exploring whether inputs of seasalt might account for soil exchangeable $\delta^{44}Ca$ that are heavier than bedrock at both Icacos, and to a greater degree, Bisley. Pett-Ridge et al. (2009) calculated that at most 17% of total atmospheric deposition of Ca at Icacos is seasalt derived, with Ca deposition dominated by dust. We infer that Saharan dust should have $\delta^{44}Ca$ close to -1.0‰ (average $\delta^{44}Ca$ for silicate rocks = -0.94‰, Fantle and Tipper 2014) but we have no direct measurements of the dust component; if carbonates (average $\delta^{44}Ca$ = -1.28‰; Fantle and Tipper, 2014) contribute significantly to Ca in Saharan dust, the $\delta^{44}Ca$ should be more negative than -1.0‰. Further support for the lack of a significant seasalt input of Ca is based on the major ion

chemistry of precipitation reported by Heartsill-Scalley (2007), who computed mean weekly precipitation composition at LEF for the period 1988-2002. The average precipitation Ca/Cl ratio (0.097 molar) is dramatically higher than that of seawater (0.0188, Pilson 1998), indicating substantial non-seasalt contributions of Ca to precipitation. Assuming precipitation Cl is derived entirely from seasalt, we calculate that seasalt contributes at most 20% of Ca to precipitation.

Our data on $\delta^{44}Ca$ in wet precipitation at Bisley, while limited to two samples, supports the inference made from Sr and major ion chemistry that seasalt is a minor contribution to Ca in precipitation. We calculate that an atmospheric source of Ca that is at most 20% seawater could be as heavy as -0.8‰, but certainly not heavy enough to account for the $\delta^{44}Ca$ (near 0‰) seen in Bisley soils. In fact our measured average precipitation $\delta^{44}Ca$ of -1.15‰ suggests that Ca in wet precipitation is not a simple mixture of dust and seasalt unless Saharan dust is much more negative than -1.0‰. This interpretation is supported by precipitation Ca/Sr ratios measured by Pett-Ridge et al. (2009), which are higher than predicted for such a mixture. The authors suggested that an unidentified source of Ca with high Ca/Sr must contribute to wet precipitation. Our data suggests that this as yet unidentified component must be isotopically light in Ca, consistent with contributions from carbonate dust. We conclude that the integrated sources of Ca to the LEF sites, although incompletely understood, likely have an average $\delta^{44}Ca$ slightly less than -1.0‰, and that relatively heavy values of $\delta^{44}Ca$ measured in the soil exchangeable pool must reflect internal

fractionation processes rather than the influence of isotopically heavy Ca sources such as seasalt.

2.5.3 Effects of internal Ca cycling on soil exchangeable $\delta^{44}Ca$

Another mechanism that can produce a soil exchangeable reservoir that is isotopically heavier than external inputs is through imbalance in the uptake and return flux of Ca between the soil exchangeable and biomass reservoir (Holmden and Bélanger 2010; Fantle and Tipper 2014). In a steady-state situation where equal amounts of Ca are being taken up from the soil exchangeable reservoir (with an accompanying isotopic fractionation) as is being returned to the soil exchangeable reservoir via above and belowground biomass decay, mass balance considerations indicate the $\delta^{44}Ca$ of the soil exchangeable reservoir will be isotopically indistinguishable from the $\delta^{44}Ca$ of external inputs (weathering and atmospheric deposition). In fact, when uptake is balanced by return, the $\delta^{44}Ca$ values of the soil exchangeable reservoir should remain identical to the $\delta^{44}Ca$ of external inputs regardless of the magnitude of isotopic fractionation. However, an imbalance in the uptake and return flux can produce a situation where the soil exchangeable reservoir is either isotopically lighter or heavier than external inputs. In this case, the difference between the $\delta^{44}Ca$ value of the soil exchangeable reservoir and the external inputs for a given imbalance in the uptake and return flux scales with the magnitude of the isotopic fractionation associated with plant uptake of Ca. We next explore this mechanism in the context of the Bisley 1 and Rio Icacos forests.

2.5.4 Mechanisms driving differences in soil exchangeable $\delta^{44}Ca$ in Bisley and Rio Icacos

Above we argued that the different soil exchangeable $\delta^{44}Ca$ values observed at each site reflect internal cycling of Ca rather than differences in the $\delta^{44}Ca$ of Ca sources. Both sites have soil exchangeable $\delta^{44}Ca$ that is heavy relative to Ca sources. Although we have measured only one soil profile from each site, and therefore cannot determine how representative these profiles are, supporting evidence for a heavy soil exchangeable Ca comes from the observation that both watersheds shift toward heavier $\delta^{44}Ca$ during stormflow. We attribute this shift to activation of shallow flowpaths, adding heavy soil-derived Ca to a baseflow component during stormflow (Kurtz et al. 2011). The observation that the difference in baseflow and stormflow $\delta^{44}Ca$ is greater at Bisley is consistent with a Ca pool that is heavier at Bisley than at Rio Icacos. Below we explore why soil exchangeable $\delta^{44}Ca$ values may be different between the two sites. Although the watersheds are located in close proximity to one another (~6km) and they share relatively similar climate (both classified as subtropical wet ecosystems, Ewel and Whitmore (1973)), there are fundamental differences in micro-climate, lithology, biology and disturbance history that may account for differences in the $\delta^{44}Ca$ values of the soil exchangeable reservoir.

2.5.5 Importance of Perturbations to the Ca cycle on soil exchangeable $\delta^{44}Ca$

Landslides and hurricanes are two of the most common perturbations to the Ca cycle within the LEF, causing changes in tree mortality and canopy structure, nutrient uptake and litterfall by vegetation, organic matter decomposition rates, and can provide additional sources of nutrients via exhumation of unweathered bedrock and minerals (Scatena 1989; Basnet et al. 1992; Scatena and Lugo 1995). On the topographic ridges where our soil samples were collected, landslides are relatively rare and hurricanes are likely the dominant disturbance mechanism (Scatena and Lugo, 1995). Hurricane disturbance, through reduction in aboveground biomass and subsequent regrowth, creates a situation where there is an imbalance in the Ca fluxes between the soil exchangeable and biomass reservoir and may provide an explanation for the observation that the soil exchangeable reservoir at each site is isotopically heavier than external inputs, and the difference in soil exchangeable $\delta^{44}Ca$ between Bisley 1 and Rio Icacos.

Hurricane Hugo made landfall in Puerto Rico on September 18, 1989 as a Category 3 with sustained winds of 166km*hr^{-1} (Walker 1991). While Hugo did not have the highest sustained wind speeds, rainfall or storm duration when compared with other hurricanes that passed over Puerto Rico in the 100 years prior to Hugo, the actual impact of each hurricane on the LEF depends heavily on their storm track over the island (Scatena and Larsen 1991). Although the island-

wide damage caused by Hugo was relative small, due to its storm track, it was estimated to be second only to a 1932 hurricane with regard to the amount of hurricane related damage to the LEF since 1899 (Scatena and Larsen, 1991). While less is known regarding the amount of damage the 1932 hurricane caused to the Bisley 1 vegetation, substantial research has been devoted to understanding the response and recovery of vegetation in Bisley 1 to Hurricane Hugo (Brokaw and Grear 1991; Basnet et al. 1992; Boose et al. 1994; Scatena et al. 1996; Beard et al. 2005). Analysis of damage to aboveground biomass as a result of Hurricane Hugo indicated that Bisley 1 was within some of the most heavily damaged areas of LEF, with only 3% of stems ≥2.5cm having more than 50% of leaves intact and 38% of stems having only the bole remaining upright (Scatena and Lugo, 1995, Boose et al, 1994). Observations and modeling of hurricane Hugo damage as it relates to topographic aspect found that north-facing slopes, which include Bisley 1, incurred the most amount of damage while south facing slopes showed less damage (Boose et al., 1994).

Scatena et al. (1996) observed that nutrient cycling was significantly impacted by Hugo, particularly in the first 5 years following the hurricane. Hurricane Hugo reduced Ca in aboveground biomass by approximately 50%, although within 5 years aboveground biomass recovered to pre-hurricane levels (Scatena et al. 1996), and by 2004 had surpassed pre-hurricane levels, reaching 124% of pre-hurricane biomass (Heartsill Scalley et al. 2010). Scatena et al. (1996) found that in the first two years following the passage of Hurricane Hugo,

between 60-75% of all Ca uptake by vegetation was retained by vegetation as opposed to returned to the soil via litterfall, indicating a net removal of Ca from the soil as biomass in Bisley 1 regrew following the hurricane. This net uptake of Ca from the soil indicates an imbalance in the uptake and return flux of Ca to the soil exchangeable reservoir that may produce the $\delta^{44}Ca$ values we observe at the two watersheds.

We used our stable Ca isotope mass balance model to simulation the impact Hurricane Hugo exerted on stable Ca isotope ratios in the soil exchangeable reservoir at Bisley 1. We force the model using net yearly biomass accumulation rates between 1989 and 2012 estimated by fitting an exponential equation to published measurements of the change in Ca biomass storage in the 15 years following the hurricane (Heartsill Scalley et al. 2010) (Figure 2.6). Depending on the trajectory of the biomass accumulation, model simulations suggest that by 2012, the net removal of Ca from the soil as a result of the regrowth of the biomass reservoir results in the $\delta^{44}Ca$ of the soil exchangeable pool becoming heavier, shifting from -1.0‰ to between -0.37 to -0.55‰ (Figure 2.7). The exact magnitude of the increase in soil $\delta^{44}Ca$ depends on the rate of biomass accumulation used in the model. No matter the exact rate of biomass Ca accumulation during regrowth, these results indicate that hurricane disturbance and subsequent biomass regrowth could drive the $\delta^{44}Ca$ of the soil exchangeable pool in Bisley 1 from an initial value of -1‰ toward more positive values, although the $\delta^{44}Ca$ of the soil exchangeable pool for our accumulation

trajectories only reached a maximum values of -0.37‰, lower than our post-hurricane soil exchangeable $\delta^{44}Ca$ measurement of -0.1‰. Our underestimation of soil exchangeable $\delta^{44}Ca$ relative to measured values may be related to our model assumption that the system was at steady-state pre-hurricane Hugo, which likely is an unrealistic scenario. Scatena and Larsen (1991) calculated that hurricanes affect the Luquillo Experimental Forest approximately every 25-30 years, and experience damage similar to that caused by Hugo every 50-60 years. For damage on the scale of Hurricane Hugo, our model indicates that the time required for the soil exchangeable $\delta^{44}Ca$ to return to a values within measurement precision of external inputs is on the order of 200 years. This suggests that it is unlikely that the system had fully recovered from past hurricanes and the $\delta^{44}Ca$ of the soil exchangeable reservoir was likely more positive than -1‰ prior to Hurricane Hugo.

There is evidence that the Rio Icacos watershed was spared the worst of the impact of Hurricane Hugo, owing to the fact that it is a south-facing watershed (Lodge et al. 1991; Boose et al. 1994; Sullivan et al. 1999). McDowell et al. (1994) used a mass balance approach to calculate a net biomass accumulation rate of 100 mol $Ca*ha^{-1}*yr^{-1}$. If we assume that this is representative of post-hurricane accumulation rate in Rio Icacos, biomass accumulation Rio Icacos in 1994 was approximately 14% of our fitted 1994 accumulation rate in Bisley 1 of 740 mol $Ca*ha^{-1}*yr^{-1}$. Our analysis suggests that if lower amounts of defoliation (and hence a smaller magnitude of biomass Ca

accumulation during regrowth) occurred at Rio Icacos, the soil exchangeable reservoir would experience a smaller positive shift in the $\delta^{44}Ca$ relative to the $\delta^{44}Ca$ of external inputs when compared with Bisley 1 (Figure 2.7).

2.5.6 Stable Ca isotope fractionation during uptake by vegetation in Bisley 1 and Rio Icacos

To this point, we have not considered how differences in the magnitude of the isotopic fractionation between soil and plant tissue at the two sites might affect the soil exchangeable $\delta^{44}Ca$ values. Previous research has established that stable Ca isotopes are fractionated during biologic uptake of Ca by roots (Cobert et al. 2011; Schmitt et al. 2013). Using greenhouse experiments, Cobert et al. (2011) identified three stable Ca isotope fractionation mechanisms during plant uptake that enrich plant organs in the light isotopes of Ca: when Ca enters the lateral roots, as Ca is transported along the xylem, and in the reproductive organs where the cell wall structures and number of available exchange sites seem to be different to those of the xylem wall. In agreement with Cobert et al. (2011) and previous research that measured the $\delta^{44}Ca$ of plant organs, the roots in all 3 species analyzed were isotopically lighter than both soil exchangeable Ca and leaf samples from the respective tree. Though we did not determine stemwood $\delta^{44}Ca$ in our 3 species, our data supports an initial fractionation as roots take Ca up from the soil ($\Delta_{soil\text{-}roots}$) and a second internal fractionation process as Ca travels along the transpiration stream ($\Delta_{leaves\text{-}roots}$).

While the $\Delta_{leaves\text{-}roots}$ doesn't exhibit significant variability among the 3 species measured in this study, $\Delta_{soil\text{-}roots}$ values did exhibit variability at the species level. In particular, the Palo Colorado specimens we sampled in Rio Icacos had significantly smaller $\Delta_{soil\text{-}roots}$ relative to the Tabonuco specimen we sampled in Bisley 1 and the Cecropia specimens sampled from both watersheds. The close similarity between $\Delta_{soil\text{-}roots}$ of Cecropia found in Bisley 1 and Rio Icacos suggest that $\Delta_{soil\text{-}roots}$ in this species was not affected by the difference in soil exchangeable Ca concentrations. While this observation contrasts finding by Cobert et al. (2011) who observed a relationship between $\Delta_{soil\text{-}roots}$ and the Ca concentration in soil solution for potted dwarf French bean (*Phaseolus vulgaris* L.) plants, we acknowledge that our limited sampling of Cecropia trees may not completely represent the species as a whole, so we caution against generalizing our finding regarding the relationship between soil Ca availability and biologically induced stable Ca isotope fractionation.

That the $\Delta_{soil\text{-}roots}$ for Palo Colorado is significantly smaller than either Tabonuco or Cecropia is intriguing with regard to differences in the soil exchangeable $\delta^{44}Ca$ we observed at each site. As mentioned previously however, differences in separation factors between the two sites cannot produce isotopic differences between the soil exchangeable reservoir and external inputs without an accompanying imbalance in the Ca fluxes between the soil exchangeable and biomass reservoir. However, the observation of different separation factors for the dominant vegetation species at each site leaves open

the possibility that if both sites were subjected to the same magnitude of disturbance and regrowth as a result of Hurricane Hugo, the $\delta^{44}Ca$ of the soil exchangeable reservoirs could evolve along different trajectories. To examine the sensitivity of the soil exchangeable $\delta^{44}Ca$ value to the vegetation uptake fractionation factor (Δ_U), we varied Δ_U between -2.0‰ and 0.0‰ while keeping the biomass Ca accumulation constant (Figure 2.8). The most negative value for Δ_U (-2.0‰) produced a soil exchangeable pool that reached a $\delta^{44}Ca$ value of ~-0.10‰ by 2012, a 0.90‰ increase relative to initial conditions, but a Δ_U = -0.5‰ only produced an increase of ~0.2‰ by 2012. If Δ_U = 0.0‰, the soil exchangeable $\delta^{44}Ca$ value remained unchanged relative to the initial soil exchangeable reservoir $\delta^{44}Ca$ value of -1.0‰. If we assume the Δ_U for Bisley 1 and Rio Icacos forest can be approximated as the average of $\Delta_{soil\text{-}roots}$ and $\Delta_{soil\text{-}leaves}$ for the dominant species in each forest, and apply the same Ca accumulation rate to both watersheds, we find that by 2012, our model would predict the soil exchangeable $\delta^{44}Ca$ at Rio Icacos to be more negative than Bisley 1, but the difference between the two is much smaller, with the modeled $\delta^{44}Ca$ at Rio Icacos over predicted and the $\delta^{44}Ca$ in Bisley underpredicted. While we acknowledge that our Δ_U values are only estimates, our results indicate that the sites may have in fact experienced differing degrees of disturbance in addition to having different Δ_U.

2.6 CONCLUSIONS

In this study, we present stable Ca isotope data and $^{87}Sr/^{86}Sr$ data for two tropical forests, Bisley 1 and Rio Icacos, within the Luquillo Critical Zone observatory in Puerto Rico. Although the sites are only 6km apart, they exhibit contrasting lithology, Ca concentration in the soil, and dominant vegetation that may produce distinct Ca cycles. Both watersheds exhibited soil exchangeable $\delta^{44}Ca$ values that were isotopically heavier than external inputs, a relatively rare observation to date. Bisley 1 soil had higher Ca concentration in the upper 1m of the soil exchangeable reservoir and significantly more positive soil exchangeable $\delta^{44}Ca$ values (average soil exchangeable $\delta^{44}Ca$ at Bisley 1 = -0.09‰) than Rio Icacos. Soil exchangeable Ca concentrations at Rio Icacos were lower and soil exchangeable $\delta^{44}Ca$ values (average soil exchangeable $\delta^{44}Ca$ at Rio Icacos = -0.72‰), were closer the $\delta^{44}Ca$ value of Ca sources into both sites. This difference was reflected in the $\delta^{44}Ca$ values of high discharge waters draining each watershed.

Given the geographic location of Puerto Rico, it may be tempting to call on a soil exchangeable reservoir dominated by sea salt Ca ($\delta^{44}Ca$ of sea salt Ca = 0.00‰) as the primary mechanism behind the isotopically heavy soil Ca, particularly at the Bisley 1 site. However, Ca and Sr isotope data do not support this conclusion. First, $^{87}Sr/^{86}Sr$ data suggest that the two sites receive similar relative contributions of atmospheric Sr. Secondly, precipitation $\delta^{44}Ca$ averages -1.15‰, suggesting that sea salt is a minor contributor to atmospheric Ca, and

making it unlikely that atmospheric deposition would drive either site to heavier values of $\delta^{44}Ca$.

Instead we propose that heavy $\delta^{44}Ca$ at these sites, and in particular at the Bisley 1 site reflect biological Ca isotope fractionation combined with a disturbance-driven imbalance in the forests' Ca cycle. Our measurements of $\delta^{44}Ca$ in roots and leaves of the dominant tree species in each watershed indicated that the isotopic separation factor ($\Delta_{soil\text{-}roots}$) between the dominant tree species in Bisley 1 and the soil exchangeable reservoir was larger than in Rio Icacos, perhaps accounting for some of the soil Ca isotopic difference between sites. However, mass balance considerations indicate that heavy soil Ca requires that Ca uptake from the soil exchange complex is larger than the flux of Ca returned to soil via decomposition.

One well documented process that can produce such non-steady state conditions in the LCZO is ecosystem disturbance from hurricanes. Box model simulations of the Ca cycle indicate that biomass regrowth following a hurricane disturbance such as the 1989 Hurricane Hugo can produce a flux imbalance that would drive the soil exchangeable reservoir to become isotopically heavier than external inputs of Ca. With regard to the differences we observe between forests, if both forests were disturbed the same degree (and experienced the same magnitude of biomass regrowth) the distinct isotopic separation factors in each forest could produce the differences in soil exchangeable $\delta^{44}Ca$ that we observe. However, to produce such a large difference in soil exchangeable $\delta^{44}Ca$ between

both sites additionally requires a different flux imbalances at Bisley and Rio Icacos, possibly driven by distinct disturbance histories and recovery trajectories.

It’s important to note that our data does not permit us to directly attribute the imbalance in the cycling of Ca between the soil and biomass reservoir to a particular event. In fact, the differences in stable Ca isotope ratios is likely a result of the culmination of multiple disturbances that have occurred over the previous 10s to 100s of years. Finally, we cannot rule that the calcium cycle in the Tabonuco forest in Bisley 1 is inherently more susceptible to disturbances compared with Palo Colorado forests possibly as a result of geomorphic, lithologic or biologic factors. Nonetheless, while we may not be able to identify definitely the mechanism driving this imbalance, our data and model simulations suggest that stable Ca isotope ratios of the soil exchangeable reservoir may provide information on the disturbance history of a terrestrial ecosystem.

2.7 REFERENCES

Ahmad R, Scatena FN, Gupta A (1993) Morphology and sedimentation in Caribbean montane streams: examples from Jamaica and Puerto Rico. Sedimentary Geology 85:157–169. doi: 10.1016/0037-0738(93)90080-O

Bagard M-L, Schmitt A-D, Chabaux F, et al (2013) Biogeochemistry of stable Ca and radiogenic Sr isotopes in a larch-covered permafrost-dominated watershed of Central Siberia. Geochimica et Cosmochimica Acta 114:169–187. doi: 10.1016/j.gca.2013.03.038

Basnet K, Likens GE, Scatena FN, Lugo AE (1992) Hurricane Hugo: Damage to a Tropical Rain Forest in Puerto Rico. Journal of Tropical Ecology 8:47–55.

Beard KH, Vogt KA, Vogt DJ, et al (2005) Structural and Functional Responses of a Subtropical Forest to 10 Years of Hurricanes and Droughts. Ecological Monographs 75:345–361. doi: 10.2307/4539103

Bélanger N, Holmden C (2010) Influence of landscape on the apportionment of Ca nutrition in a Boreal Shield forest of Saskatchewan (Canada) using ^{87} Sr/ ^{86} Sr as a tracer. Canadian Journal of Soil Science 90:267–288. doi: 10.4141/CJSS09079

Blum JD, Klaue A, Nezat CA, et al (2002) Mycorrhizal weathering of apatite as an important calcium source in base-poor forest ecosystems. Nature 417:729–731. doi: 10.1038/nature00793

Boose ER, Foster DR, Fluet M (1994) Hurricane Impacts to Tropical and Temperate Forest Landscapes. Ecological Monographs 64:370–400. doi: 10.2307/2937142

Brokaw NVL, Grear JS (1991) Forest Structure Before and After Hurricane Hugo at Three Elevations in the Luquillo Mountains, Puerto Rico. Biotropica 23:386–392. doi: 10.2307/2388256

Brown ET, Stallard RF, Larsen MC, et al (1995) Denudation rates determined from the accumulation of in situ-produced 10Be in the luquillo experimental forest, Puerto Rico. Earth and Planetary Science Letters 129:193–202. doi: 10.1016/0012-821X(94)00249-X

Brown S, Lugo AE, Silander S, Liegel L (1983) Research history and opportunities in the Luquillo Experimental Forest. Gen. Tech. Report SO-44. U.S. Dept. of Agriculture, Forest Service, Southern Forest Experiment Station, New Orleans, La.

Bullen TD, Fitzpatrick JA, White AF, et al (2004) Calcium Stable Isotope Evidence for Three Soil Calcium Pools at a Granitoid Chronosequence. In: Proceedings of the Eleventh International Symposium on Water-Rock Interaction. Taylor and Francis, London, Saratoga Sprngs, New York, pp 813–817

Buss HL, Brantley SL, Scatena FN, et al (2013) Probing the deep critical zone beneath the Luquillo Experimental Forest, Puerto Rico. Earth Surface Processes and Landforms 38:1170–1186. doi: 10.1002/esp.3409

Buss HL, Sak PB, Webb SM, Brantley SL (2008) Weathering of the Rio Blanco quartz diorite, Luquillo Mountains, Puerto Rico: Coupling oxidation, dissolution, and fracturing. Geochimica et Cosmochimica Acta 72:4488–4507. doi: 10.1016/j.gca.2008.06.020

Cenki-Tok B, Chabaux F, Lemarchand D, et al (2009) The impact of water–rock interaction and vegetation on calcium isotope fractionation in soil- and stream waters of a small, forested catchment (the Strengbach case). Geochimica et Cosmochimica Acta 73:2215–2228. doi: 10.1016/j.gca.2009.01.023

Chadwick OA, Derry LA, Vitousek PM, et al (1999) Changing sources of nutrients during four million years of ecosystem development. Nature 397:491–497. doi: 10.1038/17276

Cobert F, Schmitt A-D, Bourgeade P, et al (2011) Experimental identification of Ca isotopic fractionations in higher plants. Geochimica et Cosmochimica Acta 75:5467–5482. doi: 10.1016/j.gca.2011.06.032

Compston W, Oversby VM (1969) Lead Isotopic Analysis Using a Double Spike. Journal of Geophysical Research 74:4338–4348. doi: 10.1029/JB074i017p04338

Dahlgren RA, Driscoll CT (1994) The effects of whole-tree clear-cutting on soil processes at the Hubbard Brook Experimental Forest, New Hampshire, USA. Plant and Soil 158:239–262. doi: 10.1007/BF00009499

Dosseto A, Buss HL, Suresh P. (2012) Rapid regolith formation over volcanic bedrock and implications for landscape evolution. Earth and Planetary Science Letters 337–338:47–55. doi: 10.1016/j.epsl.2012.05.008

Driscoll CT, Cirmo CP, Fahey TJ, et al (1996) The Experimental Watershed Liming Study: Comparison of Lake and Watershed Neutralization Strategies. Biogeochemistry 32:143–174.

Ellsworth DS, Liu X (1994) Photosynthesis and canopy nutrition of four sugar maple forests on acid soils in northern Vermont. Canadian Journal of Forest Research 24:2118–2127. doi: 10.1139/x94-272

Ewel JJ, Whitmore JL; (1973) The Ecological Life Zones of Puerto Rico and the U.S. Virgin Islands.

Fantle MS, Bullen TD (2009) Essentials of iron, chromium, and calcium isotope analysis of natural materials by thermal ionization mass spectrometry. Chemical Geology 258:50–64. doi: 10.1016/j.chemgeo.2008.06.018

Fantle MS, Tipper ET (2014) Calcium isotopes in the global biogeochemical Ca cycle: Implications for development of a Ca isotope proxy. Earth-Science Reviews 129:148–177. doi: 10.1016/j.earscirev.2013.10.004

Farkaš J, Déjeant A, Novák M, Jacobsen SB (2011) Calcium isotope constraints on the uptake and sources of Ca2+ in a base-poor forest: A new concept of combining stable (δ44/42Ca) and radiogenic (εCa) signals. Geochimica et Cosmochimica Acta 75:7031–7046. doi: 10.1016/j.gca.2011.09.021

Goldsmith ST, Porder S, Kurtz AC, Takagi KA (2013) Paper No. 81-10: Evaluation of shallow flow pathways and relative contributions to solute fluxes in a tropical small mountainous river: Luquillo, Puerto Rico. In: Geological Society of America Annual Meeting. Denver, Colorado USA,

Heartsill-Scalley T, Scatena FN, Estrada C, et al (2007) Disturbance and long-term patterns of rainfall and throughfall nutrient fluxes in a subtropical wet forest in Puerto Rico. Journal of Hydrology 333:472–485. doi: 10.1016/j.jhydrol.2006.09.019

Heartsill Scalley T, Scatena FN, Lugo AE, et al (2010) Changes in Structure, Composition, and Nutrients During 15 Yr of Hurricane-Induced Succession in a Subtropical Wet Forest in Puerto Rico. Biotropica 42:455–463. doi: 10.1111/j.1744-7429.2009.00609.x

Heijden G van der, Dambrine E, Pollier B, et al (2014) Mg and Ca uptake by roots in relation to depth and allocation to aboveground tissues: results from an isotopic labeling study in a beech forest on base-poor soil. Biogeochemistry 1–19. doi: 10.1007/s10533-014-0047-2

Heuser A, Eisenhauer A, Gussone N, et al (2002) Measurement of calcium isotopes (δ44Ca) using a multicollector TIMS technique. International Journal of Mass Spectrometry 220:385–397. doi: 10.1016/S1387-3806(02)00838-2

Hindshaw RS, Reynolds BC, Wiederhold JG, et al (2012) Calcium isotope fractionation in alpine plants. Biogeochemistry. doi: 10.1007/s10533-012-9732-1

Hindshaw RS, Reynolds BC, Wiederhold JG, et al (2011) Calcium isotopes in a proglacial weathering environment: Damma glacier, Switzerland. Geochimica et Cosmochimica Acta 75:106–118. doi: 10.1016/j.gca.2010.09.038

Holmden C, Bélanger N (2010) Ca isotope cycling in a forested ecosystem. Geochimica et Cosmochimica Acta 74:995–1015. doi: 10.1016/j.gca.2009.10.020

Jolly WT, Lidiak EG, Dickin AP, Wu T-W (1998) Geochemical diversity of Mesozoic island arc tectonic blocks in eastern Puerto Rico. Geological Society of America Special Papers 322:67–98. doi: 10.1130/0-8137-2322-1.67

Jordan CF, Kline JR, Sasscer DS (1972) Relative Stability of Mineral Cycles in Forest Ecosystems. The American Naturalist 106:237–253. doi: 10.2307/2459930

Joslin JD, Kelly JM, Van Miegroet H (1992) Soil Chemistry and Nutrition of North American Spruce-Fir Stands: Evidence for Recent Change. Journal of Environmental Quality 21:12–30. doi: 10.2134/jeq1992.00472425002100010002x

Kennedy MJ, Chadwick OA, Vitousek PM, et al (1998) Changing sources of base cations during ecosystem development, Hawaiian Islands. Geology 26:1015–1018. doi: 10.1130/0091-7613(1998)026<1015:CSOBCD>2.3.CO;2

Kurtz AC, Lugolobi F, Salvucci G (2011) Germanium-silicon as a flow path tracer: Application to the Rio Icacos watershed. Water Resources Research 47:W06516. doi: 10.1029/2010WR009853

Larsen MC, Collar PD, Stallard RF (1993) Research plan for the investigation of water, energy, and biogeochemical budgets in the Luquillo Mountains, Puerto Rico. U.S. Geological Survey Open-File Report 92-150, 19pp.

Larsen MC, Torres-Sánchez AJ, Concepción IM (1999) Slopewash, surface runoff and fine-litter transport in forest and landslide scars in humid-tropical steeplands, luquillo experimental forest, Puerto Rico. Earth Surface Processes and Landforms 24:481–502. doi: 10.1002/(SICI)1096-9837(199906)24:6<481::AID-ESP967>3.0.CO;2-G

Lawrence GB, Fuller RD, Driscoll CT (1987) Release of Aluminum following Whole-Tree Harvesting at the Hubbard Brook Experimental Forest, New Hampshire1. Journal of Environment Quality 16:383. doi: 10.2134/jeq1987.00472425001600040016x

Likens GE, Driscoll CT, Buso DC, et al (1994) The biogeochemistry of potassium at Hubbard Brook. Biogeochemistry 25:61–125. doi: 10.1007/BF00000881

Lodge DJ, Scatena FN, Asbury CE, Sanchez MJ (1991) Fine Litterfall and Related Nutrient Inputs Resulting From Hurricane Hugo in Subtropical Wet and Lower Montane Rain Forests of Puerto Rico. Biotropica 23:336–342. doi: 10.2307/2388249

McDowell WH, Bowden WB, Asbury CE (1992) Riparian Nitrogen Dynamics in Two Geomorphologically Distinct Tropical Rain Forest Watersheds: Subsurface Solute Patterns. Biogeochemistry 18:53–75.

McDowell WH, Scatena FN, Waide RB, et al (2012) Geographic and ecological setting of the Luquillo Mountains.

McLaughlin SB, Wimmer R (1999) Tansley Review No. 104 Calcium Physiology and Terrestrial Ecosystem Processes. New Phytologist 142:373–417.

Moreno T, Querol X, Castillo S, et al (2006) Geochemical variations in aeolian mineral particles from the Sahara–Sahel Dust Corridor. Chemosphere 65:261–270. doi: 10.1016/j.chemosphere.2006.02.052

Muhs DR, Bush CA, Stewart KC, et al (1990) Geochemical evidence of Saharan dust parent material for soils developed on Quaternary limestones of Caribbean and western Atlantic islands. Quaternary Research 33:157–177. doi: 10.1016/0033-5894(90)90016-E

Murphy SF, Stallard RF (2012) Water quality and landscape processes of four watersheds in eastern Puerto Rico: U.S. Geological Survey Professional Paper 1789. USGS

Nezat CA, Blum JD, Yanai RD, Hamburg SP (2007) A sequential extraction to determine the distribution of apatite in granitoid soil mineral pools with application to weathering at the Hubbard Brook Experimental Forest, NH, USA. Applied Geochemistry 22:2406–2421. doi: 10.1016/j.apgeochem.2007.06.012

Page BD, Bullen TD, Mitchell MJ (2008) Influences of calcium availability and tree species on Ca isotope fractionation in soil and vegetation. Biogeochemistry 88:1–13. doi: 10.1007/s10533-008-9188-5

Perakis SS, Maguire DA, Bullen TD, et al (2006) Coupled Nitrogen and Calcium Cycles in Forests of the Oregon Coast Range. Ecosystems 9:63–74. doi: 10.1007/s10021-004-0039-5

Pett-Ridge JC, Derry LA, Barrows JK (2009) Ca/Sr and 87Sr/86Sr ratios as tracers of Ca and Sr cycling in the Rio Icacos watershed, Luquillo Mountains, Puerto Rico. Chemical Geology 267:32–45. doi: 10.1016/j.chemgeo.2008.11.022

Porder S, Johnson AH, Xing HX, et al (2015) Linking geomorphology, weathering and cation availability in the Luquillo Mountains of Puerto Rico. Geoderma 249–250:100–110. doi: 10.1016/j.geoderma.2015.03.002

Poszwa A, Dambrine E, Ferry B, et al (2002) Do Deep Tree Roots Provide Nutrients to the Tropical Rainforest? Biogeochemistry 60:97–118.

Rudge JF, Reynolds BC, Bourdon B (2009) The double spike toolbox. Chemical Geology 265:420–431. doi: 10.1016/j.chemgeo.2009.05.010

Russell WA, Papanastassiou DA (1978) Calcium isotope fractionation in ion-exchange chromatography. Analytical Chemistry 50:1151–1154. doi: 10.1021/ac50030a036

Russell WA, Papanastassiou DA, Tombrello TA (1978) Ca isotope fractionation on the Earth and other solar system materials. Geochimica et Cosmochimica Acta 42:1075–1090. doi: 10.1016/0016-7037(78)90105-9

Scatena FN (1989) An Introduction to the Physiography and History of the Bisley Experimental Watersheds in the Luquillo Mountains of Puerto Rico.

Scatena FN, Larsen MC (1991) Physical Aspects of Hurricane Hugo in Puerto Rico. Biotropica 23:317–323. doi: 10.2307/2388247

Scatena FN, Lugo AE (1995) Geomorphology, disturbance, and the soil and vegetation of two subtropical wet steepland watersheds of Puerto Rico. Geomorphology 13:199–213. doi: 10.1016/0169-555X(95)00021-V

Scatena FN, Moya S, Estrada C, Chinea JD (1996) The First Five Years in the Reorganization of Aboveground Biomass and Nutrient Use Following Hurricane Hugo in the Bisley Experimental Watersheds, Luquillo Experimental Forest, Puerto Rico. Biotropica 28:424–440. doi: 10.2307/2389086

Schellekens J (2000) The interception and runoff generating processes in the Bisley catchment, Luquillo experimental forest, Puerto Rico. Physics and Chemistry of the Earth, Part B: Hydrology, Oceans and Atmosphere 25:659–664. doi: 10.1016/S1464-1909(00)00081-2

Schellekens J, Scatena FN, Bruijnzeel LA, et al (2004) Stormflow generation in a small rainforest catchment in the Luquillo Experimental Forest, Puerto Rico. Hydrological Processes 18:505–530. doi: 10.1002/hyp.1335

Schmitt A-D, Cobert F, Bourgeade P, et al (2013) Calcium isotope fractionation during plant growth under a limited nutrient supply. Geochimica et Cosmochimica Acta 110:70–83. doi: 10.1016/j.gca.2013.02.002

Schmitt A-D, Stille P (2005) The source of calcium in wet atmospheric deposits: Ca-Sr isotope evidence. Geochimica et Cosmochimica Acta 69:3463–3468. doi: 10.1016/j.gca.2004.11.010

Silver WL, Scatena FN, Johnson AH, et al (1994) Nutrient availability in a montane wet tropical forest: Spatial patterns and methodological considerations. Plant and Soil 164:129–145. doi: 10.1007/BF00010118

Stark NM, Jordan CF (1978) Nutrient Retention by the Root Mat of an Amazonian Rain Forest. Ecology 59:434–437. doi: 10.2307/1936571

Sullivan NH, Bowden WB, McDowell WH (1999) Short-Term Disappearance of Foliar Litter in Three Species Before and After a Hurricane1. Biotropica 31:382–393. doi: 10.1111/j.1744-7429.1999.tb00380.x

Tipper ET, Galy A, Bickle MJ (2008) Calcium and magnesium isotope systematics in rivers draining the Himalaya-Tibetan-Plateau region: Lithological or fractionation control? Geochimica et Cosmochimica Acta 72:1057–1075. doi: 10.1016/j.gca.2007.11.029

Walker LR (1991) Tree Damage and Recovery From Hurricane Hugo in Luquillo Experimental Forest, Puerto Rico. Biotropica 23:379–385. doi: 10.2307/2388255

Weaver PL, Murphy PG (1990) Forest Structure and Productivity in Puerto Rico's Luquillo Mountains. Biotropica 22:69–82. doi: 10.2307/2388721

White AF, Blum AE (1995) Effects of climate on chemical weathering in watersheds. Geochimica et Cosmochimica Acta 59:1729–1747.

White AF, Blum AE, Schulz MS, et al (1998) Chemical Weathering in a Tropical Watershed, Luquillo Mountains, Puerto Rico: I. Long-Term Versus Short-Term Weathering Fluxes. Geochimica et Cosmochimica Acta 62:209–226. doi: 10.1016/S0016-7037(97)00335-9

Wiegand BA, Chadwick OA, Vitousek PM, Wooden JL (2005) Ca cycling and isotopic fluxes in forested ecosystems in Hawaii. Geophysical Research Letters 32:L11404. doi: 10.1029/2005GL022746

Wiegand BA, Schwendenmann L (2013) Determination of Sr and Ca sources in small tropical catchments (La Selva, Costa Rica) – A comparison of Sr and Ca isotopes. Journal of Hydrology 488:110–117. doi: 10.1016/j.jhydrol.2013.02.044

2.8 SUPPLEMENTAL INFORMATION

2.8.1 Figures

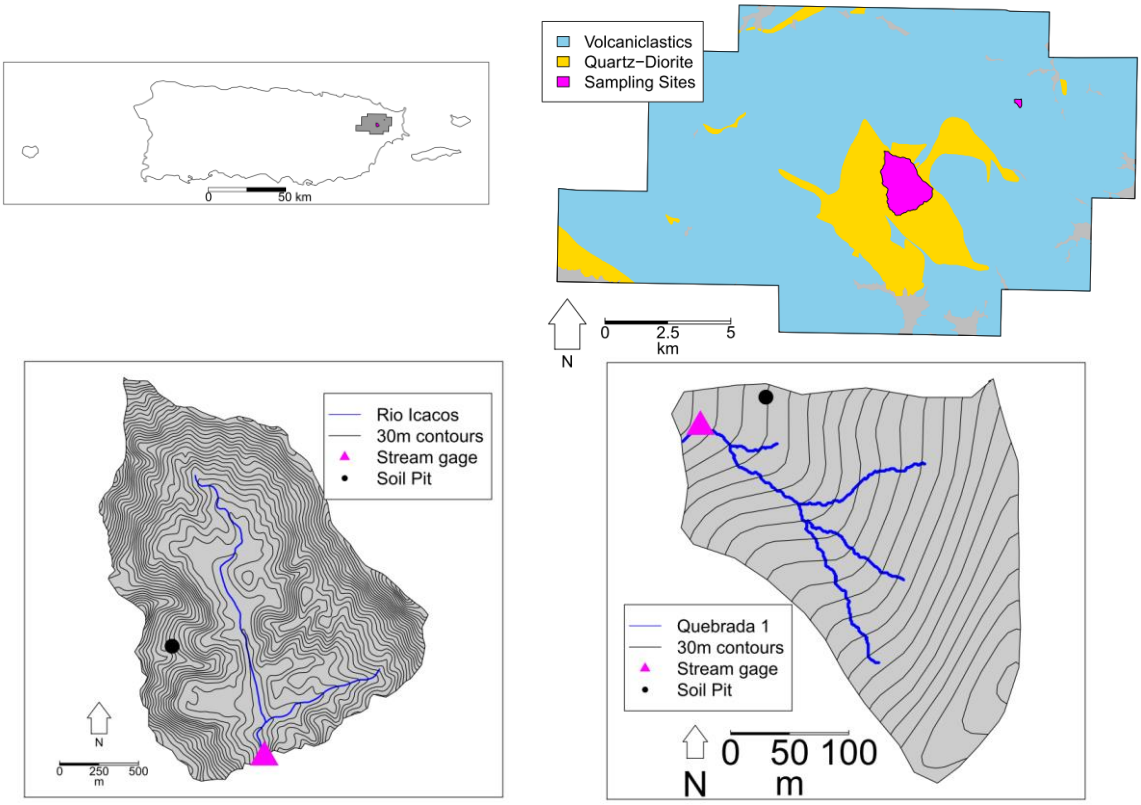

Figure 2.1. Site Map of Caribbean National Forest within the insland of Puerto Rico, b) location of Bisley and Rio Icacos within the Caribbean National Forest, c) Rio Icacos watershed and d) Bisley 1 watershed with locations of stream gage and soil pits.

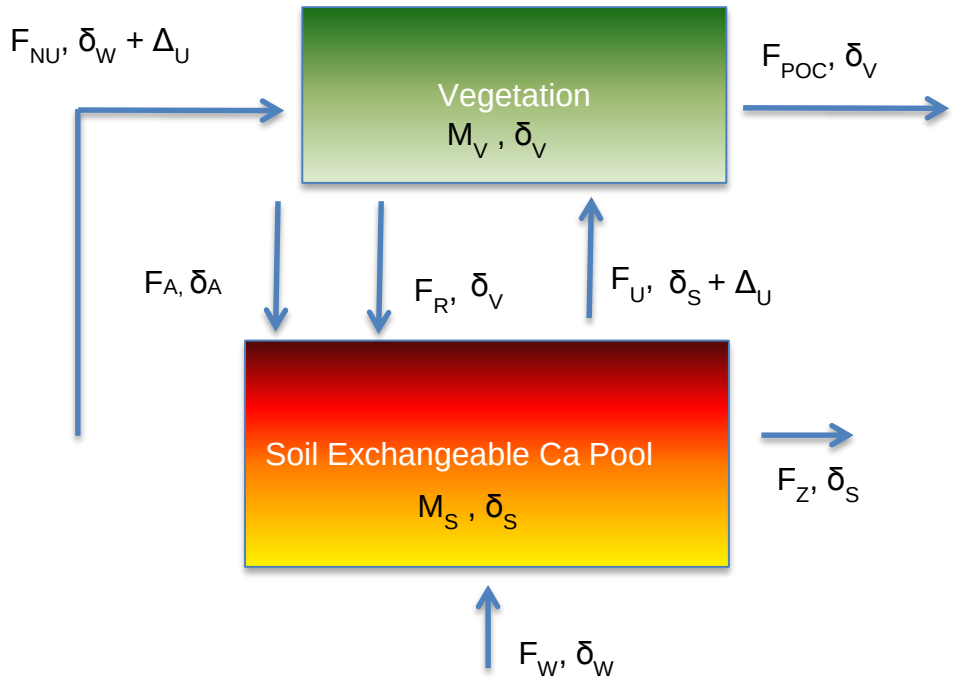

Figure 2.2. Ca stable isotope box model diagram. See text for definition of flux and reservoir abbreviations, and Appendix A2 for additional model details.

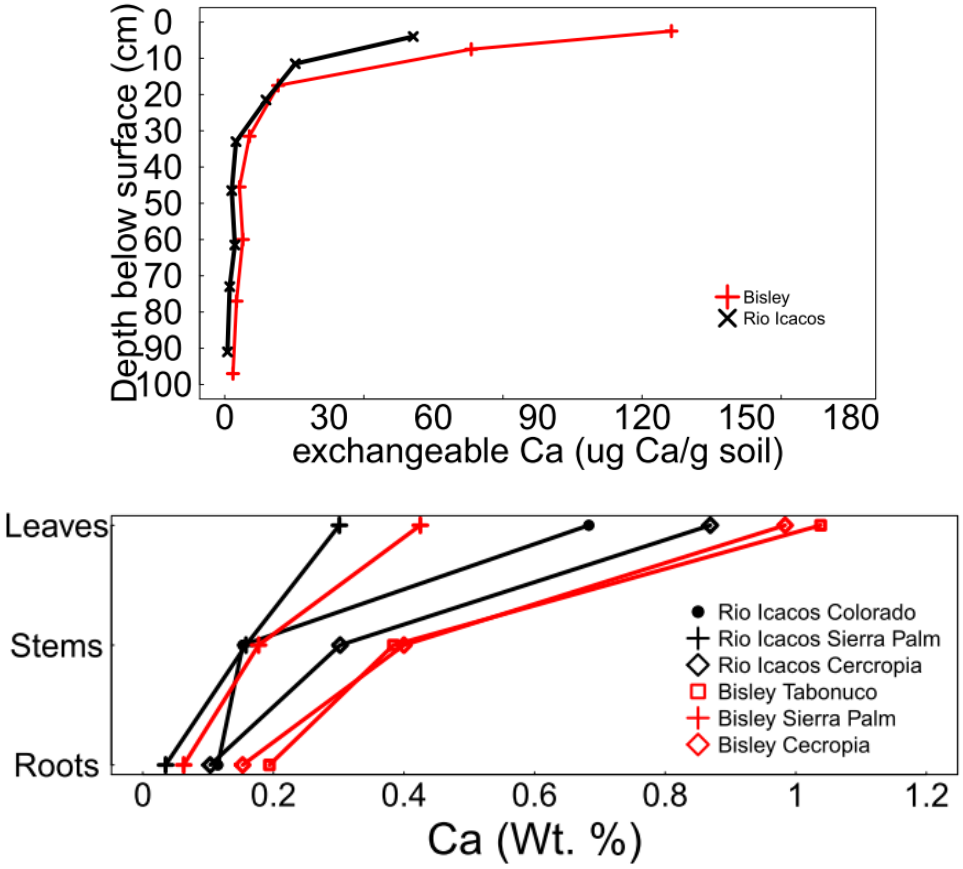

Figure 2.3. a) Soil exchangeable Ca concentrations in each watershed and b) Ca concentrations in different vegetation compartments.

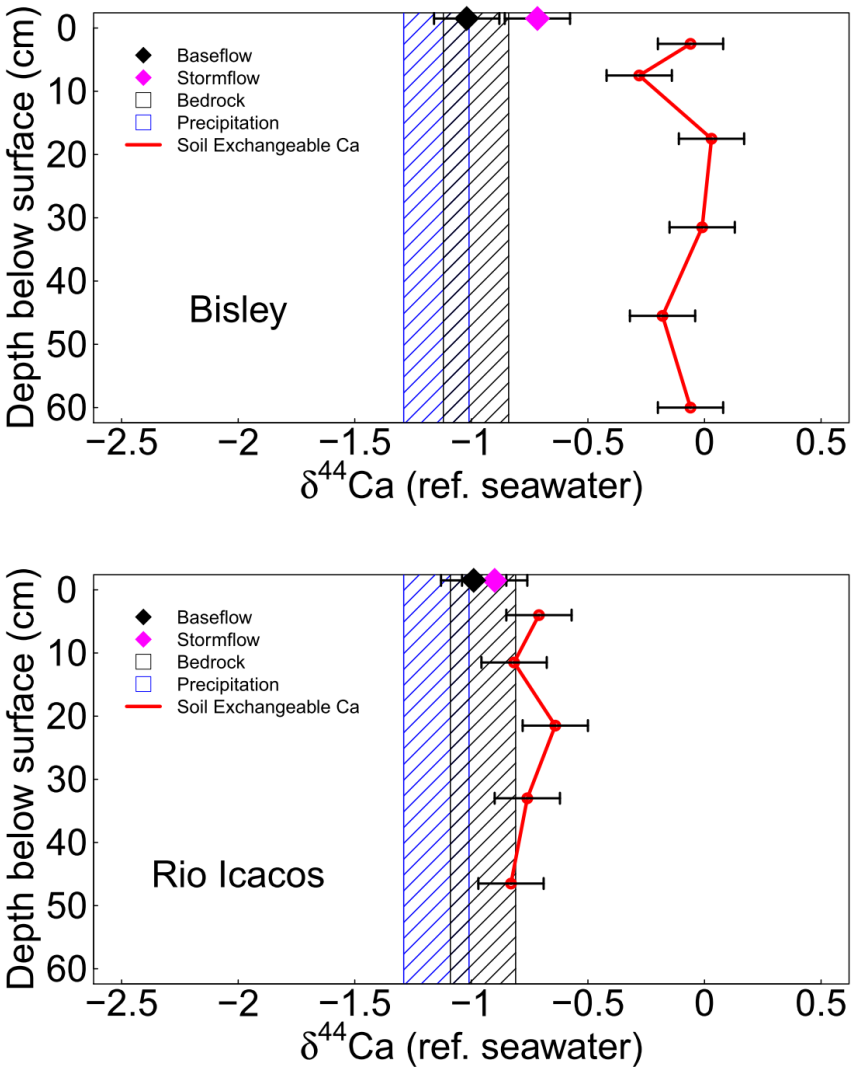

Figure 2.4. $\delta^{44}Ca$ values of external inputs, streamflow, bedrock, precipitation and soil exchangeable samples for a) Bisley 1, and b) Rio Icacos.

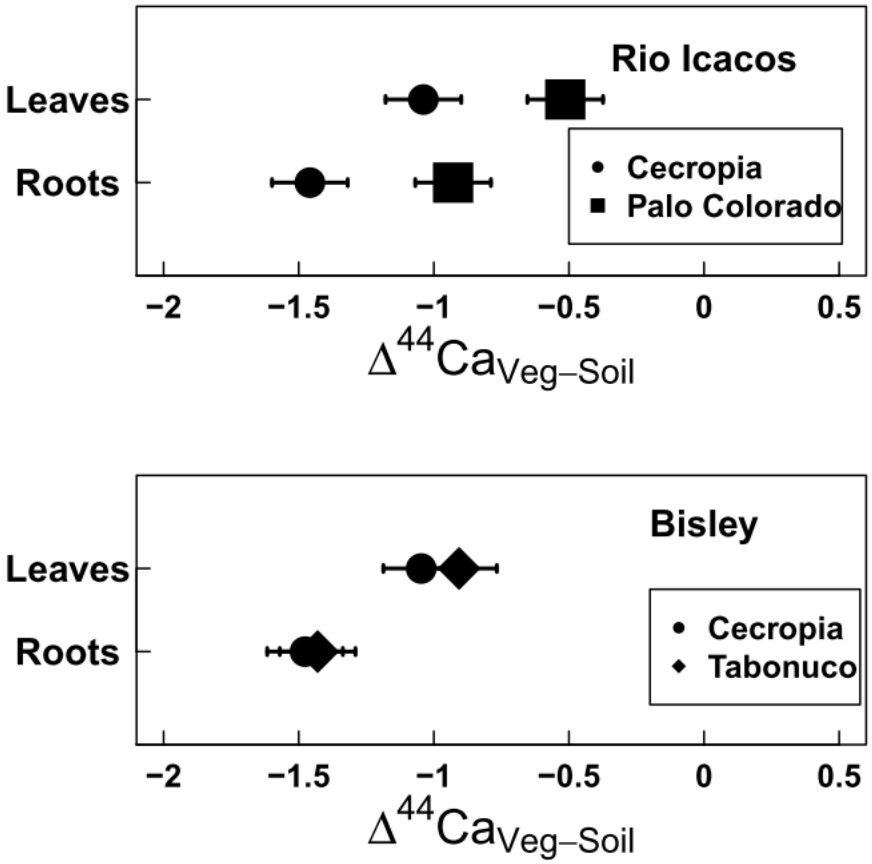

Figure 2.5. $\Delta^{44}Ca_{Veg\text{-}Soil}$ (‰ difference between average soil exchangeable $\delta^{44}Ca$ and vegetation compartment $\delta^{44}Ca$) for a) dominant vegetation (Tabonuco) and Cercropia in Bisley 1, and b) dominant vegetation (Palo Colorado) and Cercropia in Rio Icacos.

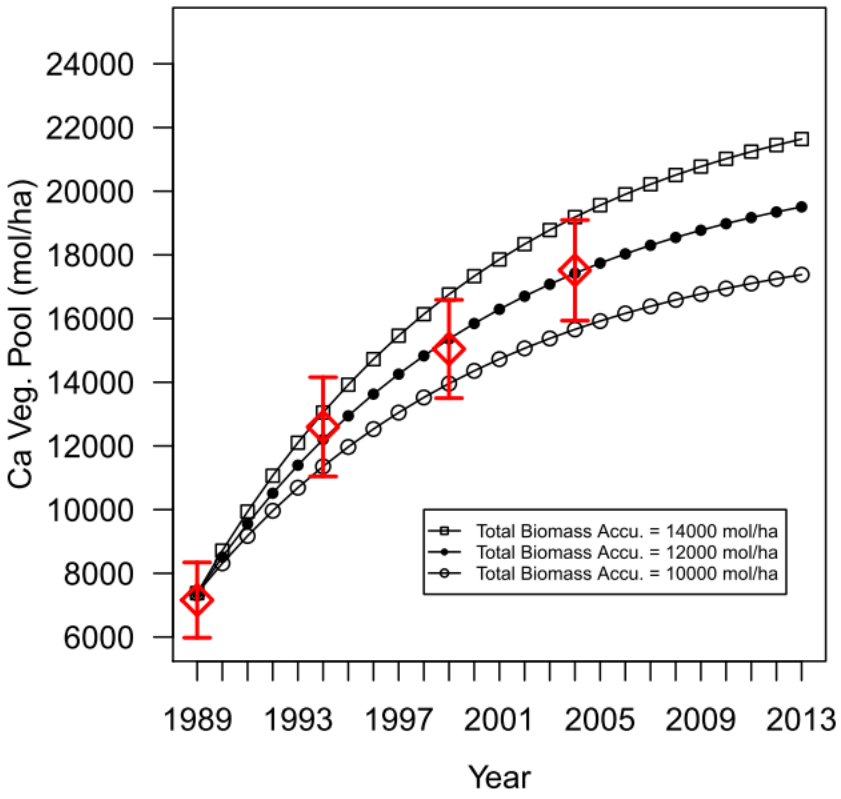

Figure 2.6. Biomass regrowth following the passing of hurricane Hugo in 1989. Red diamonds indicate observed biomass Ca storage with 1S.E. error bars (Hearsill Scaley et al. 2010), the solid symbol represent best fit of an exponential equation, while open symbols represent different biomass Ca accumulation scenarios.

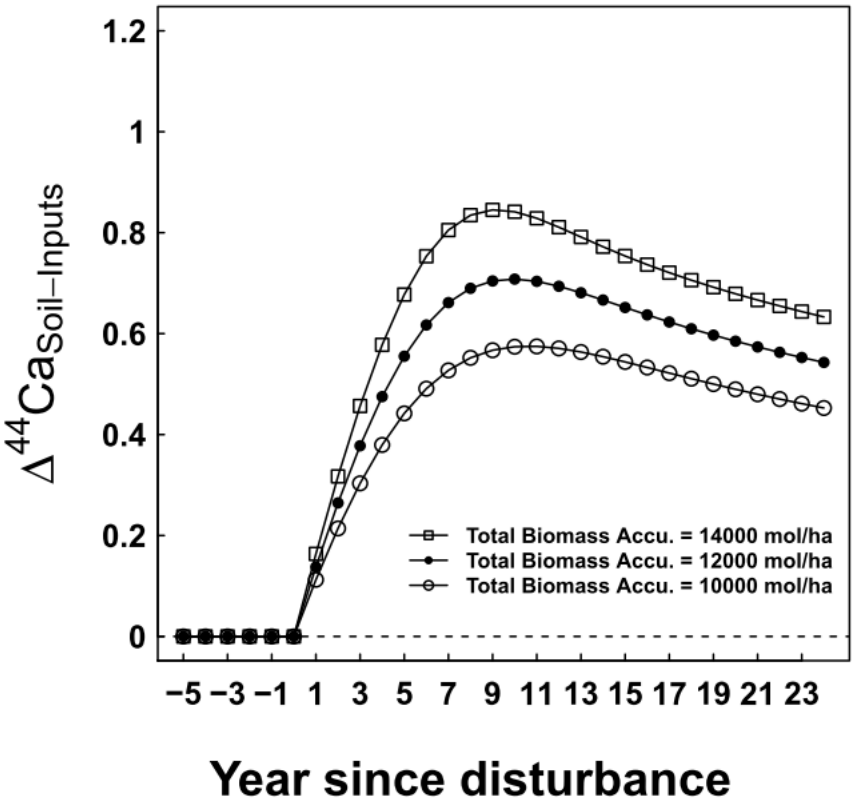

Figure 2.7. Model simulation of the time evolution of $\Delta^{44}Ca_{soil\text{-}Inputs}$ (‰ difference between the soil exchangeable reservoir and external inputs) following the passage of hurricane Hugo using the different uptake scenarios presented in Fig. 2.6. Symbols are the same as used in Fig. 2.6 for different Ca uptake scenarios. Model Parameters are represented in Table 2.5.

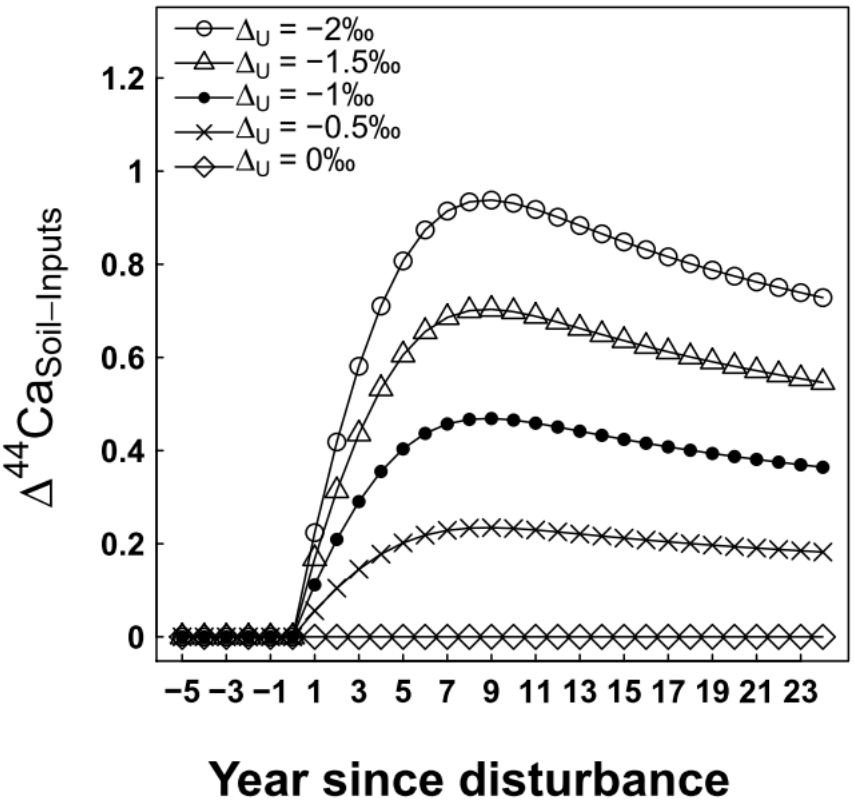

Figure 2.8. Model simulation of the time evolution of $\Delta^{44}Ca_{soil\text{-}Inputs}$ (‰ difference between the soil exchangeable reservoir and external inputs) following the passage of hurricane Hugo using different values of Δ_U (isotopic fractionation factor associated with biological uptake of Ca from the soil exchangeable reservoir).

2.8.2 Tables

Table 2.1. Elemental concentrations and Ca stable isotope ratios for external inputs into Rio Icacos and Bisley 1 forests.

Sample Type	Site	Sample ID	(Wt.% Oxide)						(µg/g sample)		molar ratio		$\delta^{44}Ca$ (‰ rel. SW)
			SiO_2	MgO	Al_2O_3	CaO	Na_2O	K_2O	Ba	Sr	Ca/Sr	Ca/Na	
Rock	Bisley 1	LTR-2	nd	2.3	16.2	7.4	1.6	1.6	601.6	696.6	165.98	2.56	-0.98
Rock	Rio Icacos	RBQD	nd	2.7	12.0	3.7	3.6	1.5	120.8	106.8	545.42	0.57	-0.95

Sample Type	Site	Date	Time	(ug/mL)									molar ratio	$\delta^{44}Ca$ (‰ rel. SW)
				Si	Mg	Al	Ca	Sr	Na	K	Cl^-	NO^{3-}	SO_4^{2-}	Ca/Na	
precipitation	Rio Icacos	11/13/2006	12:28	2.2	2.9	nd	3.5	nd	24.5	4.4	8.8	5.4	3.5	0.14	-1.17
precipitation	Rio Icacos	11/13/2006	12:54	1.4	5.2	nd	3.8	nd	50.4	7.5	16.5	8.5	6.3	0.08	-1.13

nd: Not determined.

Table 2.2. Elemental concentrations and Ca stable isotope ratios for streamwater draining Rio Icacos and Bisley 1 forests.

Sample ID	Site	Description	Date	Time	(ug/mL) Si	Mn	Fe	Mg	Ca	Sr	Na	K	($m^{3*}sec^{-1}$) Daily Q	$\delta^{44}Ca$ (‰ rel. SW)
PR-174	Icacos	Stormflow	11/13/2006	13:30	1.640	0.014	0.321	0.294	0.705	0.004	1.361	0.309	1.8	-0.90
PR-209	Icacos	Baseflow	11/14/2006	11:50	7.880	0.032	0.214	1.029	2.817	0.015	3.250	0.464	0.4	-0.99
B-2	Bisley	Stormflow	6/5/2011	9:45	2.387	bdl	0.053	0.561	0.709	0.006	2.302	0.879	2.2[a]	-0.72
B1-12	Bisley	Baseflow	6/26/2011	16:46	16.343	bdl	0.027	2.948	5.331	0.055	8.096	0.855	0.8[a]	-1.02

bdl: Below detection limit.
[a]: daily discharge recorded at Rio Mameyes stream gauge (USGS#50065500) which drains the basin that encompasses Bisley 1.

Table 2.3. Elemental concentrations, Ca stable isotope ratios and Sr isotope ratios of the soil exchangeable reservoir in Rio Icacos and Bisley 1 forests.

			(µg/g sample)								
Site	**horizon**	**Depth**	**Mg**	**Al**	**Ca**	**Sr**	**Ba**	**Na**	**K**	**δ^{44}Ca (‰ rel. SW)**	**$^{87}Sr/^{86}Sr$**
Bisley	Oa1	0-5cm	176.08	355.31	128.44	2.90	8.36	54.80	78.97	-0.06	0.70930
Bisley	Oa2	5-10cm	145.97	339.61	70.88	1.89	8.11	66.61	69.25	-0.28	0.70931
Bisley	B	10-25cm	76.57	306.35	15.34	0.54	6.93	16.89	23.98	0.03	0.70938
Bisley	B	25-38cm	37.62	273.55	7.10	0.22	9.74	12.47	17.79	-0.01	0.70924
Bisley	B2	38-53cm	23.78	336.76	4.24	0.24	14.12	13.67	8.10	-0.18	0.70956
Bisley	B3	53-67cm	28.94	584.37	5.20	0.25	9.25	10.41	6.62	-0.06	0.70950
Bisley	C	67-87cm	20.55	566.85	3.37	0.15	10.08	9.48	8.17	nd	0.70980
Bisley	C2	87-107cm	25.40	751.12	2.36	0.11	9.50	9.59	10.85	nd	0.71044
Rio Icacos	Oa1	0-8cm	71.14	176.49	54.21	0.91	3.06	45.26	70.32	-0.71	0.70950
Rio Icacos	Oa2	8-15cm	48.36	214.34	20.27	0.28	3.18	38.53	46.70	-0.82	0.70957
Rio Icacos	A	15-28cm	25.68	163.18	11.85	0.14	2.64	17.27	22.96	-0.64	0.70941
Rio Icacos	B	28-38cm	9.74	120.53	3.23	0.03	2.81	9.60	9.07	-0.76	0.70946
Rio Icacos	B2	38cm-55cm	8.01	133.38	2.00	0.01	4.74	8.52	6.46	-0.83	0.70901
Rio Icacos	B2	55-68cm	8.25	139.40	2.89	0.02	5.09	8.63	8.25	nd	0.70942
Rio Icacos	B3	68-78cm	6.95	152.00	1.42	0.02	6.45	9.15	6.31	nd	0.70934
Rio Icacos	C1	78-104cm	7.66	213.18	0.77	0.47	14.98	22.02	5.35	nd	0.70936

nd: Not determined.

Table 2.4. Elemental concentrations, Ca stable isotope ratios and Sr isotope ratios of vegetation samples collected in Rio Icacos and Bisley 1 forests.

				(µg/g sample)								
Sample ID	**Site**	**Species**	**Description**	**P**	**Mg**	**Ca**	**Sr**	**Ba**	**Na**	**K**	**δ^{44}Ca (‰ rel. SW)**	**$^{87}Sr/^{86}Sr$**
LTV-1	Bisley	tabonuco	roots	238	555	1990	22	12	1978	2741	-1.52	0.70922
LTV-1	Bisley	tabonuco	stem	276	1081	3993	42	19	3290	5599	nd	nd
LTV-1	Bisley	tabonuco	greenstem	479	4922	6602	70	42	8006	10945	nd	nd
LTV-1	Bisley	tabonuco	leaves	805	6279	10494	73	25	5961	17956	-1.00	0.70933
LTV-3	Bisley	sierra palm	roots	174	995	581	6	6	2305	1932	nd	nd
LTV-3	Bisley	sierra palm	stalk	250	2390	1834	11	7	7097	14890	nd	nd
LTV-3	Bisley	sierra palm	leaves	785	4368	4419	14	5	539	4716	nd	nd
LTV-5	Bisley	cecropia	roots	164	4972	1558	20	17	bdl	1403	-1.57	0.70922
LTV-5	Bisley	cecropia	wood/bark	207	2335	4173	38	28	bdl	7849	nd	nd
LTV-5	Bisley	cecropia	leaves	213	2230	9950	61	25	bdl	884	-1.14	0.70926
LTV-7	Icacos	colorado	roots	154	587	1122	18	23	bdl	1156	-1.68	nd
LTV-7	Icacos	colorado	stemwood	76	489	1364	25	32	387	2703	nd	nd
LTV-7	Icacos	colorado	leaves	286	6270	7061	75	53	7512	3039	-1.27	nd
LTV-9	Icacos	sierra palm	roots	96	558	281	3	4	1338	1950	nd	nd
LTV-9	Icacos	sierra palm	stalk	155	363	1633	6	4	2658	13641	nd	nd
LTV-9	Icacos	sierra palm	leaves	437	2001	2791	8	3	234	6901	nd	nd
LTV-10	Icacos	cecropia	roots	138	2680	1036	17	16	bdl	2833	-2.21	nd
LTV-10	Icacos	cecropia	bark/stemwood	130	1836	3133	40	39	bdl	3585	nd	nd
LTV-10	Icacos	cecropia	leaves	160	2255	8675	53	28	374	697	-1.79	nd

nd: Not determined.

Table 2.5. Model parameters for dynamic box model.

Parameter	Description	Units	Value	Source
M_S	Mass of Soil Exchangeable Pool	mol Ca/ha	10000	Silver et al (1994)
M_V (pre-hurricane)	Mass of vegetation pool pre-hurricane Hugo (1989)	mol Ca/ha	14171	Heartsill-Scaley et al. (2010)
M_V (post-hurricane)	Mass of vegetation pool post-hurricane Hugo (1989)	mol Ca/ha	7378	Heartsill-Scaley et al. (2010)
F_A	Atmospheric Deposition	mol ca/ha*yr^{-1}	400	Heartsill-Scaley et al. (2009)
F_W	weathering Flux	mol ca/ha*yr^{-1}	0	[a]
F_Z	Leaching Flux	mol ca/ha*yr^{-1}	400	[a]
F_R	Litterfall Flux	mol ca/ha*yr^{-1}	variable	Walker et al. (1991)
F_U	Uptake Flux	mol ca/ha*yr^{-1}	variable	Heartsill-Scaley (2010)
δ_S	Initial soil exchangeable $\delta^{44}Ca$	‰ (rel. Seawater)	-1	[a]
δ_V	Initial vegetation $\delta^{44}Ca$	‰ (rel. Seawater)	variable	[a]
δ_A	Atmospheric deposition $\delta^{44}Ca$	‰ (rel. Seawater)	-1	this study[b]
δ_W	Weathering $\delta^{44}Ca$	‰ (rel. Seawater)	-1	this study[b]
Δ_U	Δ_U	‰ (rel. Seawater)	variable	[a]

[a]: see text for explanation.
[b]: value rounded to -1‰ for modeling purposes.

CHAPTER 3: LINKING VARIABILITY IN SOIL STABLE CALCIUM ISOTOPE RATIOS TO ECOSYSTEM PROCESSES USING GLOBAL MEASUREMENTS OF STABLE CA ISOTOPES

3.1 ABSTRACT

Over the past 15 years, measurements of stable Ca isotope ratios ($\delta^{44}Ca$) in terrestrial ecosystems have become an increasingly common tool to investigate ecosystem calcium cycling. $\delta^{44}Ca$ measurements of the bioavailable soil Ca reservoir (soil exchangeable and soil solutions, $\delta^{44}Ca_{soil}$) have been a particular focus of these studies. Given the increased interest in terrestrial stable Ca isotopes, there is a need to develop a consistent framework to interpret these measurements. Here for the first time we compile global measurements of $\delta^{44}Ca_{soil}$ across 18 studies. We observe large variability in $\delta^{44}Ca_{soil}$ relative to $\delta^{44}Ca$ of external Ca sources (bedrock weathering and atmospheric deposition). We also observe that some sites are isotopically heavier that Ca sources while other sites are isotopically lighter. Across sites, high Ca concentrations were correlated with low $\delta^{44}Ca_{soil}$ values and high $\delta^{44}Ca_{soil}$ values were correlated with both low Ca concentrations and higher amounts of atmospherically derived Sr. Our observations suggest that sea salt Ca is not likely the primary driver of high $\delta^{44}Ca_{soil}$ values. Modeling work indicates that an imbalance in the uptake and return flux of Ca between vegetation and the bioavailable soil reservoir is an important control on $\delta^{44}Ca_{soil}$. We suggest that nutrient uplift by vegetation can drive sites to more negative $\delta^{44}Ca_{soil}$ relative to Ca sources. Sites with more

positive $\delta^{44}Ca_{soil}$ relative to Ca sources may be particularly sensitive to non-steady state conditions due to small soil Ca reservoirs and the lack of weathering inputs, although non-steady state conditions can produce more negative $\delta^{44}Ca_{soil}$ relative to Ca sources as well.

3.2 INTRODUCTION

The actively cycled soil Ca reservoir, defined here as dissolved Ca in soil solution or Ca electrostatically bound to soil exchange sites, is one of the primary sources of nutrients for vegetation growth. The amount of Ca in the reservoir reflects a balance between input and output fluxes of Ca, including atmospheric deposition, weathering of Ca-bearing minerals, decay of organic matter, vegetation uptake and leaching of Ca into groundwater and streams, as well as the soil cation exchange capacity (CEC). In addition, actively cycled soil Ca is sensitive to anthropogenic disturbances such as acid deposition and land use change (Reuss and Johnson 1986; Joslin et al. 1992; Likens et al. 1996). In this paper we argue that the isotope ratio of calcium in the actively cycled soil Ca reservoir is diagnostic of the state of an ecosystems calcium biogeochemical cycle.

Given the multitude of processes affecting the actively cycled Ca reservoir, researchers have long recognized the potential for this reservoir to provide information regarding nutrient cycling dynamics as well as the overall health of an ecosystem (Lawrence et al. 1987; Probst et al. 1990; Mitchell et al. 1996; Likens et al. 1998). Biogeochemists have long used $^{87}Sr/^{86}Sr$ ratios of the

actively cycled soil reservoir to determine the source of Sr (and by proxy Ca due to their similar chemical behavior in soil), and to infer which depths or minerals in the soil profile are actively contributing to Sr uptake by vegetation (Miller et al. 1993; Blum et al. 2002; Bullen and Bailey 2005; Blum et al. 2008). While the $^{87}Sr/^{86}Sr$ tracer relies on distinct $^{87}Sr/^{86}Sr$ ratios of Sr sources, variability in stable Ca isotope ratios of sources is at most a secondary control on soil Ca isotope ratios. Because stable Ca isotope ratios are fractionated during biological and pedogenic processes, soil stable Ca isotope ratios may be a useful tool for understanding internal cycling of Ca in ecosystems.

Two processes are known to fractionate Ca isotopes in terrestrial ecosystems: biological fractionation as Ca passes from the soil into roots during Ca uptake and fractionation during the precipitation of pedogenic Ca-bearing minerals such as calcium carbonate and calcium sulfate (Ewing et al. 2008; Cobert et al. 2011; Hindshaw et al. 2012; Bagard et al. 2013). Hindshaw et al (2012) associated preferential accumulation of isotopically light Ca in biomass with two processes, preferential absorption of the lighter isotopes of Ca into roots vacuoles via kinetic fractionation and preferential adsorption of isotopically light Ca onto exchange sites located in the apoplasm via equilibrium fractionation as Ca moves along the xylem. Both processes enrich biomass in the isotopically light isotopes of Ca while leaving behind isotopically heavy Ca in the soil exchangeable reservoir. Additional fractionation has been observed during biological precipitation of calcium oxalate, commonly associated with mycorrizal

fungi in soil and by vegetation in leaves, which is a relatively recalcitrant mineral that can accumulate in near surface soils (Graustein et al. 1977; Cromack Jr et al. 1979; Franceschi and Horner 1980; Gadd 1999). Observations across a wide range of species and climates suggest that biological fractionation is robust and should be expected wherever vegetation is actively growing. Ca isotopic fractionation by formation of pedogenic carbonate influences soil stable Ca isotope ratios in arid environments, and may be the dominant fractionation mechanism in low-productivity hyper-arid environments. Ewing et al. (2008) observed significant down-profile variability in Ca isotope ratios for soil profiles collected in the hyper-arid Atacama Desert in Chile, which they attributed to pedogenic precipitation of calcium carbonate and calcium sulfate. Pedogenic Ca-bearing minerals were isotopically light relative to atmospheric inputs, indicating a fractionation process that preferentially incorporates the light isotopes of Ca into the crystal lattice.

Given that these *in-situ* fractionation processes discriminate again the heavier isotopes of Ca in the soil reservoir, mass balance considerations suggest that residual soil exchangeable Ca should evolve toward Ca isotope values that are heavier than Ca sources. However, previously published studies have demonstrated that the soil exchangeable Ca reservoir can be isotopically heavier than, lighter than, or similar to Ca sources (bedrock weathering and atmospheric deposition) (Figure 3.1). A number of mechanisms have been put forth to explain these observations, including accumulation of isotopically light organically bound

Ca in near-surface soil, preferential leaching of the heavier isotopes of Ca from the upper portion of the soil profile to lower depths, or influence of sea-salt derived Ca (Bullen et al. 2004; Wiegand et al. 2005; Holmden and Bélanger 2010; Farkaš et al. 2011).

Here we build upon the model framework developed by Holmden and Bélanger (2010), and generalized by Fantle and Tipper (2014). Holmden and Belanger (Holmden and Bélanger 2010) applied a box model to a single study site in Canada, and demonstrated how variations in the uptake and return fluxes of Ca could influence the vertical profile of soil Ca isotope ratios measured there. Fantle and Tipper (2014) used a similar box modeling approach to address the question of whether variations in terrestrial Ca cycling could influence the Ca isotope ratios of rivers, and by extention, the Ca isotope ratio of seawater. Our approach is to synthesize the existing studies of Ca isotopes in terrestrial ecosystems and to interpret these data in the context of a box model of the terrestrial Ca cycle. We aim to determine whether known processes can account for the range in soil Ca isotope ratios observed globally, and to ask whether new insights on terrestrial Ca cycling can be gained by this cross-site comparison.

3.3 MATERIAL AND METHODS

3.3.1 Literature synthesis methodology

As the goal of this synthesis is to assess the variability in stable Ca isotopes in the soil exchangeable reservoir and identify the factors that produce

the variability across studies, we focus on terrestrial ecosystem studies that measured natural abundance stable Ca isotope ratios in the soil exchangeable reservoir and in soil solution. Using these criteria, we've identified 18 studies that measured soil exchangeable stable Ca isotopes and 7 studies that measured soil solution stable Ca isotopes. In 4 of these studies both soil exchangeable and soil solution stable Ca isotopes were measured. The soil exchangeable Ca pool is operationally defined in these studies using a range of lab methodologies but in all cases it is the Ca released from soil samples exposed to high ionic strength reagents (typically reagents include ammonium chloride, ammonium acetate or barium chloride). Soil solutions in these studies were collected using tension or zero-tension lysimeters installed at specific depths in the soil profile. Sites that measured both soil solution and exchangeable Ca observed a general agreement between the two types of samples (White et al. 2010; Hindshaw et al. 2011; Bagard et al. 2013), although some differences were observed (Bullen et al. 2004). Nonetheless, we treat both sets of data as representative of the actively cycled Ca reservoir.

14 of the 18 studies included measurements of local precipitation and bedrock. To better assess variability in the stable Ca isotope ratios of atmospheric deposition, we've included in our compilation two studies that primarily measured atmospheric deposition rather than soil exchangeable stable Ca (Schmitt and Stille 2005; Fantle et al. 2012).

Vegetation stable Ca isotope data was reported in 9 of the 18 studies. While we recognize that $\delta^{44}Ca$ values can vary widely with tree tissues, in order to facilitate comparison of vegetation Ca isotope data across sites, we have grouped biomass into three categories: roots, boles and leaves. Roots were measured in each study. Samples originally referred to by the studies' authors as stemwood, wood cores, branches and bark have here been grouped together as "boles", while our "leaves" category include samples originally referred to as leaves, litter, needles and cones.

Finally, we compiled published data on source partitioning of Sr (bedrock weathering derived vs. atmospherically derived) in the soil exchangeable reservoir at 6 of the sites to aid in interpreting the stable Ca isotope data. We note that Ca and Sr isotope data for some sites were not from the same study, nor necessarily from the same site, but were paired based on proximity and data availablility. The apportioning of Sr in the exchangeable reservoir is based on the assumption that the $^{87}Sr/^{86}Sr$ ratio of the soil exchangeable reservoir represents a mixture of Sr derived from bedrock weathering and from atmospheric deposition each, with a unique $^{87}Sr/^{86}Sr$ ratio (Miller et al. 1993; Capo et al. 1998; Kennedy et al. 1998; Blum et al. 2002).

A challenge in compiling stable Ca isotope data from the literature are the various ways that stable Ca isotope ratios are reported and a lack of agreement on a standards from which to reference natural samples (Fantle and Tipper 2014). For the studies reviewed here, stable Ca isotope data was reported as the

$^{44}Ca/^{40}Ca$ ratio referenced to a seawater standard ($\delta^{44}Ca_{SW}$, eg. Page et al. (2008)), the $^{44}Ca/^{40}Ca$ ratio relative to NIST 915a Ca standard ($\delta^{44}Ca_{915a}$, Bagard et al. (2013)), while others report the $^{44}Ca/^{42}Ca$ ratio relative to NIST 915a Ca standard ($\delta^{44/42}Ca_{915a}$ eg. Hindshaw et al. (2011)). To allow comparison of measurements across studies, we convert all $\delta^{44}Ca$ and $\delta^{44/42}Ca$ measurements to be $\delta^{44}Ca$ values relative to seawater. For values originally reported as $\delta^{44}Ca_{915a}$, we convert $\delta^{44}Ca_{915a}$ to $\delta^{44}Ca_{SW}$ using an accepted value of seawater (seawater $\delta^{44}Ca_{915a}$ = -1.88‰, Schmitt and Stille (2005)) and the following relationship (Schmitt et al. 2003):

$$\delta^{44}Ca_{sw} = \delta^{44}Ca_{915a} - 1.88‰ \quad (1)$$

In the case where the stable Ca isotopes ratios were originally reported as $\delta^{44/42}Ca_{915a}$, we first convert $\delta^{44/42}Ca_{915a}$ to $\delta^{44}Ca_{915a}$ follow the method outlined in equations 5 and 6 in Fantle and Tipper (2014), then insert the resulting $\delta^{44}Ca_{915a}$ into equation (1) to derive a $\delta^{44}Ca_{SW}$ value.

3.2 Steady-state box model development

In order to examine the impact biology exerts on soil exchangeable $\delta^{44}Ca$ values, we developed a two-box model of the terrestrial Ca cycle (Figure 3.2; see also Takagi 2015, Chapter 2). The model consists of 2 boxes (reservoirs) representing the mass of actively cycled soil Ca integrated over the root zone (M_S) and the mass of Ca in biomass (M_V) (mol Ca*ha^{-1}) and 7 fluxes (mol Ca*ha^{-1}*yr^{-1}) representing the movement of Ca into, out of, and between reservoirs. Two external fluxes enter the soil exchangeable reservoir, representing atmospheric

deposition (F_A) and bedrock weathering-derived (F_W) sources of Ca to the system. One external flux (F_{NU}) enters the vegetation pool directly, bypassing the soil exchange pool. This flux represents direct uptake of new Ca by roots from sources other than the exchangeable reservoir, contributing to “nutrient uplift”. Internal biomass cycling of Ca is represented by an uptake flux from the soil exchangeable reservoir (F_U), and the return of Ca from biomass back to the soil exchangeable reservoir (F_R) via decomposition. Ca is exported from the system by one of two fluxes, via leaching from the soil exchange reservoir (F_Z) to groundwater or streamwater, and as export of Ca from the vegetation reservoir (F_{POM}), for example by stream export of particulate organic matter. We use the box model to investigate steady-state scenarios that result in the $\delta^{44}Ca$ of the exchange pool, being lighter than, heavier than, or equal to the $\delta^{44}Ca$ of Ca sources to the system. We also investigate time-dependent (non-steady state) scenarios. Additional model details describing steady state and non-steady state equations is provided in Appendix A2.

3.4 RESULTS

A summary of our literature synthesis is reported in Tables 3.1-3.5. In this section we briefly present the variability of stable Ca isotope ratios of the primary Ca sources to ecosystems (bedrock weathering and atmospheric deposition), in the soil exchangeable and soil solution reservoirs, and in vegetation. Finally, we compare $\delta^{44}Ca$ values of the soil exchangeable reservoir with respective soil exchangeable Ca concentrations and Sr source apportionment calculations.

3.4.1 $\delta^{44}Ca$ of external Ca sources to terrestrial ecosystems

A compilation of $\delta^{44}Ca$ of external Ca sources is reported in Table 3.2. Bedrock weathering sources exhibited the smallest variability of Ca sources (Figure 3.3), with an average $\delta^{44}Ca$ (silicate and carbonate combined) of -1.12‰, and ranged from -1.59‰ to -0.75‰. The mean for $\delta^{44}Ca$ in precipitation (both rain and snow) was -1.11‰, not significantly different than the value for bedrock weathering, but more variable with a range in $\delta^{44}Ca$ of -2.22‰ to -0.58‰. While precipitation $\delta^{44}Ca$ values were similar across ecosystems for the most part, most of variability observed for atmospheric deposition is due to the large range at the sites in Costa Rica and Santa Cruz, CA USA (precipitation $\delta^{44}Ca$ values were between -2.22‰ and -0.58‰ in Costa Rica and -1.78‰ and -0.61‰ in Santa Cruz). Dominant inputs of Ca into terrestrial ecosystems fall within a fairly narrow range centered on -1.1‰.

3.4.2 $\delta^{44}Ca$ of the soil exchangeable reservoir

The absolute range in soil exchangeable $\delta^{44}Ca$ across all sites included in the synthesis varied from -2.35‰ in the shallow exchangeable reservoir at the Arbutus Lake watershed in New York, USA (Page et al. 2008) to +0.89‰ in the shallow exchangeable reservoir at the Kolekole site, HI USA (Wiegand et al. 2005) (Table 3.3 and 3.4). The limited variability in source $\delta^{44}Ca$ suggests that very little of the variability in soil $\delta^{44}Ca$ is accounted for by differences in the $\delta^{44}Ca$ of sources, with the possible exception of sea-salt inputs, which we discuss below.

Across all sites, the largest variability in soil $\delta^{44}Ca$ was observed in the near surface soil, with the range spanning -2.35‰ to 0.89‰. The majority of profiles have soil $\delta^{44}Ca$ values less -1.1‰ indicating that soil Ca is lighter than inputs (Figure 3.4). $\delta^{44}Ca$ in these “light profiles” generally increased with depth, often approaching typical bedrock values in the deepest samples. In only one soil profile (Santa Cruz, CA USA, White et al. 2010) is there clear evidence for deep soil $\delta^{44}Ca$ heavier than bedrock. Sites with soil $\delta^{44}Ca$ “heavier” than typical input values (i.e. > -1.1‰) are found more infrequently in our compilation. In these profiles, $\delta^{44}Ca$ is much less variable with depth, and consistently heavy.

We observe that the sites with high soil Ca concentrations tend to have light soil Ca, while sites with low concentrations of actively cycled soil Ca tend to have heavy soil Ca (Fig. 3.5). This is most apparent in the upper 50cm, and less so at depth (Figure 3.6). A related observation is that the importance of atmospheric inputs (vs. bedrock weathering) tends to scale with soil $\delta^{44}Ca$ (Fig. 3.7). Sites where more than 60% of Sr is sourced from atmospheric deposition tend to have heavy soil exchangeable $\delta^{44}Ca$. Conversely, sites where bedrock weathering contributes substantial Sr to soils tend to have light soil $\delta^{44}Ca$.

3.4.3 $\delta^{44}Ca$ of vegetation

On average across all studies and species analyzed, the roots had the most negative $\delta^{44}Ca$ ($\delta^{44}Ca$ of roots = -2.26‰) and leaves the most positive ($\delta^{44}Ca$ of leaves = -1.36‰), although significant overlap exists across all biomass compartments (Fig. 3.3). The average $\delta^{44}Ca$ of leaves was not significantly

different than that of atmospheric deposition or bedrock $\delta^{44}Ca$ values. For studies that measured more than one biomass compartment, all but one study found average root $\delta^{44}Ca$ to be more negative than average bole $\delta^{44}Ca$ (Bagard et al. 2013), and all studies found average bole $\delta^{44}Ca$ to be more negative than average leaves $\delta^{44}Ca$. There was evidence of biological fractionation at all sites. Average $\delta^{44}Ca$ values for biomass compartments (roots, boles and leaves) were more negative compared with their corresponding average soil $\delta^{44}Ca$ value. The average difference between roots and soil $\delta^{44}Ca$ was -1.25‰, between boles and soil was -1.17‰ and between leaves and soil was -0.68‰.

3.5 DISCUSSION

3.5.1 Controls on soil $\delta^{44}Ca$ inferred from model

The $\delta^{44}Ca$ value of the actively cycled soil Ca reservoir exhibits significant variability across study sites. As a starting point for interpreting this variability in the context of ecosystem processes, we utilize our 2 box model of the terrestrial ecosystem Ca cycle. As noted earlier, modeling work by Holmden and Belanger (2010) and Fantle and Tipper (2014) demonstrated that an imbalance in the uptake of Ca by vegetation and return flux of Ca via organic matter decomposition can affect the $\delta^{44}Ca$ value of the actively cycled Ca reservoir. In agreement with these earlier results, our model demonstrates that when the uptake (F_U) and return fluxes (F_R) between the actively cycled and vegetation reservoirs are in balance ($F_R=F_U$), the $\delta^{44}Ca$ of the actively cycled Ca reservoir

simply reflects the $\delta^{44}Ca$ value of the external input flux of Ca into the soil via weathering and atmospheric deposition (F_A and F_W), regardless of the magnitude of the isotopic separation factor (Δ_U) (Figure 3.8).

Actively cycled soil $\delta^{44}Ca$ values (hereafter referred to simply as soil $\delta^{44}Ca$) that differ from input values are explained in the model by one of two mechanisms. Either 1) there are multiple pathways for Ca uptake and loss from the vegetation pool that influence soil $\delta^{44}Ca$, which can persist even at steady state, or 2) a disturbance (hurricane, forest harvesting, fire, etc.) has produced an (non-steady-state) imbalance in the Ca cycle. Our model produces steady-state solutions in which soil $\delta^{44}Ca$ is lighter than inputs when the flux of Ca to vegetation directly from bedrock is significant (i.e. F_{NU} is non-zero in the model), and the loss of Ca from vegetation (F_{POC}) is zero (or at least small). At steady state, the Ca flux from vegetation to the exchange pool (F_R) is balanced by the sum of the two inputs (F_U and F_{NU}), and therefore $F_U<F_R$, and soil becomes isotopically light by the net addition of biologically fractioned (^{40}Ca enriched) Ca to the soil pool. This is a model representation of the process of “nutrient uplift” (Jobbágy and Jackson 2004), where deep roots access new Ca from bedrock, and then deliver that Ca to the exchange pool during decomposition. Conversely, the model produces steady state solutions with soil $\delta^{44}Ca$ heavier than inputs when this “nutrient uplift” source of Ca (F_{NU}) is zero (or at least small), and loss from the vegetation pool F_{POM} is non-zero. In this case, since a portion of the Ca taken from the exchange pool by vegetation is lost, uptake of Ca from the

exchange pool exceeds return of Ca to the exchange pool ($F_U > F_R$), resulting in heavy soil $\delta^{44}Ca$ through residual enrichment of the soil Ca pool by net extraction of light Ca by vegetation.

These examples illustrate simple, plausible processes that might account for both light and heavy values of soil $\delta^{44}Ca$ even in the absence of disturbance. However, our prior work (Takagi 2015, Chapter 1 and 2) demonstrates the impact that disturbance (harvesting, hurricanes) may have on soil $\delta^{44}Ca$ at some sites. Below we discuss cross-site patterns in soil $\delta^{44}Ca$ considering both the steady-state mechanisms described above, and a range of potential disturbance effects.

3.5.2 Interpretation of $\delta^{44}Ca$ trends across sites: Sites with light soil $\delta^{44}Ca$

At 7 of the 18 sites the majority of Ca in the actively cycled Ca reservoir is isotopically light relative to values typical of Ca sources. In the context of our model, these "light" sites are attributable either to active uptake of Ca from bedrock ("nutrient uplift") or a disturbance scenario where $F_U < F_R$, essentially implying net dieback rather than forest growth. We first evaluate the evidence for the "nutrient uplift" scenario.

Nutrient uplift is the process by which nutrient are transported by vegetation from depth to near surface soil horizons, thus limiting leaching losses of nutrients and maintaining sufficient stock to support plant growth (Jobbágy and Jackson 2001; Poszwa et al. 2002; Jobbágy and Jackson 2004; Porder et al. 2006; Porder and Chadwick 2009) It is regarded as an important mechanism for

maintain sufficient amount of limiting nutrients like P and N, though it has also been linked to less limiting nutrients such as Ca, Mg, and K (Jobbágy and Jackson 2004) The observation that the lightest Ca resides in the near surface of these “light” sites supports the nutrient uplift mechanism (e.g. Bullen and Chadwick, in prep): the shallow soil exchange pool is receiving more light Ca from vegetation than is being drawn from it.

The observation that “light” sites generally have soil exchangeable $\delta^{44}Ca$ values lighter than external Ca sources throughout the soil depth profile suggest that biomass isn’t simply shifting actively cycled Ca from deeper to shallower depths, but instead are accessing a deep secondary soil Ca reservoir, likely mineral bound Ca. If biomass were taking up actively cycled Ca at depth and returning it to the near surface horizons, mass balance considerations would indicate that $\delta^{44}Ca$ values of the actively cycled reservoir at depth should be isotopically heavier than external Ca sources, something that is only observed at one site (Santa Cruz, CA USA, White et al. 2010).

The generally positive relationship between the fraction of atmospherically derived Sr and soil $\delta^{44}Ca$ supports our conclusion that biomass is actively acquiring Ca from mineral sources. Sr apportionment at Hubbard Brook and Huntington Forest (which encompasses the Arbutus Lake watershed), two sites with an actively cycled Ca reservoir isotopically lighter than external sources, indicate a relatively high reliance on mineral bound Ca (Miller et al. 1993; Blum et al. 2002). In fact, it was speculated that the abundance of Ca rich minerals in the

soil profile would reduce the impact that acid rain associated leaching losses of Ca from the soil exchangeable complex would have on biomass growth (Mitchell et al. 1996). Sr isotope data indicate that vegetation at Arbutus Lake watershed contains ~20% Sr from new mineral weathering while 60-95% of foliar Sr at Hubbard Brook is from apatite derived Ca (Miller et al. 1993; Blum et al. 2002). Similarly, at a permafrost dominated watershed in Siberia (Bagard et al. 2013), the actively cycled reservoir was isotopically lighter than external sources and atmospherically derived Sr was calculated to account for only 6 to 33% of total exchangeable Sr in the upper soil profile, decreasing to 1 to 5% in deeper soil horizons. Farkas et al. (2011) observed the near surface soil exchangeable reservoir to be isotopically lighter than external Ca sources at a study site in central Massachusetts, USA. While the researchers classified the soil as “base-poor”, they did find abundant accessory apatite and Ca-rich plagioclase feldspar, suggesting the opportunity for plants to directly access these minerals for nutrient uptake and bypass the soil exchangeable reservoir altogether. Overall, sites with isotopically light soil Ca have been observed in a wide variety of climates, including in Hawaii and the South Island of New Zealand (Chadwick and Bullen, in prep., Moore et al. 2013). Our synthesis suggests isotopically light soil Ca may be a consequence of landscape age, weathering extent and availability of bedrock Ca to vegetation.

Our work specifically focused on the effects of disturbance on soil $\delta^{44}Ca$, using Hubbard Brook as an example, produced surprising results (Takagi, 2015,

Chapter 1). Following whole-tree harvest and removal of above-ground biomass, a time series of soil samples shows that soil exchangeable $\delta^{44}Ca$ decreases from initially light pre-harvest (and perhaps steady-state) values to become lighter yet in the 8 years following disturbance. If the transient response of soil $\delta^{44}Ca$ to forest recovery were dominated by biomass Ca uptake, we would expect soils to become heavier, rather than lighter with time. We attributed this trend towards lighter soil $\delta^{44}Ca$ to increased decomposition of belowground biomass immediately following the disturbance. This example highlights the delicate balance between uptake and return of Ca to the soil exchangeable reservoir. Extending these results, we might expect a forest experiencing decline to similarly exhibit decreasing soil $\delta^{44}Ca$ values as biomass decomposition would exceed uptake flux by biomass.

3.5.3 Interpretation of $\delta^{44}Ca$ trends across sites: Sites with heavy soil $\delta^{44}Ca$

Several sites (Hawaii, Luquillo, Puerto Rico, La Ronge, Canada, Strengbach, France) exhibit an actively cycled Ca reservoir that is majority isotopically heavy relative to values of typical sources. Within our modeling framework, “heavy” sites can be explained by unusually heavy $\delta^{44}Ca$ in the atmospheric source, by the absence of a significant “nutrient uplift” flux coupled with loss of Ca in the form of POM, or by disturbance. We first address the atmospheric mechanism.

The observation that sites with heavy $\delta^{44}Ca$ tend to have significant contributions of cations from atmospheric sources might suggest that we are

simply observing a source effect. If rainfall Ca is isotopically heavy, sites that receive a substantial fraction of their Ca from the atmosphere would be expected to be heavy as a result. Weigand et al. (2005) in their study of soils along a Hawaii chronosequence called upon sea salt Ca (which should have $\delta^{44}Ca$ =0‰) to at least in part explain isotopically heavy soils in older, more highly weathered sites. This remains a plausible explanation but a few observations suggest that alternative explanations should be explored. Weigand et al. (2005) did not report rainfall data, so it is unclear whether precipitation in Hawaii actually delivers Ca with $\delta^{44}Ca$ approaching 0‰. Fantle and Tipper's (2014) compilations found rainfall tends to be ~-1.0‰ lighter than sea water (average rainfall $\delta^{44}Ca_{SW}$ = -1.16‰). This indicates that atmospherically derived Ca is likely a mixture of sea salt, silicate and carbonate dust sources (Schmitt and Stille 2005; Farkaš et al. 2011) and unlikely to be purely sea salt Ca, perhaps even in Hawaii. Furthermore, at least one of the Hawaii sites measured by Weigand et al. (2005) was in fact heavier than seawater (see Table 4.3), requiring an additional mechanism to account for heavy soil Ca. Measurements by Takagi (2015, Chapter 2) similarly observed rainfall $\delta^{44}Ca$ to be too negative to produce the observed $\delta^{44}Ca$ values in the Bisley 1 and Rio Icacos forests, and Ca/Sr and $^{87}Sr/^{86}Sr$ data indicate that precipitation is unlikely to be sea salt dominated. As such, rainfall measured to date doesn't appear to have the isotopic leverage to produce a soil exchangeable reservoir significantly heavier than approximately -1.0‰.

Alternatively, if a portion of litterfall bypasses the soil reservoir altogether, as described in our model above, soils could maintain heavy $\delta^{44}Ca$ unrelated to source effects or disturbance. This could occur for example by the export of isotopically light particulate organic matter via streamwater. However, our model suggests that even with a large isotopic separation factor (ie. Δ_U = -2‰), this particulate Ca export flux would have to be on the order of 50% of the return flux (F_R) to drive the actively cycled Ca reservoir toward the most positive $\delta^{44}Ca$ values observed in our synthesis (Fig. 3.8). With regard to the Bisley site in Puerto Rico, where actively cycle $\delta^{44}Ca$ approached 1‰ more positive than Ca sources, estimates by Heartsill Scalley et al. (2012) indicate that less than 0.1% of litterfall in Bisley is directly exported out of the watershed as coarse particulate organic matter (CPOM) (>12.7mm), an insignificant flux compared with litterfall and not larger enough to significantly alter the $\delta^{44}Ca$ value. While other mechanisms exist that allow biomass Ca to bypass the actively cycled reservoir altogether, it is difficult to envision a process that would allow enough biomass Ca to bypass the actively cycled reservoir to significantly alter the $\delta^{44}Ca$ value.

In light of these observations, the relationship between the amounts of atmospherically derived cations in the actively cycled reservoir and $\delta^{44}Ca$ values may not be a causal relationship, but merely indicative of other processes controlling the stable Ca isotope ratios. Sites with a high proportion of atmospherically derived cations lack alternative sources of Ca in the soil. Without a substantial weathering source to draw from, the role of nutrient uplift, and its

effect in producing light soil $\delta^{44}Ca$ is minimized. This observation is supported by work along a Hawaiian chronosequence that found older, more weathered soils exhibited reduced nutrient uplift (Porder and Chadwick, 2009). Additional support comes from two chronosequence studies included here (Hawaii, USA and Santa Cruz, CA USA, Bullen et al. 2004; Wiegand et al. 2005) which observed an increase in $\delta^{44}Ca$ values with increasing age. Furthermore, our observation that more positive $\delta^{44}Ca$ values are coupled with lower Ca concentrations, supports modeling work that indicates a smaller soil exchangeable reservoir will more fully express biological fractionation and be particularly sensitive to a flux imbalance (Fantle and Tipper 2014).

It thus appears unlikely that a steady-state situation could shift the entire actively cycled reservoir $\delta^{44}Ca$ values by the amounts observed at sites globally. Therefore we suggest that a non-steady state situation, possibly arising from an aggrading biomass Ca reservoir, is driving older, Ca-poor sites to heavy soil $\delta^{44}Ca$. At the Bisley watershed in Puerto Rico, significant regrowth occurred following the passage of Hurricane Hugo over Puerto Rico in 1989 (Scatena et al. 1996; Beard et al. 2005; Heartsill Scalley et al. 2010). Takagi (2015, Chapter 2) demonstrated this regrowth has the leverage to drive the soil exchangeable $\delta^{44}Ca$ toward values that approach measured $\delta^{44}Ca$ values. Similarly, Holmden and Belanger (2010) measured isotopically heavy soil exchangeable and soil solution Ca in a boreal forest in Saskachewan, Canada (La Ronge) that is subjected to forest fires approximately every 100 years. Measurements at La

Ronge indicated that all but one plot had attained steady-state, indicating the forest may still be recovering. Similarly, the Strengbach catchment in Aubure, France has been subject to anthropogenic acid deposition and has soil solutions $\delta^{44}Ca$ values that are more positive than external Ca sources (Probst et al. 1992; Cenki-Tok et al. 2009). Unlike similar acid rain affected sites like HBEF and Arbutus Lake watersheds which have abundant mineral bound Ca in the soil and where nutrient uplift is prevalent, Strengbach contains Ca poor soil with only trace amounts of apatite, and soil exchangeable Sr isotope ratios indicate the actively cycled reservoir is atmospherically dominated (Dambrine et al. 1995; Fichter et al. 1998; Probst et al. 2000) There is evidence that the spruce forest in the Strengbach watershed experienced a period of decline in the 1980s in part due to elevated acid deposition (Probst et al. 1990). If the watershed is now in a period of recovery from acid deposition, this accompanied by a lack of nutrient uplift may partially explain why Strengbach exhibits isotopically heavy actively cycled Ca while HBEF and Arbutus Lake do not.

We note that biomass is not necessarily required to be aggrading at the time of sample collection for the soil exchangeable reservoir to reflect a previous period of aggradation. Dynamic model runs that incorporate disturbance (reduction in the size of the biomass reservoir) and subsequent regrowth indicate that a soil exchangeable reservoir remains isotopically heavier than inputs for a significant period of time following the disturbance, depending on the magnitude of biomass regrowth and the sizes of the biomass and soil exchangeable

reservoir. For example, modeling of hurricane disturbance in the Luquillo Experiment Forest, Puerto Rico by Takagi (2015, Chapter 2) indicates that it would take ~200 years for the soil exchangeable reservoir in the Bisley watershed to return to pre-hurricane $\delta^{44}Ca$ values. If an ecosystem is subjected to repeated disturbance events, as would be the case with reoccurring forest fires or hurricanes, the soil exchangeable reservoir can evolve such that it is always isotopically heavier than external inputs (Fig. 3.9).

3.6 CONCLUSIONS

Synthesizing published Ca stable isotope data across study sites provides a unique perspective on ecosystem processes that control the observed $\delta^{44}Ca$ values of the actively cycled soil Ca pool. Several observations from this study may provide a framework for interpreting future measurements of soil Ca stable isotope ratios, and may generate new hypotheses regarding the behavior or Ca stable isotope in terrestrial ecosystems and Ca cycling as a whole and motivate future applications of Ca stables isotopes in terrestrial ecosystems.

First we observed exhibit significant variability in soil exchangeable $\delta^{44}Ca$ values across study sites and relative to observed variability in the dominant external inputs of Ca (bedrock weathering and atmospheric deposition). More specifically, the majority of sites exhibited soil exchangeable $\delta^{44}Ca$ values that were isotopically lighter than external inputs, while a few sites exhibited soil exchangeable $\delta^{44}Ca$ values that were isotopically heavier than external inputs. While this observation may seem rather inconsequential, modeling indicates that

in order to produce a soil exchangeable reservoir that is isotopically different than external inputs, there must be an imbalance in the flux of Ca that is taken up by vegetation (accompanied by an isotopic fractionation) and the flux of Ca that is returned from the biomass reservoir to the soil exchangeable reservoir. This observation allows us to develop a framework for interpreting the observed soil exchangeable $\delta^{44}Ca$ values in the context of ecosystem process that could produce this imbalance in fluxes.

Based on our observation that sites where the soil exchangeable reservoir is isotopically lighter than external inputs also generally have an exchangeable reservoir that is dominated by bedrock weathering inputs, we hypothesize that the ability for biomass to obtain nutrients from a source other than the soil exchangeable reservoir (i.e. “nutrient uplift”) is an important factor in determining whether the soil exchangeable reservoir will evolve to be isotopically lighter than external inputs..

The most intriguing situation is where the soil exchangeable reservoir is isotopically heavier than external inputs. Global measurements have observed that precipitation is a likely mix of sea salt, silicate and carbonate dust, with a $\delta^{44}Ca$ value too negative to produce soil $\delta^{44}Ca$ significantly heavier than external sources. To achieve this situation the biomass reservoir must be taking up more Ca from the soil exchangeable reservoir than it returns back to the soil exchangeable reservoir. Interestingly, these sites also have an exchangeable reservoir dominated by atmospheric inputs, potentially indicative of a situation

where the soil exchangeable reservoir is the dominant soil reservoir of Ca, as compared with sites that have a significant reservoir of mineral-bound Ca in the soil. While there are number of mechanisms that can allow biomass Ca to bypass the soil exchangeable reservoir, including direct deposition of litterfall on to stream channels and removal of biomass Ca via biological vectors, an aggrading biomass reservoir is an important mechanism for producing the observed soil exchangeable $\delta^{44}Ca$ values. In particular, this processes must be considered when interpreting soil exchangeable $\delta^{44}Ca$ values at study sites that are subjected to ecosystem-scale disturbance.

3.7 REFERENCES

Bagard M-L, Schmitt A-D, Chabaux F, et al (2013) Biogeochemistry of stable Ca and radiogenic Sr isotopes in a larch-covered permafrost-dominated watershed of Central Siberia. Geochimica et Cosmochimica Acta 114:169–187. doi: 10.1016/j.gca.2013.03.038

Beard KH, Vogt KA, Vogt DJ, et al (2005) Structural and Functional Responses of a Subtropical Forest to 10 Years of Hurricanes and Droughts. Ecological Monographs 75:345–361. doi: 10.2307/4539103

Blum JD, Dasch AA, Hamburg SP, et al (2008) Use of Foliar Ca/Sr Discrimination and $^{87}Sr/^{86}Sr$ Ratios to Determine Soil Ca Sources to Sugar Maple Foliage in a Northern Hardwood Forest. Biogeochemistry 87:287–296.

Blum JD, Klaue A, Nezat CA, et al (2002) Mycorrhizal weathering of apatite as an important calcium source in base-poor forest ecosystems. Nature 417:729–731. doi: 10.1038/nature00793

Bullen TD, Bailey SW (2005) Identifying calcium sources at an acid deposition-impacted spruce forest: a strontium isotope, alkaline earth element multi-tracer approach. Biogeochemistry 74:63–99. doi: 10.1007/s10533-004-2619-z

Bullen TD, Bailey SW, McGuire KJ, et al (2010) Understanding metal sources and transport processes in watersheds: a hydropedologic approach (Invited),Abstract B23K-06 presented at 2010 Fall Meeting, AGU, San Francisco, Calif., 13-17 Dec.

Bullen TD, Fitzpatrick JA, White AF, et al (2004) Calcium Stable Isotope Evidence for Three Soil Calcium Pools at a Granitoid Chronosequence. In: Proceedings of the Eleventh International Symposium on Water-Rock Interaction. Taylor and Francis, London, Saratoga Sprngs, New York, pp 813–817

Capo RC, Stewart BW, Chadwick OA (1998) Strontium isotopes as tracers of ecosystem processes: theory and methods. Geoderma 82:197–225. doi: 10.1016/S0016-7061(97)00102-X

Cenki-Tok B, Chabaux F, Lemarchand D, et al (2009) The impact of water–rock interaction and vegetation on calcium isotope fractionation in soil- and stream waters of a small, forested catchment (the Strengbach case). Geochimica et Cosmochimica Acta 73:2215–2228. doi: 10.1016/j.gca.2009.01.023

Cobert F, Schmitt A-D, Bourgeade P, et al (2011) Experimental identification of Ca isotopic fractionations in higher plants. Geochimica et Cosmochimica Acta 75:5467–5482. doi: 10.1016/j.gca.2011.06.032

Cromack Jr K, Sollins P, Graustein WC, et al (1979) Calcium oxalate accumulation and soil weathering in mats of the hypogeous fungus Hysterangium crassum. Soil Biology and Biochemistry 11:463–468. doi: 10.1016/0038-0717(79)90003-8

Dambrine E, Bonneau M, Ranger J, et al (1995) Cycling and Budgets of Acidity and Nutrients in Norway Spruce Stands in Northeastern France and the Erzgebirge (Czech Republic). In: Landmann G, Bonneau M, Kaennel M (eds) Forest Decline and Atmospheric Deposition Effects in the French Mountains. Springer Berlin Heidelberg, pp 233–258

Ewing SA, Yang W, DePaolo DJ, et al (2008) Non-biological fractionation of stable Ca isotopes in soils of the Atacama Desert, Chile. Geochimica et Cosmochimica Acta 72:1096–1110. doi: 10.1016/j.gca.2007.10.029

Fantle MS, Tipper ET (2014) Calcium isotopes in the global biogeochemical Ca cycle: Implications for development of a Ca isotope proxy. Earth-Science Reviews 129:148–177. doi: 10.1016/j.earscirev.2013.10.004

Fantle MS, Tollerud H, Eisenhauer A, Holmden C (2012) The Ca isotopic composition of dust-producing regions: Measurements of surface sediments in the Black Rock Desert, Nevada. Geochimica et Cosmochimica Acta 87:178–193. doi: 10.1016/j.gca.2012.03.037

Farkaš J, Déjeant A, Novák M, Jacobsen SB (2011) Calcium isotope constraints on the uptake and sources of Ca2+ in a base-poor forest: A new concept of combining stable (δ44/42Ca) and radiogenic (εCa) signals. Geochimica et Cosmochimica Acta 75:7031–7046. doi: 10.1016/j.gca.2011.09.021

Fichter J, Dambrine E, Turpault M-P, Ranger J (1998) Base Cation Supply in Spruce and Beech Ecosystems of the Strengbach Catchment (Vosges Mountains, N-E France). Water, Air, and Soil Pollution 104:125–148. doi: 10.1023/A:1004966302517

Franceschi VR, Horner HT (1980) Calcium Oxalate Crystals in Plants. Botanical Review 46:361–427.

Gadd GM (1999) Fungal Production of Citric and Oxalic Acid: Importance in Metal Speciation, Physiology and Biogeochemical Processes. In: Advances in Microbial Physiology. Academic Press, pp 47–92

Graustein WC, Cromack K, Sollins P (1977) Calcium Oxalate: Occurrence in Soils and Effect on Nutrient and Geochemical Cycles. Science 198:1252–1254. doi: 10.1126/science.198.4323.1252

Heartsill Scalley T, Scatena FN, Lugo AE, et al (2010) Changes in Structure, Composition, and Nutrients During 15 Yr of Hurricane-Induced Succession in a Subtropical Wet Forest in Puerto Rico. Biotropica 42:455–463. doi: 10.1111/j.1744-7429.2009.00609.x

Heartsill Scalley T, Scatena FN, Moya S, Lugo AE (2012) Long-term dynamics of organic matter and elements exported as coarse particulates from two Caribbean montane watersheds. Journal of Tropical Ecology 28:127–139. doi: 10.1017/S0266467411000733

Hindshaw RS, Reynolds BC, Wiederhold JG, et al (2012) Calcium isotope fractionation in alpine plants. Biogeochemistry. doi: 10.1007/s10533-012-9732-1

Hindshaw RS, Reynolds BC, Wiederhold JG, et al (2011) Calcium isotopes in a proglacial weathering environment: Damma glacier, Switzerland. Geochimica et Cosmochimica Acta 75:106–118. doi: 10.1016/j.gca.2010.09.038

Holmden C, Bélanger N (2010) Ca isotope cycling in a forested ecosystem. Geochimica et Cosmochimica Acta 74:995–1015. doi: 10.1016/j.gca.2009.10.020

Jobbágy EG, Jackson RB (2004) The Uplift of Soil Nutrients by Plants: Biogeochemical Consequences across Scales. Ecology 85:2380–2389.

Jobbágy EG, Jackson RB (2001) The Distribution of Soil Nutrients with Depth: Global Patterns and the Imprint of Plants. Biogeochemistry 53:51–77.

Joslin JD, Kelly JM, Van Miegroet H (1992) Soil Chemistry and Nutrition of North American Spruce-Fir Stands: Evidence for Recent Change. Journal of Environmental Quality 21:12–30. doi: 10.2134/jeq1992.00472425002100010002x

Kennedy MJ, Chadwick OA, Vitousek PM, et al (1998) Changing sources of base cations during ecosystem development, Hawaiian Islands. Geology 26:1015–1018. doi: 10.1130/0091-7613(1998)026<1015:CSOBCD>2.3.CO;2

Lawrence GB, Fuller RD, Driscoll CT (1987) Release of Aluminum following Whole-Tree Harvesting at the Hubbard Brook Experimental Forest, New Hampshire1. Journal of Environment Quality 16:383. doi: 10.2134/jeq1987.00472425001600040016x

Likens GE, Driscoll CT, Buso DC (1996) Long-Term Effects of Acid Rain: Response and Recovery of a Forest Ecosystem. Science 272:244–246. doi: 10.1126/science.272.5259.244

Likens GE, Driscoll CT, Buso DC, et al (1998) The Biogeochemistry of Calcium at Hubbard Brook. Biogeochemistry 41:89–173.

Miller EK, Blum JD, Friedland AJ (1993) Determination of soil exchangeable-cation loss and weathering rates using Sr isotopes. Nature 362:438–441. doi: 10.1038/362438a0

Mitchell MJ, Raynal DJ, Driscoll CT (1996) Biogeochemistry of a forested watershed in the central Adirondack Mountains: Temporal changes and mass balances. Water, Air, and Soil Pollution 88:355–369. doi: 10.1007/BF00294111

Moore J, Jacobson AD, Holmden C, Craw D (2013) Tracking the relationship between mountain uplift, silicate weathering, and long-term CO2 consumption with Ca isotopes: Southern Alps, New Zealand. Chemical Geology 341:110–127. doi: 10.1016/j.chemgeo.2013.01.005

Page BD, Bullen TD, Mitchell MJ (2008) Influences of calcium availability and tree species on Ca isotope fractionation in soil and vegetation. Biogeochemistry 88:1–13. doi: 10.1007/s10533-008-9188-5

Porder S, Chadwick OA (2009) Climate and Soil-Age Constraints on Nutrient Uplift and Retention by Plants. Ecology 90:623–636.

Porder S, Clark DA, Vitousek PM (2006) Persistence of Rock-Derived Nutrients in the Wet Tropical Forests of La Selva, Costa Rica. Ecology 87:594–602.

Poszwa A, Dambrine E, Ferry B, et al (2002) Do Deep Tree Roots Provide Nutrients to the Tropical Rainforest? Biogeochemistry 60:97–118.

Probst A, Dambrine E, Viville D, Fritz B (1990) Influence of acid atmospheric inputs on surface water chemistry and mineral fluxes in a declining spruce stand within a small granitic catchment (Vosges Massif, France). Journal of Hydrology 116:101–124. doi: 10.1016/0022-1694(90)90118-H

Probst A, El Gh'mari A, Aubert D, et al (2000) Strontium as a tracer of weathering processes in a silicate catchment polluted by acid atmospheric inputs, Strengbach, France. Chemical Geology 170:203–219. doi: 10.1016/S0009-2541(99)00248-X

Probst A, Viville D, Fritz B, et al (1992) Hydrochemical budgets of a small forested granitic catchment exposed to acid deposition: The strengbach catchment case study (Vosges massif, France). Water, Air, and Soil Pollution 62:337–347. doi: 10.1007/BF00480265

Reuss JO, Johnson DW (1986) Acid depostion and acidification of soils and waters. viii + 119pp.

Scatena FN, Moya S, Estrada C, Chinea JD (1996) The First Five Years in the Reorganization of Aboveground Biomass and Nutrient Use Following Hurricane Hugo in the Bisley Experimental Watersheds, Luquillo Experimental Forest, Puerto Rico. Biotropica 28:424–440. doi: 10.2307/2389086

Schmitt A-D, Chabaux F, Stille P (2003) The calcium riverine and hydrothermal isotopic fluxes and the oceanic calcium mass balance☆. Earth and Planetary Science Letters 213:503–518. doi: 10.1016/S0012-821X(03)00341-8

Schmitt A-D, Stille P (2005) The source of calcium in wet atmospheric deposits: Ca-Sr isotope evidence. Geochimica et Cosmochimica Acta 69:3463–3468. doi: 10.1016/j.gca.2004.11.010

Tipper ET, Galy A, Bickle MJ (2006) Riverine evidence for a fractionated reservoir of Ca and Mg on the continents: Implications for the oceanic Ca cycle. Earth and Planetary Science Letters 247:267–279. doi: 10.1016/j.epsl.2006.04.033

White AF, Schulz M, Bullen T, et al (2010) Use of elemental and isotopic ratios to distinguish between lithogenic and biogenic sources of soil mineral nutrients. In: 19 th World Congress of Soil Science, Soil Solutions for a Changing World. Brisbane, Australia, pp 214–217

Wiegand BA, Chadwick OA, Vitousek PM, Wooden JL (2005) Ca cycling and isotopic fluxes in forested ecosystems in Hawaii. Geophysical Research Letters 32:L11404. doi: 10.1029/2005GL022746

Wiegand BA, Schwendenmann L (2013) Determination of Sr and Ca sources in small tropical catchments (La Selva, Costa Rica) – A comparison of Sr and Ca isotopes. Journal of Hydrology 488:110–117. doi: 10.1016/j.jhydrol.2013.02.044

3.8 SUPPLEMENTAL INFORMATION

3.8.1 Figures

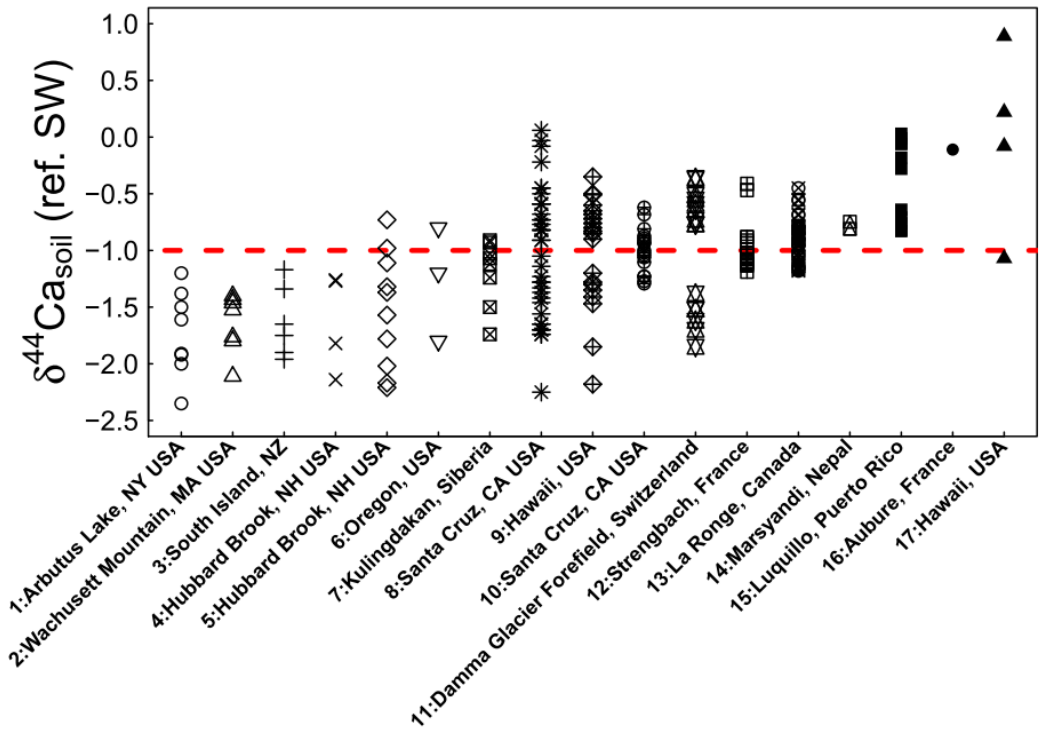

Figure 3.1. Plot of studies that measured actively cycled soil Ca stable Ca isotope ratios. Studies shown in order of most negative $\delta^{44}Ca_{soil}$ to most positive. Red dashed line indicates approximate average of external Ca sources (atmospheric deposition and weathering). Study ID is indicated by number preceding study location. Refer to table 4.1 for Study ID key.

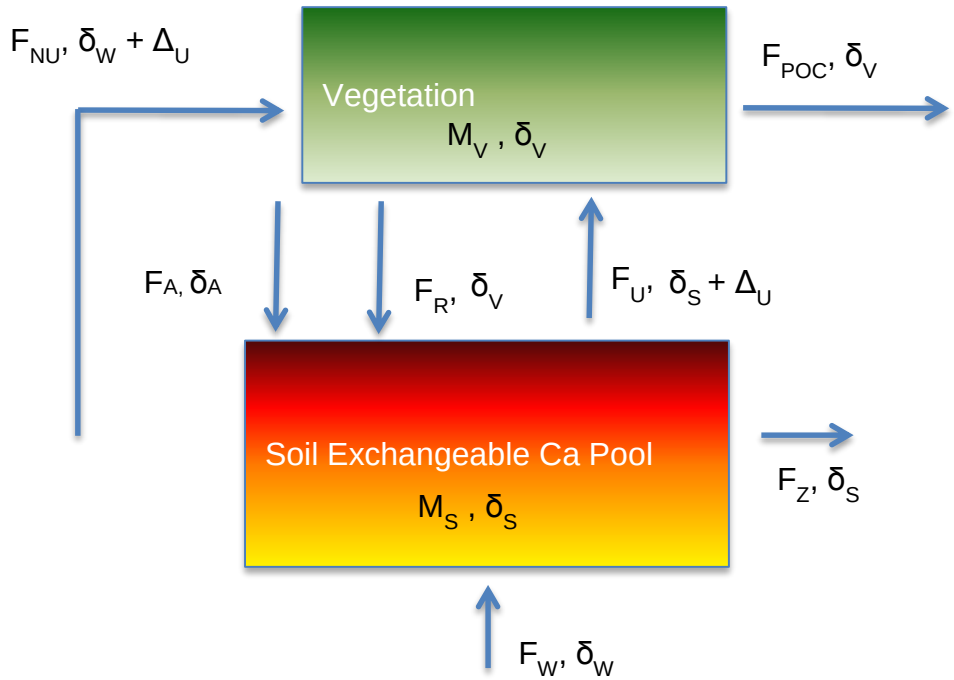

Figure 3.2. Ca stable isotope box model diagram. See text for definition of flux and reservoir abbreviations.

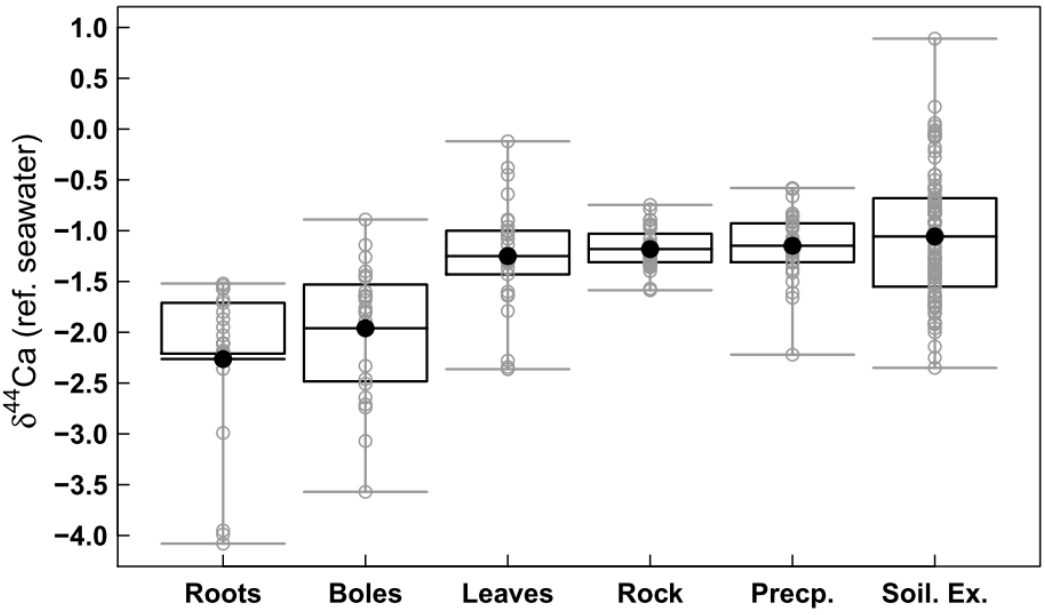

Figure 3.3. Compilation of vegetation compartment and external Ca source input (rock and precipitation) $\delta^{44}Ca$ values. Solid circle represents average value, top and bottom of box represent 1st and 3rd quartiles, respectively, and wiskers represent maximum and minimum values, respectively.

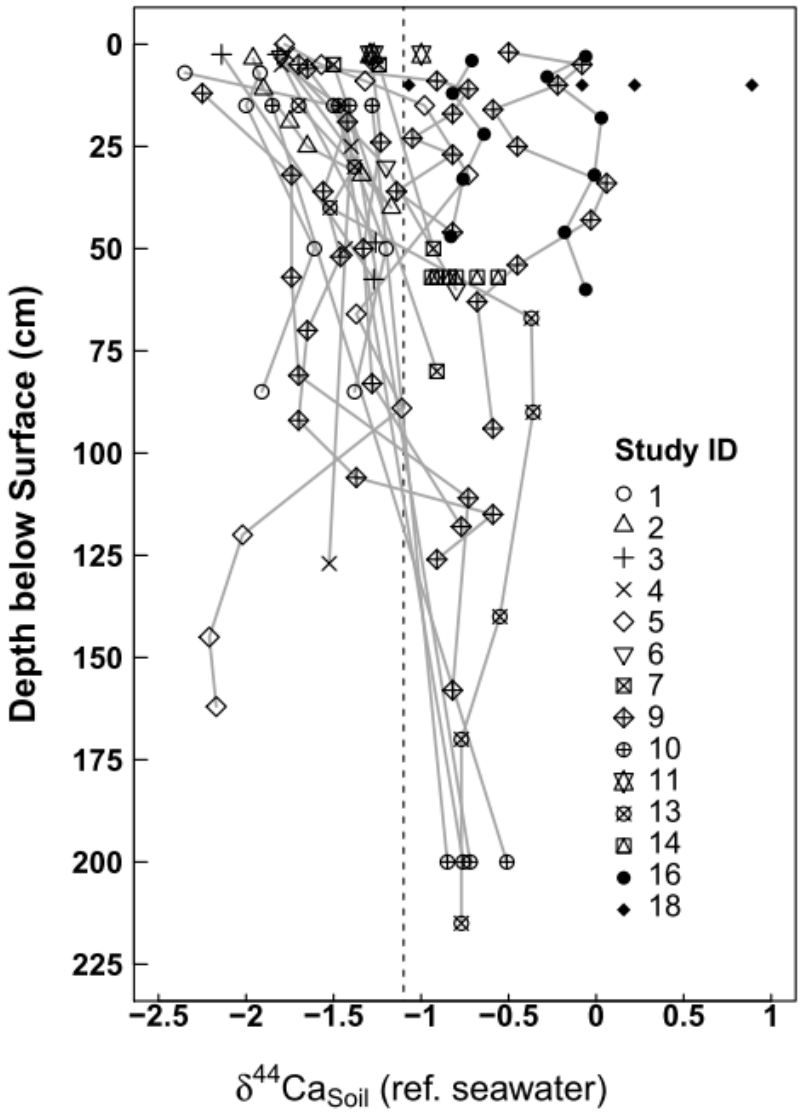

Figure 3.4. Soil depth profiles for soil exchangeable $\delta^{44}Ca$ ($\delta^{44}Ca_{soil}$). See table 1 for study ID key.

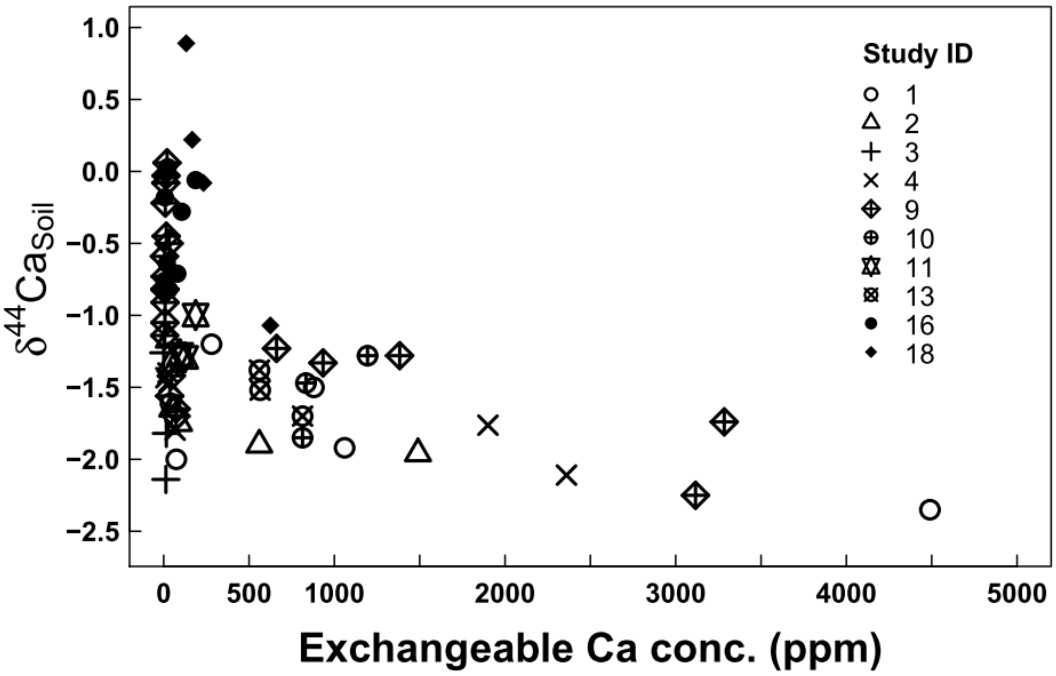

Figure 3.5. Relationship between $\delta^{44}Ca_{soil}$ (soil exchangeable Ca only) and soil exchangeable Ca concentration (ppm) for samples in the upper 50cm of soil.

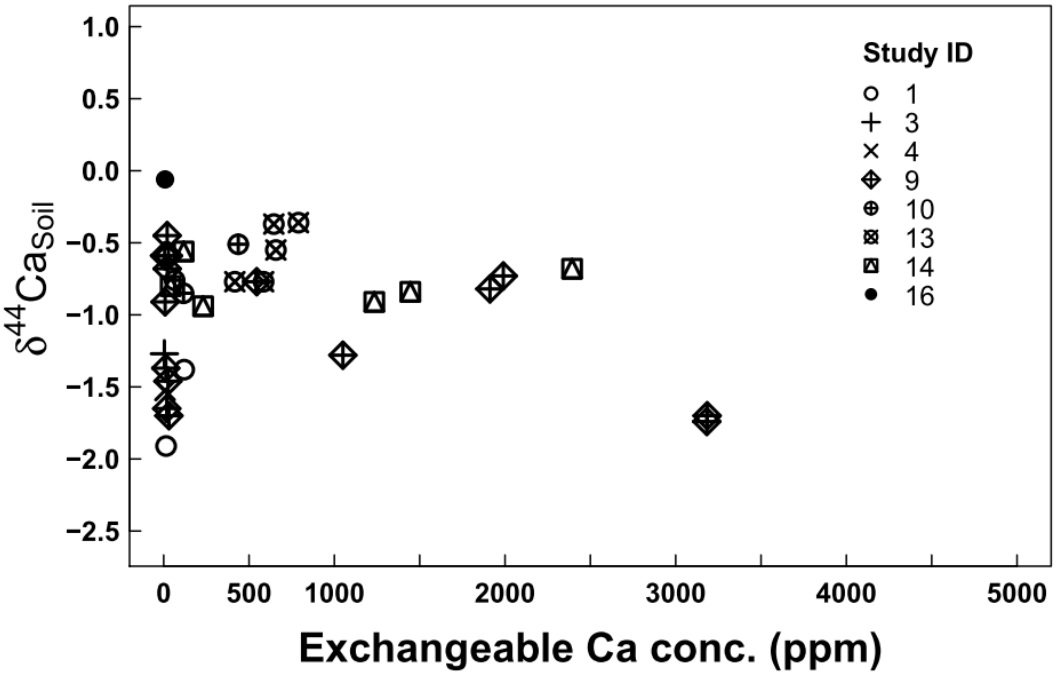

Figure 3.6. Relationship between $\delta^{44}Ca_{soil}$ (soil exchangeable Ca only) and soil exchangeable Ca concentration (ppm) for samples collected greater than 50cm below soil surface.

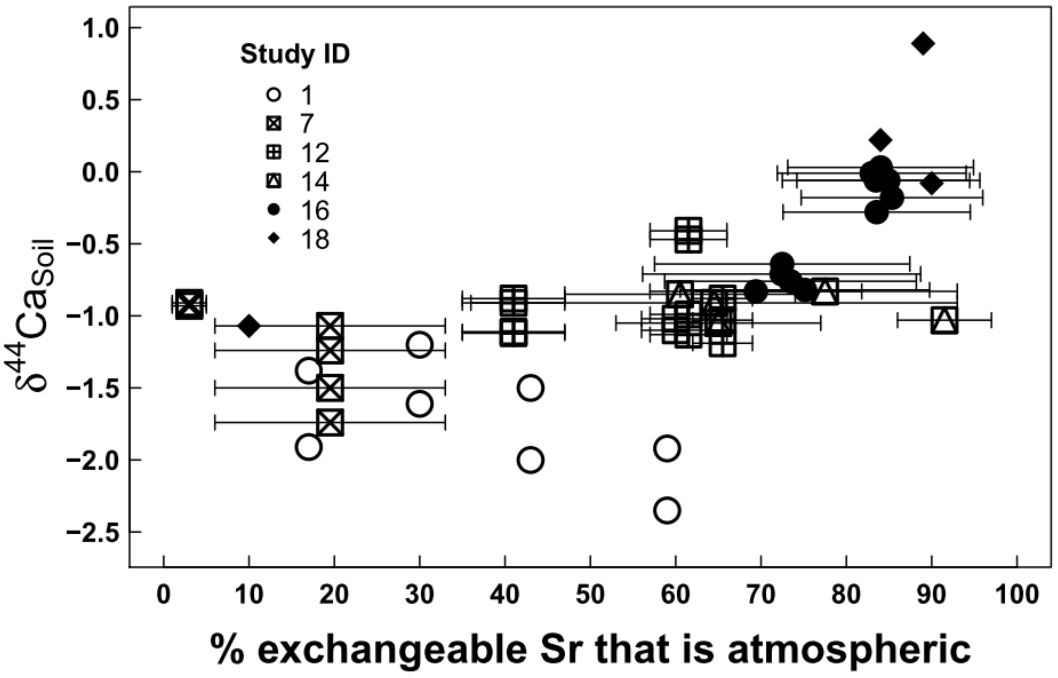

Figure 3.7. Relationship between $\delta^{44}Ca_{soil}$ and the percentage of exchangeable Sr that was derived from atmospheric deposition. See table 4.1 for Study ID key.

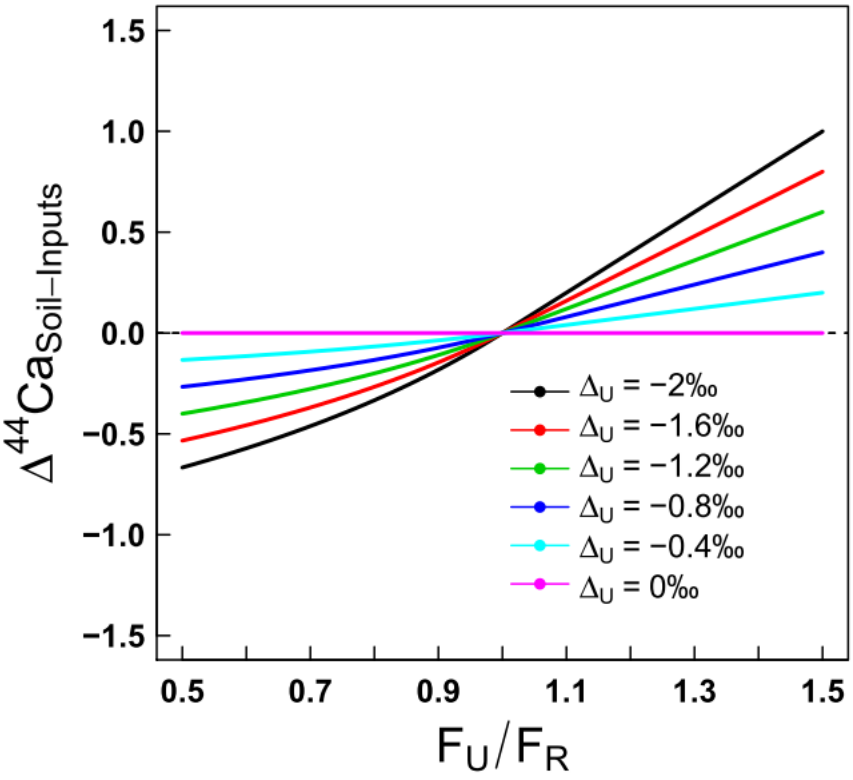

Figure 3.8. Steady-state model results for $\Delta^{44}Ca_{soil\text{-}Inputs}$ (permil difference between the soil exchangeable reservoir and external inputs) for various values of Δ_U and the ratio F_U/F_R. See text for definition of F_U and F_R.

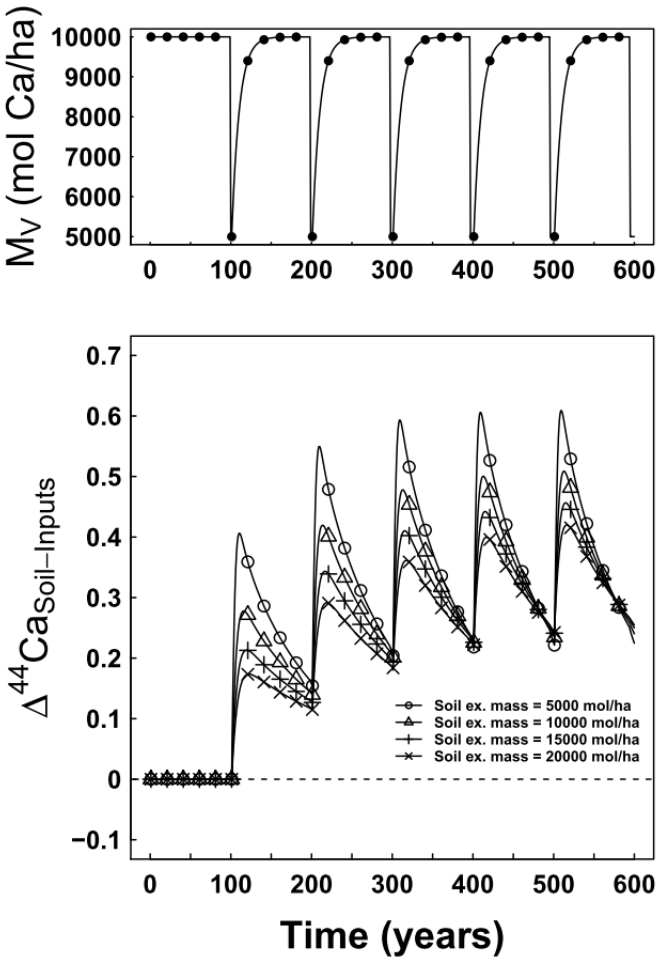

Fig. 3.9. Dynamic model run simulating the effect of a reoccurring disturbance on soil exchangeable $\delta^{44}Ca$, here represented as $\Delta^{44}Ca_{soil\text{-}Inputs}$ (‰ difference between the soil exchangeable reservoir and external inputs). In this simulation, the disturbance occurs every 100 year and reduces biomass by 50%. To demonstrate the effect of soil reservoir size on the excursion in soil $\delta^{44}Ca$ from initial conditions, the model was run with different initial sizes of soil exchangeable reservoir as shown in the bottom panel.

3.8.2 Tables

Table 3.1. Study ID and reference key.

Study ID	Reference	Location
1	Page et al. (2008)	Arbutus Lake Watershed, NY USA
2	Farkas et al. (2011)	Wachusett Mountain, MA USA
3	Moore et al. (2013)	South Island, NZ
4	Takagi (2015)	Hubbard Brook, NH USA
5	Bullen (2011)	Hubbard Brook, NH USA
6	Perakis et al. (2006)	Oregon, USA
7	Bagard et al. (2013)	Kulingdakan watershed, Central Siberian Plateau
8	White et al. (2010)	Santa Cruz, CA, USA
9	Chadwick and Bullen (in prep.)	Hawaii, USA
10	Bullen et al. (2004)	Santa Cruz, CA USA
11	Hindshaw et al. (2010)	Damma Glacier Forefield, Switzerland
12	Cenki-tok et al. (2009)	Strengbach, France
13	Holmden and Belanger (2009)	La Ronge, Canada
14	Tipper et al. (2006)	Marsyandi_catchment_Nepal
15	Takagi (2015)	Luquillo, Puerto Rico
16	Schmitt et al. (2003)	Aubure, France
17	Wiegand et al. (2005)	Hawaii, USA
18	Schmitt et al. (2005)	Multiple Sites
19	Wiegand and Schwendenmann (2013)	La Selva, Costa Rica

Table 3.2. Summary of Atmospheric deposition and bedrock Ca stable Isotopes measurements.

StudyID	Study Site	$\delta^{44}Ca_{SW}$ (‰ ref. seawater)	Type	$\delta^{44}Ca$ reported	Sample Type	Method
2	Wachusett Mountain, MA USA	-0.98	Rainfall	$^{44/40}Ca$ (ref. 915a)	-	-
2	Wachusett Mountain, MA USA	-0.92	Snow	$^{44/40}Ca$ (ref. 915a)	-	-
2	Wachusett Mountain, MA USA	-1.24	Rock	$^{44/40}Ca$ (ref. 915a)	Wachusett_Granodiorite	1N_HNO3_Leach
2	Wachusett Mountain, MA USA	-1.31	Rock	$^{44/40}Ca$ (ref. 915a)	Wachusett_Granodiorite	15N_HNO3_Leach
2	Wachusett Mountain, MA USA	-1.30	Rock	$^{44/40}Ca$ (ref. 915a)	Wachusett_Granodiorite	Bulk
3	South Island, NZ	-1.14	Rock	$^{44/40}Ca$ (ref. seawater)	Greywacke	Residue
3	South Island, NZ	-1.17	Rock	$^{44/40}Ca$ (ref. seawater)	Greywacke	Residue
3	South Island, NZ	-1.35	Rock	$^{44/40}Ca$ (ref. seawater)	Argillite	Residue
3	South Island, NZ	-1.31	Rock	$^{44/40}Ca$ (ref. seawater)	Schist	Residue
3	South Island, NZ	-1.32	Rock	$^{44/40}Ca$ (ref. seawater)	Schist	Residue
3	South Island, NZ	-1.26	Rock	$^{44/40}Ca$ (ref. seawater)	Schist	Residue
3	South Island, NZ	-1.21	Rock	$^{44/40}Ca$ (ref. seawater)	Schist	Residue
4	Hubbard Brook, NH USA	-1.27	Rock	$^{44/40}Ca$ (ref. seawater)	Rangely_Formation	Bulk
7	Kulingdakan, Siberia	-1.15	Snow	$^{44/40}Ca$ (ref. 915a)	-	-
7	Kulingdakan, Siberia	-1.1	Snow	$^{44/40}Ca$ (ref. 915a)	-	-
7	Kulingdakan, Siberia	-1.08	Rock	$^{44/40}Ca$ (ref. 915a)	Basalt	Bulk
8	Santa Cruz, CA USA	-1.7761	Rainfall	$^{44/40}Ca$ (ref. seawater)	-	-
8	Santa Cruz, CA USA	-1.5914	Rainfall	$^{44/40}Ca$ (ref. seawater)	-	-
8	Santa Cruz, CA USA	-1.4158	Rainfall	$^{44/40}Ca$ (ref. seawater)	-	-
8	Santa Cruz, CA USA	-1.3482	Rainfall	$^{44/40}Ca$ (ref. seawater)	-	-
8	Santa Cruz, CA USA	-0.7896	Rainfall	$^{44/40}Ca$ (ref. seawater)	-	-
8	Santa Cruz, CA USA	-0.605	Rainfall	$^{44/40}Ca$ (ref. seawater)	-	-
11	Damma Glacier Forefield, Switzerland	-0.91	Rainfall	$^{44/42}Ca$ (ref. 915a)	-	-

Table 3.2. Continued.

StudyID	Study Site	$\delta^{44}Ca_{SW}$ (‰ ref. seawater)	Type	$\delta^{44}Ca$ reported	Sample Type	Method
11	Damma Glacier Forefield, Switzerland	-1.12	Rainfall	$^{44/42}Ca$ (ref. 915a)	-	-
11	Damma Glacier Forefield, Switzerland	-1.12	Rainfall	$^{44/42}Ca$ (ref. 915a)	-	-
11	Damma Glacier Forefield, Switzerland	-0.85	Snow	$^{44/42}Ca$ (ref. 915a)	-	-
11	Damma Glacier Forefield, Switzerland	-0.66	Snow	$^{44/42}Ca$ (ref. 915a)	-	-
11	Damma Glacier Forefield, Switzerland	-0.89	Rock	$^{44/42}Ca$ (ref. 915a)	-	Bulk
11	Damma Glacier Forefield, Switzerland	-1.15	Rock	$^{44/42}Ca$ (ref. 915a)	-	Bulk
11	Damma Glacier Forefield, Switzerland	-0.96	Rock	$^{44/42}Ca$ (ref. 915a)	-	Bulk
11	Damma Glacier Forefield, Switzerland	-0.75	Rock	$^{44/42}Ca$ (ref. 915a)	-	Bulk
11	Damma Glacier Forefield, Switzerland	-1.12	Rock	$^{44/42}Ca$ (ref. 915a)	-	Bulk
11	Damma Glacier Forefield, Switzerland	-0.94	Rock	$^{44/42}Ca$ (ref. 915a)	-	Bulk
11	Damma Glacier Forefield, Switzerland	-0.89	Rock	$^{44/42}Ca$ (ref. 915a)	-	Bulk
11	Damma Glacier Forefield, Switzerland	-0.83	Mineral	$^{44/42}Ca$ (ref. 915a)	Biotite	-
11	Damma Glacier Forefield, Switzerland	-0.89	Mineral	$^{44/42}Ca$ (ref. 915a)	Plagioclase	-
11	Damma Glacier Forefield, Switzerland	-1.12	Mineral	$^{44/42}Ca$ (ref. 915a)	K_Feldspar	-
12	Strengbach, France	-1.31	Rainfall	$^{44/40}Ca$ (ref. 915a)	-	-
12	Strengbach, France	-0.95	Rainfall	$^{44/40}Ca$ (ref. 915a)	-	-
12	Strengbach, France	-0.59	Snow	$^{44/40}Ca$ (ref. 915a)	-	-
12	Strengbach, France	-1.59	Throughfall	$^{44/40}Ca$ (ref. 915a)	-	-
12	Strengbach, France	-1.08	Throughfall	$^{44/40}Ca$ (ref. 915a)	-	-
13	La Ronge, Canada	-1.31	Rainfall	$^{44/40}Ca$ (ref. seawater)	-	-
13	La Ronge, Canada	-1.31	Rainfall	$^{44/40}Ca$ (ref. seawater)	-	-
13	La Ronge, Canada	-1.21	Snow	$^{44/40}Ca$ (ref. seawater)	-	-
13	La Ronge, Canada	-1.20	Snow	$^{44/40}Ca$ (ref. seawater)	-	-

Table 3.2. Continued.

StudyID	Study Site	$\delta^{44}Ca_{SW}$ (‰ ref. seawater)	Type	$\delta^{44}Ca$ reported	Sample Type	Method
13	La Ronge, Canada	-1.41	Snow	$^{44/40}Ca$ (ref. seawater)	-	-
13	La Ronge, Canada	-1.25	Snow	$^{44/40}Ca$ (ref. seawater)	-	-
13	La Ronge, Canada	-1.22	Snow	$^{44/40}Ca$ (ref. seawater)	-	-
13	La Ronge, Canada	-1.27	Rock	$^{44/40}Ca$ (ref. seawater)	Granite	Bulk
13	La Ronge, Canada	-1.36	Rock	$^{44/40}Ca$ (ref. seawater)	Granite	1N_HNO3_Leach
13	La Ronge, Canada	-1.57	Rock	$^{44/40}Ca$ (ref. seawater)	Granite	15N_HNO3_Leach
14	Marsyandi, Nepal	-1.23	Rock	$^{44/42}Ca$ (ref. 915a)	High_Himalayan_para-gneiss	Bulk
14	Marsyandi, Nepal	-1.23	Rock	$^{44/42}Ca$ (ref. 915a)	High_Himalayan_para-gneiss	residue
14	Marsyandi, Nepal	-0.79	Rock	$^{44/42}Ca$ (ref. 915a)	High_Himalayan_para-gneiss	leachate
14	Marsyandi, Nepal	-1.25	Rock	$^{44/42}Ca$ (ref. 915a)	Limestone_leachate	leachate
14	Bhote Kosi, Nepal	-1.59	Rock	$^{44/42}Ca$ (ref. 915a)	Travertine	Bulk
14	Bhote Kosi, Nepal	-1.33	Rock	$^{44/42}Ca$ (ref. 915a)	Travertine	Bulk
14	Bhote Kosi, Nepal	-1.40	Rock	$^{44/42}Ca$ (ref. 915a)	Travertine	Bulk
15	Luquillo, Puerto Rico	-1.07	Rainfall	$^{44/40}Ca$ (ref. seawater)	-	-
15	Luquillo, Puerto Rico	-0.98	Rock	$^{44/40}Ca$ (ref. seawater)	Vocanoclastics	Bulk
15	Luquillo, Puerto Rico	-0.95	Rock	$^{44/40}Ca$ (ref. seawater)	Granodiorite	Bulk
16	Aubure, France	-1.31	Rainfall	$^{44/40}Ca$ (ref. seawater)	-	-
16	Aubure, France	-0.87	Rainfall	$^{44/40}Ca$ (ref. seawater)	-	-
16	Aubure, France	-1.48	Mineral	$^{44/40}Ca$ (ref. seawater)	Apatite	-
18	Strausburg,France	-1.19	Rainfall	$^{44/40}Ca$ (ref. 915a)	-	-
18	Luxemburg, Lux	-1.61	Rainfall	$^{44/40}Ca$ (ref. 915a)	-	-
18	Berkeley, CA USA	-1.50	Rainfall	$^{44/40}Ca$ (ref. 915a)	-	-
18	Normandie, France	-1.15	Rainfall	$^{44/40}Ca$ (ref. 915a)	-	-

Table 3.2. Continued.

StudyID	Study Site	$\delta^{44}Ca_{SW}$ (‰ ref. seawater)	Type	$\delta^{44}Ca$ reported	Sample Type	Method
18	Zweisimmen	-1.38	Rainfall	$^{44/40}Ca$ (ref. 915a)	-	-
18	Cadarache	-1.66	Snow	$^{44/40}Ca$ (ref. 915a)	-	-
18	Japan	-1.20	Snow	$^{44/40}Ca$ (ref. 915a)	-	-
18	Aubure_France	-1.13	Throughfall	$^{44/40}Ca$ (ref. 915a)	-	-
19	La Selva, Costa Rica	-0.58	Rainfall	$^{44/40}Ca$ (ref. seawater)	-	-
19	La Selva, Costa Rica	-0.83	Rainfall	$^{44/40}Ca$ (ref. seawater)	-	-
19	La Selva, Costa Rica	-2.22	Rainfall	$^{44/40}Ca$ (ref. seawater)	-	-
19	La Selva, Costa Rica	-0.90	Rainfall	$^{44/40}Ca$ (ref. seawater)	-	-
19	La Selva, Costa Rica	-0.96	Rainfall	$^{44/40}Ca$ (ref. seawater)	-	-

Table 3.3. Summary of soil exchangeable Ca stable Isotopes measurements. See Table 3.1 for Study ID key.

StudyID	Study Site	Plot	Horizon or depth interval	$\delta^{44}Ca_{SW}$ (‰ ref. seawater)	[Ca] (ppm)	Exchangeable Method	$\delta^{44}Ca$ reported	Exch.Sr atm. derived
1	Arbutus Lake, NY USA	Catchment 14	Oe_and_Oa	-2.35	4490	1N NH4OAc	$^{44/40}Ca$ (ref. seawater)	59[a]
1	Arbutus Lake, NY USA	Catchment 14	15	-1.5	880	1N NH4OAc	$^{44/40}Ca$ (ref. seawater)	43[a]
1	Arbutus Lake, NY USA	Catchment 14	50	-1.2	280	1N NH4OAc	$^{44/40}Ca$ (ref. seawater)	30[a]
1	Arbutus Lake, NY USA	Catchment 14	70-100	-1.38	120	1N NH4OAc	$^{44/40}Ca$ (ref. seawater)	17[a]
1	Arbutus Lake, NY USA	Catchment 15	Oe_and_Oa	-1.92	1060	1N NH4OAc	$^{44/40}Ca$ (ref. seawater)	59[a]
1	Arbutus Lake, NY USA	Catchment 15	15	-2	74	1N NH4OAc	$^{44/40}Ca$ (ref. seawater)	43[a]
1	Arbutus Lake, NY USA	Catchment 15	50	-1.61	40	1N NH4OAc	$^{44/40}Ca$ (ref. seawater)	30[a]
1	Arbutus Lake, NY USA	Catchment 15	70-100	-1.91	14	1N NH4OAc	$^{44/40}Ca$ (ref. seawater)	17[a]
2	Wachusett Mountain, MA USA	1	0-7	-1.96	1490	0.1M BaCl-H2O	$^{44/40}Ca$ (ref. 915a)	-
2	Wachusett Mountain, MA USA	1	7-15	-1.9	560	0.1M BaCl-H2O	$^{44/40}Ca$ (ref. 915a)	-
2	Wachusett Mountain, MA USA	1	15-22	-1.75	90	0.1M BaCl-H2O	$^{44/40}Ca$ (ref. 915a)	-
2	Wachusett Mountain, MA USA	1	22-29	-1.65	50	0.1M BaCl-H2O	$^{44/40}Ca$ (ref. 915a)	-
2	Wachusett Mountain, MA USA	1	29-36	-1.34	40	0.1M BaCl-H2O	$^{44/40}Ca$ (ref. 915a)	-
2	Wachusett Mountain, MA USA	1	36-45	-1.17	30	0.1M BaCl-H2O	$^{44/40}Ca$ (ref. 915a)	-
3	South Island, NZ	SL01	0-5	-1.82	15.6	1M NH4Cl	$^{44/40}Ca$ (ref. seawater)	-
3	South Island, NZ	SL01	46-51	-1.26	0.34	1M NH4Cl	$^{44/40}Ca$ (ref. seawater)	-
3	South Island, NZ	SL04	0-5	-2.14	12.9	1M NH4Cl	$^{44/40}Ca$ (ref. seawater)	-
3	South Island, NZ	SL04	55-60	-1.27	4.03	1M NH4Cl	$^{44/40}Ca$ (ref. seawater)	-
4	Hubbard Brook, NH USA	WS-5	Oie	-2.11	2360	1M NH4Cl	$^{44/40}Ca$ (ref. seawater)	-
4	Hubbard Brook, NH USA	WS-5	Oa	-1.763	1899.86	1M NH4Cl	$^{44/40}Ca$ (ref. seawater)	-
4	Hubbard Brook, NH USA	WS-5	0-10	-1.798	66.98	1M NH4Cl	$^{44/40}Ca$ (ref. seawater)	-
4	Hubbard Brook, NH USA	WS-5	10-20	-1.463	31.19	1M NH4Cl	$^{44/40}Ca$ (ref. seawater)	-
4	Hubbard Brook, NH USA	WS-5	20+	-1.4	25.03	1M NH4Cl	$^{44/40}Ca$ (ref. seawater)	-
4	Hubbard Brook, NH USA	WS-5	C	-1.433	12.76	1M NH4Cl	$^{44/40}Ca$ (ref. seawater)	-

Table 3.3. Continued.

StudyID	Study Site	Plot	Horizon or depth interval	$\delta^{44}Ca_{SW}$ (‰ ref. seawater)	[Ca] (ppm)	Exchangeable Method	$\delta^{44}Ca$ reported	Exch.Sr atm. derived
4	Hubbard Brook, NH USA	WS-5	Till	-1.525	7.76	1M NH4Cl	$^{44/40}Ca$ (ref. seawater)	-
5	Hubbard Brook, NH USA	WS-1	0	-1.78	NA	-	$^{44/40}Ca$ (ref. seawater)	-
5	Hubbard Brook, NH USA	WS-1	5	-1.57	NA	-	$^{44/40}Ca$ (ref. seawater)	-
5	Hubbard Brook, NH USA	WS-1	9	-1.32	NA	-	$^{44/40}Ca$ (ref. seawater)	-
5	Hubbard Brook, NH USA	WS-1	15	-0.98	NA	-	$^{44/40}Ca$ (ref. seawater)	-
5	Hubbard Brook, NH USA	WS-1	32	-0.73	NA	-	$^{44/40}Ca$ (ref. seawater)	-
5	Hubbard Brook, NH USA	WS-1	66	-1.37	NA	-	$^{44/40}Ca$ (ref. seawater)	-
5	Hubbard Brook, NH USA	WS-1	89	-1.11	NA	-	$^{44/40}Ca$ (ref. seawater)	-
5	Hubbard Brook, NH USA	WS-1	120	-2.02	NA	-	$^{44/40}Ca$ (ref. seawater)	-
5	Hubbard Brook, NH USA	WS-1	145	-2.21	NA	-	$^{44/40}Ca$ (ref. seawater)	-
5	Hubbard Brook, NH USA	WS-1	162	-2.17	NA	-	$^{44/40}Ca$ (ref. seawater)	-
6	Oregon, USA	1	3	-1.8	NA	1N NH4OAc	$^{44/40}Ca$ (ref. seawater)	-
6	Oregon, USA	1	30	-1.2	NA	1N NH4OAc	$^{44/40}Ca$ (ref. seawater)	-
6	Oregon, USA	1	60	-0.8	NA	1N NH4OAc	$^{44/40}Ca$ (ref. seawater)	-
7	Kulingdakan, Siberia	North Facing Hillslope	0-10	-1.24	NA	acetic acid	$^{44/40}Ca$ (ref. 915a)	6-33
7	Kulingdakan, Siberia	North Facing Hillslope	40-60	-0.93	NA	acetic acid	$^{44/40}Ca$ (ref. 915a)	1-5
7	Kulingdakan, Siberia	South Facing Hillslope	0-10	-1.5	NA	acetic acid	$^{44/40}Ca$ (ref. 915a)	6-33
7	Kulingdakan, Siberia	South Facing Hillslope	60-100	-0.91	NA	acetic acid	$^{44/40}Ca$ (ref. 915a)	1-5
8	Santa Cruz, CA USA	65 kya	15	-1.7	813.624	1N NH4OAc	$^{44/40}Ca$ (ref. seawater)	-
8	Santa Cruz, CA USA	65 kya	30	-1.38	561.12	1N NH4OAc	$^{44/40}Ca$ (ref. seawater)	-
8	Santa Cruz, CA USA	65 kya	40	-1.52	565.128	1N NH4OAc	$^{44/40}Ca$ (ref. seawater)	-
8	Santa Cruz, CA USA	65 kya	67	-0.37	645.288	1N NH4OAc	$^{44/40}Ca$ (ref. seawater)	-
8	Santa Cruz, CA USA	65 kya	90	-0.36	789.576	1N NH4OAc	$^{44/40}Ca$ (ref. seawater)	-
8	Santa Cruz, CA USA	65 kya	140	-0.55	657.312	1N NH4OAc	$^{44/40}Ca$ (ref. seawater)	-

Table 3.3. Continued.

StudyID	Study Site	Plot	Horizon or depth interval	$\delta^{44}Ca_{SW}$ (‰ ref. seawater)	[Ca] (ppm)	Exchangeable Method	$\delta^{44}Ca$ reported	Exch.Sr atm. derived
8	Santa Cruz, CA USA	65 kya	170	-0.77	416.832	1N NH4OAc	$^{44/40}Ca$ (ref. seawater)	-
8	Santa Cruz, CA USA	65 kya	215	-0.77	585.168	1N NH4OAc	$^{44/40}Ca$ (ref. seawater)	-
9	Hawaii, USA	Site B	4	-1.28	1382.76	0.1N NH4OAc	$^{44/40}Ca$ (ref. seawater)	-
9	Hawaii, USA	Site B	24	-1.23	661.32	0.1N NH4OAc	$^{44/40}Ca$ (ref. seawater)	-
9	Hawaii, USA	Site B	50	-1.33	933.864	0.1N NH4OAc	$^{44/40}Ca$ (ref. seawater)	-
9	Hawaii, USA	Site B	83	-1.28	1050.096	0.1N NH4OAc	$^{44/40}Ca$ (ref. seawater)	-
9	Hawaii, USA	Site B	118	-0.77	545.088	0.1N NH4OAc	$^{44/40}Ca$ (ref. seawater)	-
9	Hawaii, USA	Site I	12	-2.25	3116.22	0.1N NH4OAc	$^{44/40}Ca$ (ref. seawater)	-
9	Hawaii, USA	Site I	32	-1.74	3284.556	0.1N NH4OAc	$^{44/40}Ca$ (ref. seawater)	-
9	Hawaii, USA	Site I	57	-1.74	3182.352	0.1N NH4OAc	$^{44/40}Ca$ (ref. seawater)	-
9	Hawaii, USA	Site I	81	-1.7	3184.356	0.1N NH4OAc	$^{44/40}Ca$ (ref. seawater)	-
9	Hawaii, USA	Site I	111	-0.73	1989.972	0.1N NH4OAc	$^{44/40}Ca$ (ref. seawater)	-
9	Hawaii, USA	Site I	158	-0.82	1911.816	0.1N NH4OAc	$^{44/40}Ca$ (ref. seawater)	-
9	Hawaii, USA	Site L	2	-0.5	31.8836321	0.1N NH4OAc	$^{44/40}Ca$ (ref. seawater)	-
9	Hawaii, USA	Site L	5	-0.08	12.6006877	0.1N NH4OAc	$^{44/40}Ca$ (ref. seawater)	-
9	Hawaii, USA	Site L	10	-0.22	9.52873155	0.1N NH4OAc	$^{44/40}Ca$ (ref. seawater)	-
9	Hawaii, USA	Site L	16	-0.59	4.72143532	0.1N NH4OAc	$^{44/40}Ca$ (ref. seawater)	-
9	Hawaii, USA	Site L	25	-0.45	15.2812384	0.1N NH4OAc	$^{44/40}Ca$ (ref. seawater)	-
9	Hawaii, USA	Site L	34	0.06	19.7950082	0.1N NH4OAc	$^{44/40}Ca$ (ref. seawater)	-
9	Hawaii, USA	Site L	43	-0.03	14.3372083	0.1N NH4OAc	$^{44/40}Ca$ (ref. seawater)	-
9	Hawaii, USA	Site L	54	-0.45	20.3512548	0.1N NH4OAc	$^{44/40}Ca$ (ref. seawater)	-
9	Hawaii, USA	Site L	63	-0.68	20.8874758	0.1N NH4OAc	$^{44/40}Ca$ (ref. seawater)	-
9	Hawaii, USA	Site L	94	-0.59	28.0588433	0.1N NH4OAc	$^{44/40}Ca$ (ref. seawater)	-
9	Hawaii, USA	Site MF	5	-1.7	72.1977436	0.1N NH4OAc	$^{44/40}Ca$ (ref. seawater)	-

Table 3.3. Continued.

StudyID	Study Site	Plot	Horizon or depth interval	$\delta^{44}Ca_{SW}$ (‰ ref. seawater)	[Ca] (ppm)	Exchangeable Method	$\delta^{44}Ca$ reported	Exch.Sr atm. derived
9	Hawaii, USA	Site MF	9	-0.91	8.28393515	0.1N NH4OAc	$^{44/40}Ca$ (ref. seawater)	-
9	Hawaii, USA	Site MF	11	-0.73	8.6287953	0.1N NH4OAc	$^{44/40}Ca$ (ref. seawater)	-
9	Hawaii, USA	Site MF	17	-0.82	7.02495202	0.1N NH4OAc	$^{44/40}Ca$ (ref. seawater)	-
9	Hawaii, USA	Site MF	23	-1.05	7.3712586	0.1N NH4OAc	$^{44/40}Ca$ (ref. seawater)	-
9	Hawaii, USA	Site MF	27	-0.82	6.95095283	0.1N NH4OAc	$^{44/40}Ca$ (ref. seawater)	-
9	Hawaii, USA	Site MF	36	-1.14	5.65984341	0.1N NH4OAc	$^{44/40}Ca$ (ref. seawater)	-
9	Hawaii, USA	Site MF	46	-0.82	8.31809161	0.1N NH4OAc	$^{44/40}Ca$ (ref. seawater)	-
9	Hawaii, USA	Site M	6	-1.65	73.1692808	0.1N NH4OAc	$^{44/40}Ca$ (ref. seawater)	-
9	Hawaii, USA	Site M	19	-1.42	45.252491	0.1N NH4OAc	$^{44/40}Ca$ (ref. seawater)	-
9	Hawaii, USA	Site M	36	-1.56	35.821291	0.1N NH4OAc	$^{44/40}Ca$ (ref. seawater)	-
9	Hawaii, USA	Site M	52	-1.46	25.0704336	0.1N NH4OAc	$^{44/40}Ca$ (ref. seawater)	-
9	Hawaii, USA	Site M	70	-1.65	18.0376591	0.1N NH4OAc	$^{44/40}Ca$ (ref. seawater)	-
9	Hawaii, USA	Site M	92	-1.7	30.8431778	0.1N NH4OAc	$^{44/40}Ca$ (ref. seawater)	-
9	Hawaii, USA	Site M	106	-1.37	12.3996221	0.1N NH4OAc	$^{44/40}Ca$ (ref. seawater)	-
9	Hawaii, USA	Site M	115	-0.59	5.30961381	0.1N NH4OAc	$^{44/40}Ca$ (ref. seawater)	-
9	Hawaii, USA	Site M	126	-0.91	8.36242001	0.1N NH4OAc	$^{44/40}Ca$ (ref. seawater)	-
10	Santa Cruz, CA USA	90 kya	15	-1.85	813.6	1N NH4OAc	$^{44/40}Ca$ (ref. seawater)	-
10	Santa Cruz, CA USA	137 kya	15	-1.47	833.7	1N NH4OAc	$^{44/40}Ca$ (ref. seawater)	-
10	Santa Cruz, CA USA	182 kya	15	-1.41	NA	1N NH4OAc	$^{44/40}Ca$ (ref. seawater)	-
10	Santa Cruz, CA USA	227 kya	15	-1.28	1194.4	1N NH4OAc	$^{44/40}Ca$ (ref. seawater)	-
10	Santa Cruz, CA USA	90 kya	200	-0.51	436.9	1N NH4OAc	$^{44/40}Ca$ (ref. seawater)	-
10	Santa Cruz, CA USA	137 kya	200	-0.76	64.1	1N NH4OAc	$^{44/40}Ca$ (ref. seawater)	-
10	Santa Cruz, CA USA	182 kya	200	-0.72	NA	1N NH4OAc	$^{44/40}Ca$ (ref. seawater)	-
10	Santa Cruz, CA USA	227 kya	200	-0.85	116.2	1N NH4OAc	$^{44/40}Ca$ (ref. seawater)	-

Table 3.3. Continued.

StudyID	Study Site	Plot	Horizon or depth interval	$\delta^{44}Ca_{SW}$ (‰ ref. seawater)	[Ca] (ppm)	Exchangeable Method	$\delta^{44}Ca$ reported	Exch.Sr atm. derived
11	Damma Glacier Forefield, Switzerland	BL4a-1	0-5	-1.271157305	96.192	1M_NH4Cl	$^{44/42}Ca$ (ref. 915a)	-
11	Damma Glacier Forefield, Switzerland	BL17a-1	0-5	-1.292151881	125.0496	1M_NH4Cl	$^{44/42}Ca$ (ref. 915a)	-
11	Damma Glacier Forefield, Switzerland	BL24a-1	0-5	-0.998227821	187.1736	1M_NH4Cl	$^{44/42}Ca$ (ref. 915a)	-
13	La Ronge, Canada	Plot 1.1	50-65	-0.8	41.1	BaCl2	$^{44/40}Ca$ (ref. seawater)	-
13	La Ronge, Canada	Plot 1.2	50-65	-0.56	117	BaCl2	$^{44/40}Ca$ (ref. seawater)	-
13	La Ronge, Canada	Plot 1.3	50-65	-0.68	2393	BaCl2	$^{44/40}Ca$ (ref. seawater)	-
13	La Ronge, Canada	Plot 2.1	50-65	-0.84	1445	BaCl2	$^{44/40}Ca$ (ref. seawater)	-
13	La Ronge, Canada	Plot 2.2	50-65	-0.94	231	BaCl2	$^{44/40}Ca$ (ref. seawater)	-
13	La Ronge, Canada	Plot 2.3	50-65	-0.91	1234	BaCl2	$^{44/40}Ca$ (ref. seawater)	-
15	Luquillo, Puerto Rico	Bisley1	0-5	-0.06	187.16	1M NH4Cl	$^{44/40}Ca$ (ref. seawater)	72-94
15	Luquillo, Puerto Rico	Bisley1	5-10	-0.28	105.58	1M NH4Cl	$^{44/40}Ca$ (ref. seawater)	73-95
15	Luquillo, Puerto Rico	Bisley1	10-25	0.03	23.48	1M NH4Cl	$^{44/40}Ca$ (ref. seawater)	73-95
15	Luquillo, Puerto Rico	Bisley1	25-38	-0.01	11.79	1M NH4Cl	$^{44/40}Ca$ (ref. seawater)	72-94
15	Luquillo, Puerto Rico	Bisley1	38-53	-0.18	6.93	1M NH4Cl	$^{44/40}Ca$ (ref. seawater)	75-96
15	Luquillo, Puerto Rico	Bisley1	53-67	-0.06	7.91	1M NH4Cl	$^{44/40}Ca$ (ref. seawater)	74-96
15	Luquillo, Puerto Rico	Bisley1	67-87	NA	5.94	1M NH4Cl	$^{44/40}Ca$ (ref. seawater)	77-97
15	Luquillo, Puerto Rico	Bisley1	87-107	NA	4.27	1M NH4Cl	$^{44/40}Ca$ (ref. seawater)	82-100
15	Luquillo, Puerto Rico	Rio Icacos	0-8	-0.71	79.66	1M NH4Cl	$^{44/40}Ca$ (ref. seawater)	56-89
15	Luquillo, Puerto Rico	Rio Icacos	8-15	-0.82	30.11	1M NH4Cl	$^{44/40}Ca$ (ref. seawater)	61-90
15	Luquillo, Puerto Rico	Rio Icacos	15-28	-0.64	18.19	1M NH4Cl	$^{44/40}Ca$ (ref. seawater)	58-87
15	Luquillo, Puerto Rico	Rio Icacos	28-38	-0.76	5.97	1M NH4Cl	$^{44/40}Ca$ (ref. seawater)	59-88
15	Luquillo, Puerto Rico	Rio Icacos	38-55	-0.83	3.62	1M NH4Cl	$^{44/40}Ca$ (ref. seawater)	57-82
15	Luquillo, Puerto Rico	Rio Icacos	55-68	NA	5.13	1M NH4Cl	$^{44/40}Ca$ (ref. seawater)	-
15	Luquillo, Puerto Rico	Rio Icacos	68-78	NA	2.77	1M NH4Cl	$^{44/40}Ca$ (ref. seawater)	-

Table 3.3. Continued.

StudyID	Study Site	Plot	Horizon or depth interval	$\delta^{44}Ca_{SW}$ (‰ ref. seawater)	[Ca] (ppm)	Exchangeable Method	$\delta^{44}Ca$ reported	Exch.Sr atm. derived
15	Luquillo, Puerto Rico	Rio Icacos	78-104	NA	1.92	1M NH4Cl	$^{44/40}Ca$ (ref. seawater)	-
17	Hawaii, USA	Thurston	0-20	-1.07	625	1N NH4OAc	$^{44/40}Ca$ (ref. seawater)	10[b]
17	Hawaii, USA	Kohala	0-20	-0.08	233	1N NH4OAc	$^{44/40}Ca$ (ref. seawater)	90[b]
17	Hawaii, USA	kolekole	0-20	0.89	132	1N NH4OAc	$^{44/40}Ca$ (ref. seawater)	89[b]
17	Hawaii, USA	kokee	0-20	0.22	167	1N NH4OAc	$^{44/40}Ca$ (ref. seawater)	84[b]

[a]: exchangeable Sr isotope data from Miller et al. (1993)
[b]: exchangeable Sr isotope data from Kennedy et al. (1998).

Table 3.4. Summary of soil solution Ca stable Isotopes measurements. See Table 3.1 for Study ID key.

StudyID	Study Site	Plot	Horizon or depth interval	$\delta^{44}Ca_{SW}$ (‰ ref. seawater)	[Ca] (ppm)	δ^{44}Ca reported	Exch.Sr atm. derived
7	Kulingdakan watershed, Central Siberian Plateau	North Facing Hillslope	O_horizon	-1.07	3.65	$^{44/40}$Ca (ref. 915a)	6-33
7	Kulingdakan watershed, Central Siberian Plateau	South Facing Hillslope	O_horizon	-1.74	4.85	$^{44/40}$Ca (ref. 915a)	6-33
8	Santa Cruz, CA, USA	65 kya	15	-1.85	NA	$^{44/40}$Ca (ref. seawater)	-
8	Santa Cruz, CA, USA	65 kya	30	-1.62	NA	$^{44/40}$Ca (ref. seawater)	-
8	Santa Cruz, CA, USA	65 kya	45	-1.52	NA	$^{44/40}$Ca (ref. seawater)	-
8	Santa Cruz, CA, USA	65 kya	61	-0.64	NA	$^{44/40}$Ca (ref. seawater)	-
8	Santa Cruz, CA, USA	65 kya	91	-0.51	NA	$^{44/40}$Ca (ref. seawater)	-
8	Santa Cruz, CA, USA	65 kya	152	-0.73	NA	$^{44/40}$Ca (ref. seawater)	-
8	Santa Cruz, CA, USA	65 kya	213	-0.59	NA	$^{44/40}$Ca (ref. seawater)	-
10	Santa Cruz, CA, USA	90 kya	15	-2.18	NA	$^{44/40}$Ca (ref. seawater)	-
10	Santa Cruz, CA, USA	137 kya	15	-1.30	NA	$^{44/40}$Ca (ref. seawater)	-
10	Santa Cruz, CA, USA	182 kya	15	-0.65	NA	$^{44/40}$Ca (ref. seawater)	-
10	Santa Cruz, CA, USA	227 kya	15	-0.50	NA	$^{44/40}$Ca (ref. seawater)	-
10	Santa Cruz, CA, USA	90 kya	200	-0.35	NA	$^{44/40}$Ca (ref. seawater)	-
10	Santa Cruz, CA, USA	137 kya	200	-0.90	NA	$^{44/40}$Ca (ref. seawater)	-
10	Santa Cruz, CA, USA	182 kya	200	-1.20	NA	$^{44/40}$Ca (ref. seawater)	-
10	Santa Cruz, CA, USA	227 kya	200	-1.35	NA	$^{44/40}$Ca (ref. seawater)	-
10	Santa Cruz, CA, USA	90 kya	700	-0.68	NA	$^{44/40}$Ca (ref. seawater)	-
10	Santa Cruz, CA, USA	137 kya	700	-0.83	NA	$^{44/40}$Ca (ref. seawater)	-
10	Santa Cruz, CA, USA	182 kya	700	-0.80	NA	$^{44/40}$Ca (ref. seawater)	-
10	Santa Cruz, CA, USA	227 kya	700	-0.60	NA	$^{44/40}$Ca (ref. seawater)	-

Table 3.4. Continued.

StudyID	Study Site	Plot	Horizon or depth interval	$\delta^{44}Ca_{SW}$ (‰ ref. seawater)	[Ca] (ppm)	δ^{44}Ca reported	Exch.Sr atm. derived
11	Damma Glacier Forefield, Switzerland	-	5-25	-0.94	6.09	$^{44/42}$Ca (ref. 915a)	-
11	Damma Glacier Forefield, Switzerland	-	5-25	-0.91	3.02	$^{44/42}$Ca (ref. 915a)	-
11	Damma Glacier Forefield, Switzerland	-	5-25	-1.23	18.13	$^{44/42}$Ca (ref. 915a)	-
12	Strengbach, France	spruce site A	5	-1.03	0.44	$^{44/40}$Ca (ref. 915a)	62-69[a]
12	Strengbach, France	spruce site B	5	-0.88	0.84	$^{44/40}$Ca (ref. 915a)	62-69[a]
12	Strengbach, France	spruce site B	10	-1.11	0.48	$^{44/40}$Ca (ref. 915a)	35-47[a]
12	Strengbach, France	spruce site B	30	-1.10	0.60	$^{44/40}$Ca (ref. 915a)	56-64[a]
12	Strengbach, France	spruce site B	60	-0.99	0.48	$^{44/40}$Ca (ref. 915a)	57-66[a]
12	Strengbach, France	spruce site C	5	-1.19	0.68	$^{44/40}$Ca (ref. 915a)	62-69[a]
12	Strengbach, France	spruce site C	10	-1.12	0.60	$^{44/40}$Ca (ref. 915a)	35-47[a]
12	Strengbach, France	spruce site C	30	-1.02	0.32	$^{44/40}$Ca (ref. 915a)	56-64[a]
12	Strengbach, France	spruce site C	60	-1.13	0.28	$^{44/40}$Ca (ref. 915a)	57-66[a]
12	Strengbach, France	beech site A	10	-0.88	0.20	$^{44/40}$Ca (ref. 915a)	35-47[a]
12	Strengbach, France	beech site A	60	-0.41	0.28	$^{44/40}$Ca (ref. 915a)	57-66[a]
12	Strengbach, France	beech site B	10	-0.91	0.20	$^{44/40}$Ca (ref. 915a)	35-47[a]
12	Strengbach, France	beech site B	60	-0.47	0.04	$^{44/40}$Ca (ref. 915a)	57-66[a]
13	La Ronge, Canada	Plot 1.1	10	-1.02	6.40	$^{44/40}$Ca (ref. seawater)	-
13	La Ronge, Canada	Plot 1.1	35	-0.79	NA	$^{44/40}$Ca (ref. seawater)	-
13	La Ronge, Canada	Plot 1.2	10	-1.05	16.60	$^{44/40}$Ca (ref. seawater)	53-77[b]
13	La Ronge, Canada	Plot 1.2	35	-0.69	6.23	$^{44/40}$Ca (ref. seawater)	-
13	La Ronge, Canada	Plot 1.3	10	-0.85	7.46	$^{44/40}$Ca (ref. seawater)	47-74[b]

Table 3.4. Continued.

StudyID	Study Site	Plot	Horizon or depth interval	$\delta^{44}Ca_{SW}$ (‰ ref. seawater)	[Ca] (ppm)	$\delta^{44}Ca$ reported	Exch.Sr atm. derived
13	La Ronge, Canada	Plot 1.3	20	-0.55	7.58	$^{44/40}Ca$ (ref. seawater)	-
13	La Ronge, Canada	Plot 1.3	36	-0.45	10.22	$^{44/40}Ca$ (ref. seawater)	-
13	La Ronge, Canada	Plot 2.1	10	-1.03	7.71	$^{44/40}Ca$ (ref. seawater)	86-97[b]
13	La Ronge, Canada	Plot 2.1	35	-0.88	6.55	$^{44/40}Ca$ (ref. seawater)	-
13	La Ronge, Canada	Plot 2.2	10	-0.83	3.59	$^{44/40}Ca$ (ref. seawater)	62-93[b]
13	La Ronge, Canada	Plot 2.2	35	-0.78	2.8	$^{44/40}Ca$ (ref. seawater)	-
13	La Ronge, Canada	Plot 2.3	10	-0.91	5.63	$^{44/40}Ca$ (ref. seawater)	36-93[b]
13	La Ronge, Canada	Plot 2.3	20	-0.90	6.03	$^{44/40}Ca$ (ref. seawater)	-
13	La Ronge, Canada	Plot 2.3	35	-0.81	5.9	$^{44/40}Ca$ (ref. seawater)	-
16	Aubure, France	-	10	-0.11	0.36	$^{44/40}Ca$ (ref. seawater)	-

[a]: exchangeable Sr isotope data from Probst et al. (2000)
[b]: exchangeable Sr isotope data from Belanger and Holmden (2010).

Table 3.5. Summary of Vegetation Ca stable Isotopes measurements. See Table 3.1 for Study ID key.

StudyID	Study Site	Plot	Species	Vegetation Type	$\delta^{44}Ca_{SW}$ (‰ ref. seawater)	$\delta^{44}Ca$ reported
1	Arbutus Lake, NY USA	Catchment14	Sugar_Maple	Litter	-1.66	$^{44/40}Ca$ (ref. seawater)
1	Arbutus Lake, NY USA	Catchment14	Sugar_Maple	Stemwood	-2.74	$^{44/40}Ca$ (ref. seawater)
1	Arbutus Lake, NY USA	Catchment14	Sugar_Maple	Roots	-4.08	$^{44/40}Ca$ (ref. seawater)
1	Arbutus Lake, NY USA	Catchment14	Beech	Litter	-1.80	$^{44/40}Ca$ (ref. seawater)
1	Arbutus Lake, NY USA	Catchment14	Beech	Stemwood	-2.71	$^{44/40}Ca$ (ref. seawater)
1	Arbutus Lake, NY USA	Catchment14	Beech	Roots	-3.99	$^{44/40}Ca$ (ref. seawater)
1	Arbutus Lake, NY USA	Catchment15	Sugar_Maple	Litter	-1.34	$^{44/40}Ca$ (ref. seawater)
1	Arbutus Lake, NY USA	Catchment15	Sugar_Maple	Stemwood	-3.57	$^{44/40}Ca$ (ref. seawater)
1	Arbutus Lake, NY USA	Catchment15	Sugar_Maple	Roots	-3.95	$^{44/40}Ca$ (ref. seawater)
1	Arbutus Lake, NY USA	Catchment15	Beech	Litter	-1.27	$^{44/40}Ca$ (ref. seawater)
1	Arbutus Lake, NY USA	Catchment15	Beech	Stemwood	-3.07	$^{44/40}Ca$ (ref. seawater)
1	Arbutus Lake, NY USA	Catchment15	Beech	Roots	-2.99	$^{44/40}Ca$ (ref. seawater)
2	Wachusett Mountain, MA USA	-	Red_Oak	Wood_Core	-2.70	$^{44/40}Ca$ (ref. 915a)
2	Wachusett Mountain, MA USA	-	Red_Oak	Wood_Core	-2.61	$^{44/40}Ca$ (ref. 915a)
2	Wachusett Mountain, MA USA	-	Red_Oak	Wood_Core	-2.69	$^{44/40}Ca$ (ref. 915a)
2	Wachusett Mountain, MA USA	-	Red_Oak	Wood_Core	-2.68	$^{44/40}Ca$ (ref. 915a)
2	Wachusett Mountain, MA USA	-	Red_Oak	Wood_Core	-2.46	$^{44/40}Ca$ (ref. 915a)
2	Wachusett Mountain, MA USA	-	Red_Oak	Wood_Core	-2.61	$^{44/40}Ca$ (ref. 915a)
2	Wachusett Mountain, MA USA	-	Red_Oak	Wood_Core	-2.69	$^{44/40}Ca$ (ref. 915a)
2	Wachusett Mountain, MA USA	-	Red_Oak	Wood_Core	-2.67	$^{44/40}Ca$ (ref. 915a)
2	Wachusett Mountain, MA USA	-	Red_Oak	Wood_Core	-2.80	$^{44/40}Ca$ (ref. 915a)

Table 3.5. Continued.

StudyID	Study Site	Plot	Species	Vegetation Type	$\delta^{44}Ca_{SW}$ (‰ ref. seawater)	$\delta^{44}Ca$ reported
2	Wachusett Mountain, MA USA	-	Red_Oak	Wood_Core	-2.46	$^{44/40}Ca$ (ref. 915a)
2	Wachusett Mountain, MA USA	-	Red_Oak	Wood_Core	-2.78	$^{44/40}Ca$ (ref. 915a)
2	Wachusett Mountain, MA USA	-	Red_Oak	Wood_Core	-2.55	$^{44/40}Ca$ (ref. 915a)
2	Wachusett Mountain, MA USA	-	Red_Oak	Wood_Core	-2.45	$^{44/40}Ca$ (ref. 915a)
2	Wachusett Mountain, MA USA	-	Red_Oak	Wood_Core	-2.47	$^{44/40}Ca$ (ref. 915a)
2	Wachusett Mountain, MA USA	-	Red_Oak	Wood_Core	-2.32	$^{44/40}Ca$ (ref. 915a)
2	Wachusett Mountain, MA USA	-	Red_Oak	Wood_Core	-2.32	$^{44/40}Ca$ (ref. 915a)
2	Wachusett Mountain, MA USA	-	Red_Oak	Wood_Core	-2.31	$^{44/40}Ca$ (ref. 915a)
2	Wachusett Mountain, MA USA	-	Red_Oak	Wood_Core	-2.29	$^{44/40}Ca$ (ref. 915a)
2	Wachusett Mountain, MA USA	-	Red_Oak	Wood_Core	-2.24	$^{44/40}Ca$ (ref. 915a)
2	Wachusett Mountain, MA USA	-	Red_Oak	Wood_Core	-2.26	$^{44/40}Ca$ (ref. 915a)
2	Wachusett Mountain, MA USA	-	Red_Oak	Wood_Core	-2.32	$^{44/40}Ca$ (ref. 915a)
2	Wachusett Mountain, MA USA	-	Red_Oak	Wood_Core	-2.46	$^{44/40}Ca$ (ref. 915a)
3	South Island, NZ	-	grass	leaves	-2.01	$^{44/40}Ca$ (ref. seawater)
3	South Island, NZ	-	grass	leaves	-1.91	$^{44/40}Ca$ (ref. seawater)
7	Kulingdakan, Siberia	Kulingdakan watershed	Litter	Leaves	-1.37	$^{44/40}Ca$ (ref. 915a)
7	Kulingdakan, Siberia	Kulingdakan watershed	Lichen	Lichen	-1.46	$^{44/40}Ca$ (ref. 915a)
7	Kulingdakan, Siberia	Kulingdakan watershed	Larch	Roots	-1.95	$^{44/40}Ca$ (ref. 915a)
7	Kulingdakan, Siberia	Kulingdakan watershed	Larch	Roots	-2.11	$^{44/40}Ca$ (ref. 915a)
7	Kulingdakan, Siberia	Kulingdakan watershed	Larch	Bark	-2.84	$^{44/40}Ca$ (ref. 915a)
7	Kulingdakan, Siberia	Kulingdakan watershed	Larch	Stem	-1.76	$^{44/40}Ca$ (ref. 915a)

Table 3.5. Continued.

StudyID	Study Site	Plot	Species	Vegetation Type	$\delta^{44}Ca_{SW}$ (‰ ref. seawater)	$\delta^{44}Ca$ reported
7	Kulingdakan, Siberia	Kulingdakan watershed	Larch	Branches	-2.33	$^{44/40}Ca$ (ref. 915a)
7	Kulingdakan, Siberia	Kulingdakan watershed	Larch	Branches	-2.64	$^{44/40}Ca$ (ref. 915a)
7	Kulingdakan, Siberia	Kulingdakan watershed	Larch	Cone	-1.96	$^{44/40}Ca$ (ref. 915a)
7	Kulingdakan, Siberia	Kulingdakan watershed	Larch	Needles	-1.48	$^{44/40}Ca$ (ref. 915a)
7	Kulingdakan, Siberia	Kulingdakan watershed	Larch	Needles	-1.22	$^{44/40}Ca$ (ref. 915a)
8	Santa Cruz, CA, USA	65 kya	grass	Leaves	-2.08	$^{44/40}Ca$ (ref. seawater)
8	Santa Cruz, CA, USA	65 kya	grass	Leaves	-2.03	$^{44/40}Ca$ (ref. seawater)
8	Santa Cruz, CA, USA	65 kya	grass	Leaves	-1.93	$^{44/40}Ca$ (ref. seawater)
11	Damma Glacier Forefield, Switzerland	-	Rhododendron Ferrugineum	Leaves	-2.362875241	$^{44/42}Ca$ (ref. 915a)
11	Damma Glacier Forefield, Switzerland	-	Rhododendron Ferrugineum	Leaves	-2.278896938	$^{44/42}Ca$ (ref. 915a)
11	Damma Glacier Forefield, Switzerland	-	Rhododendron Ferrugineum	Leaves	-2.341880665	$^{44/42}Ca$ (ref. 915a)
12	Strengbach, France	beech site	Beech	Leaves	-1.24	$^{44/40}Ca$ (ref. 915a)
12	Strengbach, France	beech site	Beech	Leaves	-1.64	$^{44/40}Ca$ (ref. 915a)
12	Strengbach, France	beech site	Beech	Stemwood	-1.89	$^{44/40}Ca$ (ref. 915a)
12	Strengbach, France	beech site	Beech	Roots	-1.71	$^{44/40}Ca$ (ref. 915a)
12	Strengbach, France	beech site	Beech	Roots	-1.8	$^{44/40}Ca$ (ref. 915a)
12	Strengbach, France	beech site	Beech	Roots	-2.36	$^{44/40}Ca$ (ref. 915a)
12	Strengbach, France	beech site	Beech	Litter	-1.38	$^{44/40}Ca$ (ref. 915a)
12	Strengbach, France	spruce site	Spruce	Leaves	-1.6	$^{44/40}Ca$ (ref. 915a)
12	Strengbach, France	spruce site	Spruce	Leaves	-1.08	$^{44/40}Ca$ (ref. 915a)
12	Strengbach, France	spruce site	Spruce	Stemwood	-1.46	$^{44/40}Ca$ (ref. 915a)

Table 3.5. Continued.

StudyID	Study Site	Plot	Species	Vegetation Type	$\delta^{44}Ca_{SW}$ (‰ ref. seawater)	$\delta^{44}Ca$ reported
12	Strengbach, France	spruce site	Spruce	Roots	-1.87	$^{44/40}Ca$ (ref. 915a)
12	Strengbach, France	spruce site	Spruce	Litter	-1.24	$^{44/40}Ca$ (ref. 915a)
14	La Ronge, Canada	Plot 1.1	Jack Pine	Foliage	-0.64	$^{44/40}Ca$ (ref. seawater)
14	La Ronge, Canada	Plot 1.1	Jack Pine	Stemwood	-1.14	$^{44/40}Ca$ (ref. seawater)
14	La Ronge, Canada	Plot 1.1	Jack Pine	Roots	-1.57	$^{44/40}Ca$ (ref. seawater)
14	La Ronge, Canada	Plot 1.1	Trembling Aspen	Foliage	-1.3	$^{44/40}Ca$ (ref. seawater)
14	La Ronge, Canada	Plot 1.1	Trembling Aspen	Stemwood	-1.79	$^{44/40}Ca$ (ref. seawater)
14	La Ronge, Canada	Plot 1.1	Trembling Aspen	Roots	-2.18	$^{44/40}Ca$ (ref. seawater)
14	La Ronge, Canada	Plot 1.2	Trembling Aspen	Foliage	-0.96	$^{44/40}Ca$ (ref. seawater)
14	La Ronge, Canada	Plot 1.2	Trembling Aspen	Stemwood	-1.44	$^{44/40}Ca$ (ref. seawater)
14	La Ronge, Canada	Plot 1.2	Trembling Aspen	Roots	-2.03	$^{44/40}Ca$ (ref. seawater)
14	La Ronge, Canada	Plot 1.2	Black Spruce	Foliage	-1.24	$^{44/40}Ca$ (ref. seawater)
14	La Ronge, Canada	Plot 1.2	Black Spruce	Stemwood	-1.68	$^{44/40}Ca$ (ref. seawater)
14	La Ronge, Canada	Plot 1.2	Black Spruce	Roots	-2.11	$^{44/40}Ca$ (ref. seawater)
14	La Ronge, Canada	Plot 1.3	Trembling Aspen	Foliage	-0.89	$^{44/40}Ca$ (ref. seawater)
14	La Ronge, Canada	Plot 1.3	Trembling Aspen	Stemwood	-1.4	$^{44/40}Ca$ (ref. seawater)
14	La Ronge, Canada	Plot 1.3	Black Spruce	Foliage	-1.31	$^{44/40}Ca$ (ref. seawater)
14	La Ronge, Canada	Plot 1.3	Black Spruce	Stemwood	-1.6	$^{44/40}Ca$ (ref. seawater)
14	La Ronge, Canada	Plot 1.3	White Spruce	Foliage	-1.32	$^{44/40}Ca$ (ref. seawater)
14	La Ronge, Canada	Plot 1.3	White Spruce	Stemwood	-1.64	$^{44/40}Ca$ (ref. seawater)
14	La Ronge, Canada	Plot 1.3	Balsam Poplar	Foliage	-0.9	$^{44/40}Ca$ (ref. seawater)

Table 3.5. Continued.

StudyID	Study Site	Plot	Species	Vegetation Type	$\delta^{44}Ca_{SW}$ (‰ ref. seawater)	$\delta^{44}Ca$ reported
14	La Ronge, Canada	Plot 1.3	Balsam Poplar	Stemwood	-1.64	$^{44/40}Ca$ (ref. seawater)
14	La Ronge, Canada	Plot 2.1	Black Spruce	Foliage	-1.04	$^{44/40}Ca$ (ref. seawater)
14	La Ronge, Canada	Plot 2.1	Black Spruce	Stemwood	-1.26	$^{44/40}Ca$ (ref. seawater)
14	La Ronge, Canada	Plot 2.1	Black Spruce	Roots	-2.11	$^{44/40}Ca$ (ref. seawater)
14	La Ronge, Canada	Plot 2.2	Black Spruce	Foliage	-1.22	$^{44/40}Ca$ (ref. seawater)
14	La Ronge, Canada	Plot 2.2	Black Spruce	Stemwood	-1.81	$^{44/40}Ca$ (ref. seawater)
14	La Ronge, Canada	Plot 2.2	Black Spruce	Roots	-2.2	$^{44/40}Ca$ (ref. seawater)
14	La Ronge, Canada	Plot 2.2	Jack Pine	Foliage	-0.38	$^{44/40}Ca$ (ref. seawater)
14	La Ronge, Canada	Plot 2.2	Jack Pine	Stemwood	-0.89	$^{44/40}Ca$ (ref. seawater)
14	La Ronge, Canada	Plot 2.2	Jack Pine	Roots	-1.54	$^{44/40}Ca$ (ref. seawater)
14	La Ronge, Canada	Plot 2.3	Black Spruce	Foliage	-1.43	$^{44/40}Ca$ (ref. seawater)
14	La Ronge, Canada	Plot 2.3	Black Spruce	Stemwood	-1.65	$^{44/40}Ca$ (ref. seawater)
16	Luquillo, Puerto Rico	Bisley1	Tabonuco	Roots	-1.52	$^{44/40}Ca$ (ref. seawater)
16	Luquillo, Puerto Rico	Bisley1	Tabonuco	Leaves	-1	$^{44/40}Ca$ (ref. seawater)
16	Luquillo, Puerto Rico	Bisley1	Cecropia	Roots	-1.57	$^{44/40}Ca$ (ref. seawater)
16	Luquillo, Puerto Rico	Bisley1	Cecropia	Leaves	-1.14	$^{44/40}Ca$ (ref. seawater)
16	Luquillo, Puerto Rico	Rio Icacos	Palo Colorado	Roots	-1.68	$^{44/40}Ca$ (ref. seawater)
16	Luquillo, Puerto Rico	Rio Icacos	Palo Colorado	Leaves	-1.27	$^{44/40}Ca$ (ref. seawater)
16	Luquillo, Puerto Rico	Rio Icacos	Cecropia	Roots	-2.21	$^{44/40}Ca$ (ref. seawater)
16	Luquillo, Puerto Rico	Rio Icacos	Cecropia	Leaves	-1.79	$^{44/40}Ca$ (ref. seawater)
17	Aubure, France	-	Beech	Leaves	-1.63	$^{44/40}Ca$ (ref. seawater)
14	La Ronge, Canada	Plot 1.3	Balsam Poplar	Stemwood	-1.64	$^{44/40}Ca$ (ref. seawater)
14	La Ronge, Canada	Plot 2.1	Black Spruce	Foliage	-1.04	$^{44/40}Ca$ (ref. seawater)

Table 3.5. Continued.

StudyID	Study Site	Plot	Species	Vegetation Type	$\delta^{44}Ca_{SW}$ (‰ ref. seawater)	$\delta^{44}Ca$ reported
17	Aubure, France	-	Beech	Branches	-2.46	$^{44/40}Ca$ (ref. seawater)
18	Hawaii, USA	Thurston	Ohia	Leaves	-1.29	$^{44/40}Ca$ (ref. seawater)
18	Hawaii, USA	Kohala	Ohia	Leaves	-1.01	$^{44/40}Ca$ (ref. seawater)
18	Hawaii, USA	kolekole	Ohia	Leaves	-0.12	$^{44/40}Ca$ (ref. seawater)
18	Hawaii, USA	kokee	Ohia	Leaves	-0.45	$^{44/40}Ca$ (ref. seawater)

Appendix A1: Measurement of Ca stable Isotopes at Boston University

I have refined the methodology for measuring calcium isotope ratios at the BU TIMS facility that was initiated in 2007 under the direction of Prof. Andrew Kurtz. High-precision Ca isotopic analysis by TIMS employs the double-spike technique to correct for any mass fractionation that occurs during preparation of the sample or when running the sample in the TIMS. At BU, we utilize a ^{42}Ca, ^{48}Ca double spike and have demonstrated the ability to isolate calcium in our sample and minimize isobaric interference during TIMS runs (for calcium these include $^{88}Sr^{2+}$, $^{40}K^{+}$, $^{46}Ti^{+}$, and $^{48}Ti^{+}$). To date, we have run 50 samples of spiked 915a Ca standard and 46 samples of spiked seawater (SW) standard. 20 spiked 915A standards and 17 SW standards were run using the original cup configuration which required 3 measurement “hops” to calculate the 3 isotope ratios required for the double spike correction method. The mean $\delta^{44}Ca_{915a}$ (relative to seawater) for these early samples was -1.86‰ with a 2-sigma external precision of 0.31‰ while $\delta^{44}Ca_{sw}$ = -0.01‰ (2σ ext. prec. = 0.69‰, n=17). In April 2012, we updated our cup configuration so that all the necessary isotope ratios could be measured in only 2 hops (Table A1.1). In May 2013, the faraday cups were replaced due to cup degradation. Between May of 2013 and January 2014, $\delta^{44}Ca_{915a}$ =of -1.85‰ (2σ ext. prec. = 0.12‰, n = 14) and $\delta^{44}Ca_{sw}$ = 0.09‰ (2σ ext. prec. = 0.15‰, n=8). During this period, we observed significant drift in normalized stable Ca isotopes ratios which commonly accepted mass fractionation laws were unable to correct. Beginning in December of 2013, a

concerted effort was conducted to determine the source of the drift in samples and standards. It was determined in January of 2014 that parafilm “dams”, used to prevent the spread of sample on the filament, were introducing calcium contamination into the sample load and leading to uncorrectable apparent mass fractionation. Beginning in January of 2014, we stopped using parafilm dams and we observed immediate improvement in our external precision. Between January of 2014 to present day, we’ve run 10 double spiked 915A ($\delta^{44}Ca_{915a}$ = -1.84‰, 2σ ext. prec. = 0.09‰) and 11 SW ($\delta^{44}Ca_{sw}$ = 0.05‰, 2σ ext. prec. = 0.11‰). For my dissertation, I’ve only included samples that were run between April 2012 and present day. The long term average during this period was $\delta^{44}Ca_{915a}$=-1.87‰ (2σ ext. prec. = 0.14‰, n=30) and $\delta^{44}Ca_{sw}$=0.06‰ (2σ ext. prec.=0.13‰, n=29). We have currently reached precision levels achieved by labs with more experience in Ca analysis (typically ≤ 100 ppm 2σ external error for the 915a standard) (Holmden and Bélanger 2010).

What follows are a series of checklists I created in order to standardize the procedure for stable Ca isotope column chemistry as well as analyzing a sample on the TIMS at Boston University. As with any laboratory procedure, there is a learning curve that is only overcome with experience. Therefore, simply following these procedures is no guarantee that similar levels of precision will be achieved. Good luck.

Appendix A1. Supplimentary Information

Table A1.1. Current Faraday cup configuration for measuring stable Ca isotopes at Boston University.

Cup:	L4	L3	L2	L1	C	H1	H2	H3	H4
Hop 1			^{40}Ca			^{42}Ca		^{44}Ca	
Hop 2			^{42}Ca				^{48}Ca		

Checklist for Ca Column Chemistry (updated 2/12/2014) Date: _____

For Seawater or Unknown Sample

Note: Frit in columns 5-8 may be loose. Make sure frit is secure BEFORE adding sample!

Sample ID: _____ _____ _____ _____

	Column #:	√	√	√	√
Take mixture (ie. Seawater/Unknown and DS)					
Dry down mixture to salt on hotplate					
Bring back up in 250uL 1N nitric					
Column Chemistry	Start:	_____	_____	_____	_____
Remove Column from MQ Bath					
Remove MQ from column reservoir using pipetter. Do not suck resin up. Use big pipetter to leave a few mL in top then switch to smaller pipetter to remove remainder of acid. Leave small amount near column neck and let drip through.					
W Don't let column go dry. Add 10mL of 4N nitric. Drip slowly at first, and then can speed up as column fills. Wait until all 4N nitric has passed through before proceeding. It takes about 6 min. per 1mL to pass through column.					
W Add 3mL MilliQ DI water to push through 4N nitric. Wait till all passes through.					
W Add 3mL 1N nitric to condition column. Wait till all passes through.					
Add 0.250mL Unknown/Seawater in 1 N nitric (from above).					
W Add 0.750mL 1 N nitric. VERY CAREFUL! Very important not to kick up resin. Wait till all passes through.					
W Add 29mL 1 N nitric. Wait till all passes through.					
W Add 3mL 1.5 N nitric (to columns 1-4) OR 6ml 1.5N nitric (to columns 5-9). Wait till all passes through.					
Place large beaker under column for collection.					
C Add 14mL 1.5 N nitric. Collect all these for analysis.					
W Add 20mL 4 N nitric to fill reservoir and elute remaining cations.					
W Add 10mL MilliQ DI water to clean column.					
Column Storage	Finish:	_____	_____	_____	_____
After finishing above steps:					
Add 10mL MilliQ to column and loosely put top back on and place back into MilliQ bath.					
Sample Preparation for Loading					
Dry down to "bead" on hotplate (optional: transfer bead to small 7ml teflon beaker)					
Bring back up in 50uL Optima Hydrogen Peroxide (H_2O_2) + 100uL concetrated Nitric. Sonicate					
Dry down to salt on hotplate					
Bring back up in 100uL concentrated nitric (14-15 N). Sonicate					
Dry down to salt on hotplate					
Bring back up in 100uL concentrated nitric (14-15 N). Sonicate					
Dry down to salt and bring back up in 2uL 2 N nitric for loading onto filament					

Figure A1.1. Checklist for stable Ca isotope column chemistry at Boston University.

Checklist for running Ca on TIMS

For morning warm-up (before first sample of the day):

- [ ] Detection Calibration Tab -> GAIN (takes about 10-15 mins.)
- [ ] Detection Calibration Tab -> Dark Noise (takes about 5 mins.)
- [ ] Update "watch parameter.txt" file (Start Menu -> Recent Documents -> watch parameters)

Setup method and Cup Configuration

- [ ] Under Cup Configuration -> Open file -> Ca_2scan_dkh_kt.ccf
- [ ] Under Methods window -> Open Method file -> Ca_DS_13_04_12.met
- [ ] Press Set Collection to move cups into proper configuration

If loading new barrel:

- [ ] Sample Wheel -> INITIALIZE, then enter in sample names

Before opening analyzer gate:

- [ ] Center Cup -> Faraday Box checked -> green light next to "Faraday" must be ON!!!

Running a sample:

- [ ] Select wheel position: Sample Wheel -> POSITION
- [ ] Check position on Filament Control match Sample Wheel position
- [ ] Make one diagonal slash through position number on sample log
- [ ] Make sure Current, not Temperature is selected
- [ ] Filament Control -> set speed of IONI to 500.00 mA/min
- [ ] Filament Control -> set current of IONI to 3000
- [ ] START heating IONI filament to 1410C
- [ ] hit STOP when pyrometer reaches 1410C
- [ ] Filament Control -> set speed of EVAP to 500.00 mA/min
- [ ] Filament Control -> set current of EVAP to 1600
- [ ] START heating EVAP filament to 1600mA

Once EVAP @ 1600mA:

- [ ] Open Analyzer Gate and H.V. If largest beam (40Ca) >10V, close gate and wait a few minutes, then reopen.
- [ ] Under Scan Control -> Set mass to 42Ca and Cup to H1
- [ ] Hit Set and match scale of Chart Recorder to beam intensity

Ramp of EVAP filament

- [ ] Run an Auto Focus first. This usually can only be run when beam >0.001V.
- [ ] Start heating EVAP filament in 50-100mA increments @ 50-100mA/min. Don't do it too fast.
- [ ] Run Auto Focus frequently while ramping up (approximately when beam has increased 50-100% or every 100mA).

Beam may start increasing on it's own. Let it increase/decrease without changing voltage, usually it will plateau.
If beam goes above 10V, close gate, and let beam decrease. If beam starting "running away" (ie.
Increases fast above 10V, you may need to ramp down EVAP.)

- [ ] Ramp up until largest beam is ~5-9V and make sure beam is steady. More important that beam is steady, but slight decreasing/increasing OK.

May take about 40-60mins. Depending on skill level :)

Check Mass Calibration and Peak Coincidence, and cup position:

- [ ] Make sure 42Ca and H1 are selected: Scan Control -> set mass to 42Ca and cup to H1 -> hit SET
- [ ] Run Peak Center. Make sure vertical lines match up.
- [ ] Run Peak Scan. Use Tracer Icon to select cups L2, H1 and H3 and normalize to individual.
- [ ] Scan Control -> set mass to 44Ca and cup to L2 -> hit SET
- [ ] Peak center on 44Ca in L2 optional. If you run peak center, this may create a "hump" in the mass calibration line. I haven't noticed any impact of this "hump" on the ratios, but theoretically probably not a good thing. Run Peak Scan. Use Tracer Icon to select cups L2 and H2 and normalize to individual.

If you want, can run a Mass Scan to check peak coincidence. Essentially the same as doing a Peak Scan:

- [ ] To scan 2nd Hop: Scan Control -> MASS SCAN -> Start : 45.0, End: 45.12, Steps: 200, integration time: 0.131
- [ ] Hit START
- [ ] Select cups L2 and H2. The peaks should be coincident over the dummy mass in C cup.

If cups not aligned during peak scan (L2 cup sometimes not aligned). THIS IS ADVANCED, SO DON'T DO ANY CUP MOVEMENT
IF YOU ARE NOT TRAINED PROPERLY! FIND KEN, DENISE OR ANDY. These are INCOMPLETE instructions on how to move cups!!!

- [ ] Make note whether mis-aligned cup is low (L) or high (H) cup, which direction it is off
- [ ] Under Cup Configuration -> make sure Advanced box is checked

If L cup is mis-aligned:
    Increase ADJUST TARGET POSITION on cup to move cup RIGHT
    Decrease ADJUST TARGET POSITION on cup to move cup LEFT
If H cup is mis-aligned:
    Decrease ADJUST TARGET POSITION on cup to move cup RIGHT
    Increase ADJUST TARGET POSITION on cup to move cup LEFT
Always run a peak center after moving cups and make sure cup(s) moved in the right direction using Peak Scan or Mass Scan.

Prepare to Run:

- [ ] Double check that the largest Ca beam is at ~5-9V and stable.
- [ ] If needed, adjust current to get stable beam.
- [ ] Run one last Auto Focus

Start Run:

- [ ] Go to Method Editor hit play button at top
- [ ] Make sure "After Run" box is checked and "fildown_vclose.pex" script is set. This will automatically close valve and ramp down filaments.
- [ ] Enter in file name. Can hit dropdown menu, select last run, and modify name (ie. YR_MTH_DAY_pos#_NameOfSample.exp)

Hit save and run will start.

Figure A1.2. Checklist for running stable Ca isotope samples on the Boston University TIMS.

Appendix A2: Additional stable Ca isotope box model description

A2.1 Model Equations

In this appendix I provide a more detailed description of the two-box model of the terrestrial ecosystem presented earlier in Chapters 2 and 3 (Figure 2.2 and Figure 3.2). The model consists of 2 boxes (reservoirs) representing the mass of actively cycled soil Ca integrated over the root zone (M_S) and the mass of Ca in biomass (M_V) (mol Ca*ha^{-1}) and 7 fluxes (mol Ca*ha^{-1}*yr^{-1}) representing the movement of Ca into, out of, and between reservoirs. Two external fluxes enter the soil exchangeable reservoir, representing atmospheric deposition (F_A) and bedrock weathering-derived (F_W) sources of Ca to the system. One external flux (F_{NU}) enters the vegetation pool directly, bypassing the soil exchange pool. This flux represents direct uptake of new Ca by roots from sources other than the exchangeable reservoir, contributing to “nutrient uplift”. Internal biomass cycling of Ca is represented by an uptake flux from the soil exchangeable reservoir (F_U), and the return of Ca from biomass back to the soil exchangeable reservoir (F_R) via decomposition. Ca is exported from the system by one of two fluxes, via leaching from the soil exchange reservoir (F_Z) to groundwater or streamwater, and as export of Ca from the vegetation reservoir (F_{POM}), for example by stream export of particulate organic matter.

We start with an isotope mass balance for the soil exchangeable Ca reservoir (M_S) and Ca biomass reservoir (M_V):

$$\frac{d(M_S\delta_S)}{dt} = F_A\delta_A + F_W\delta_W + F_R\delta_V - F_U(\delta_S + \Delta_U) - F_Z\delta_S \qquad (1)$$

$$\frac{d(M_v\delta_v)}{dt} = F_U(\delta_S + \Delta_U) - F_R\delta_V + F_{NU}(\delta_W + \Delta_U) - F_{POM}\delta_V \qquad (2)$$

Where M represents the mass of Ca in a particular reservoir (mol Ca*ha^{-1}), F represents a Ca flux into or out of a Ca reservoir (mol Ca*ha^{-1}*yr^{-1}), δ represents δ^{44}Ca values for the respective reservoir or flux (‰, relative to seawater standard) and Δ_U is a isotopic separation factor that represents the isotopic fractionation of Ca isotopes that occurs when Ca moves from the soil exchangeable reservoir into the biomass reservoir (‰ difference between the δ^{44}Ca of the soil exchangeable reservoir and the δ^{44}Ca value of the biomass reservoir).

At steady state, M_V and M_S are constant in time. To achieve this, the input of Ca must balance the output of Ca from each reservoir. In the case of M_S, we treat F_Z as the residual of F_A, F_W, F_R and F_U with the additional constraint that F_Z is always positive (ie. F_Z is always exiting M_S). In the case of M_V, if F_R and F_U and equal, then F_{NU} and F_{POM} must also be equal. However, we can set F_R and F_U not equal to one another, as long as the difference in F_{NU} and F_{POM} accounts for the difference between F_R and F_U, and maintain steady state conditions. It should be noted that F_A and F_W are assumed to be constant in time. An example of results from our steady-state box model (for various Δ_U values) can be seen in figure 3.8.

The box model can also be run in a non-steady state scenario, where we are no longer required to keep M_V and M_S constant. In this dynamic scenario, we do not need to call on additional fluxes into and out of the biomass reservoir (F_{NU}

and F_{POM}) to maintain a constant M_V, although these fluxes can be included in non-steady state model runs if deemed necessary. To run the model in a dynamic fashion, we define first order rate constants (k) based on the magnitude of the flux and size of the respective reservoir the flux exits at initial steady-state conditions:

$$k_i = \frac{F_i}{M_x} \qquad (3)$$

Where k_i is the rate constant associated with flux F_i, and M_x is either the mass of the soil or biomass reservoir, depending on where the flux originates. We note that F_A and F_W are not defined using first order rate constants as these are independent of the size of the Ca reservoirs, and k_{NU} is defined using the reservoir F_{NU} enters (M_V), as this uptake flux is biologically mediated. Finally, we have chosen to parameterize the model such that F_U is not dependent on the size of the Ca reservoirs, but instead explicitly determine by the user. The advantage of this model design is that we can directly incorporate into our model real world observations of the growth (or decline) in the size of the biomass reservoir through time. For example, Figure 2.6 shows the regrowth of the biomass reservoir in Bisley 1 following hurricane Hugo as measured by Hearsill Scaley et al. (2010). We can convert the real world time series of biomass size measurements to net yearly Ca accumulation and incorporate them directly into the model through the use of (F_U). I believe this provides more realistic results regarding how $\delta^{44}Ca$ values respond to disturbance events.

With the first order rate constants relating the evolving masses with individual fluxes, we can apply the chain rule to the left hand side of equation (1) and (2) to calculate the time evolution of the soil exchangeable δ^{44}Ca value (δ_S) and vegetation δ^{44}Ca value (δ_V):

$$\frac{d\delta_S}{dt} = \frac{1}{M_S}\left[\left(\frac{dM_S}{dt}\right) - \delta_S(F_A\delta_A + F_W\delta_W + k_R M_V\delta_V - F_U(\delta_S + \Delta_U) - k_z M_S\delta_S)\right] \quad (4)$$

$$\frac{d\delta_V}{dt} = \frac{1}{M_V}\left[\left(\frac{dM_V}{dt}\right) - \delta_V(F_U(\delta_S + \Delta_U) - k_R M_V\delta_V + k_{NU} M_V(\delta_W + \Delta_U) - k_{POM} M_V\delta_V)\right] \quad (5)$$

Where $\frac{dM_S}{dt}$ and $\frac{dM_v}{dt}$ are the mass balance of the soil and vegetation pool, respectively:

$$\frac{dM_S}{dt} = (F_A + F_W + F_R - F_U - F_Z) \quad (6)$$

$$\frac{dM_V}{dt} = (F_U - F_R + F_{NU} - F_{POM}) \quad (7)$$

We can then solve the ordinary differential equations presented in (4) and (5) for δ^{44}Ca values at each time step using numerical techniques. In the next section we provide an example of how to run the model in non-steady state mode to examine the formation of a forest over existing soil.

A2.2 Modeling the formation of a forest over soil

It is worth exploring the observation that terrestrial ecosystems can exhibit an isotopically light vegetation reservoir without an accompanying isotopically heavy soil Ca reservoir. In a closed system, it would be expected that a forest

would produce an isotopically heavy soil reservoir given that the isotopic fractionation during vegetation uptake of Ca from soil discriminates against the heavy Ca isotopes. However, as the terrestrial Ca cycle is an open system with respect to the movement of Ca into and out of the soil reservoir, we will demonstrate that soil underlying a forest at steady state (size of the biomass reservoir constant in time) will be isotopically indistinguishable from the isotopic value of external sources into the soil (weathering of bedrock and atmospheric deposition), assuming enough time has passed since the forest achieved steady state.

We first define steady state initial conditions from which our system will evolve through time. Initially M_V = 1 mol Ca*ha^{-1} and M_S = 5,000 mol Ca*ha^{-1}, and the F_U and F_R and equal and set to 1 mol Ca*ha^{-1}*yr^{-1}. The sum of external sources (F_W + F_A) is equal to 150 mol Ca*ha^{-1}*yr^{-1} and are assigned a δ^{44}Ca value of -1‰. Lastly, Δ_U = -1‰, F_{NU} and F_{POM} = 0 mol Ca*ha^{-1}*yr^{-1} (biomass obtains all Ca from the soil reservoir and returns all Ca to soil reservoir), and the model is run for 600 years, with the forest starting to grow at year 100. These values are summarized in Table A.2.1. Results of this model simulation are show in Figure A.2.1. Our model indicates that during the forest growth phase that begins at model year 100, the δ^{44}Ca values of both the soil and vegetation increase synchronously by approximately 0.6‰, and the mass of soil reservoir decreases to account for the increase in biomass Ca (remember F_{NU} is set to 0 mol Ca*ha^{-1}, so biomass obtains Ca only from the soil reservoir). After the forest

reaches a steady state mass (uptake from the soil equal to the return to the soil) at approximately model year 150, the $\delta^{44}Ca$ values of both the soil and vegetation *decrease* synchronously back to their initial steady state values. Concurrently, the mass of the soil reservoir returns to its initial steady state size and $\delta^{44}Ca$ value, as a result of the continued inputs of Ca from external sources. We note that the difference between the soil and vegetation $\delta^{44}Ca$ values remains constant at -1‰ (the value of Δ_U). While simple, this model demonstrates an important consequence of the "open" nature of the terrestrial Ca cycle. It is only when there is an imbalance between the Ca fluxes linking the biomass and soil reservoir does the stable Ca isotope value of the soil reservoir differ from external Ca sources.

Conceptually, as the forest grew, there was a net removal of Ca from the soil as Ca was being stored in biomass. This net uptake of isotopically light Ca drove the soil reservoir toward isotopically heavier values compared with initial conditions. The isotopic value of biomass responded similarly to soil due to the fact that the biomass reservoir obtained all its Ca from the soil reservoir. However, as the forest ceased growing and returned to steady state conditions (albeit at a larger reservoir size), the uptake of isotopically light Ca is balanced by the return of isotopically light Ca, effectively canceling out the isotopic fractionation. The continued input of Ca from external sources into the soil reservoir drove the isotopic value of the soil reservoir back toward the values of external sources. The return of the soil $\delta^{44}Ca$ value to initial, pre-growth conditions can be viewed

as the result of soil Ca originally fractionated during forest growth being “flushed out” and replaced with new Ca from external sources. Hence, it is the “open system” nature of the terrestrial Ca cycle that can produce a situation where isotopically light biomass is not necessarily balanced by isotopically heavy soil.

For completeness, we have included fully reproducible R scripts for the model simulation described above so that others interested in the model can extend or alter the model as they see fit.

A2.3 Supplimentary Information

A2.3.1. R script for simulation a forest growth over soil

```
### Forest growth simulation using2 box stable Ca Isotope Model
### Created: 6/1/2015
### By: Ken Takagi
### Filename: CaIsoModel_2box_GrowingForest.R
### Notes: This script simulates the creation of a forest over an existing
### soil Ca pool. First the regrowth trajectory is created, then we define
### initial steady-state fluxes, masses, and d44Ca values in the model funcion
### call, and lastly we plot results.
##############################################################################

#Hypothetical biomass regrowth
x <- c(1,2,3,4)
y <- c(0.287, 0.505, 0.603, 0.702)
a1 = 1
b1 = -0.25
xfit <- seq(1, 50, 0.25)
yfit<- nls(y ~ a*(1-exp(x*b)), start = list(a = a1, b = b1))
yfitParm <- summary(yfit)$para[,1]
dStorage <- ((yfitParm[1])*(1 - exp(xfit*yfitParm[2])))*500*1000/40.08
dStorage.norm <- (dStorage - dStorage[1])/max(dStorage - dStorage[1])*5000
accum <- c(diff(dStorage.norm), rep(0, (500-length(diff(dStorage.norm)))))

# Define time dependent fluxes. Here only accumulation flux changes. Rest 0.
accFlux.all <- c(rep(0, 100), rep(accum,1))
lossFlux.all <- rep(0, length(accum)+100)

# Define reminder of initial steady state fluxes, masses and d44Ca value, and call
# model file to run model.
source("filepath/to/dynamic_CaIsoModel_2Box.R"))
out <- dynamic_CaIsoModel_2Box(soilCaMass = 5000,
                               delSoil = -1,
                               vegCaMass = 0.001,
                               delVeg = -2,
                               atmFlux = 75,
                               delAtm = -1,
                               wthFlux = 75,
                               delWth = -1,
                               lchSoilFlux = 150,
                               inVegFlux = 0, #No nutrient uplift flux
                               delInVeg = -1,
                               lchVegFlux = 0, #No POM flux
                               uptakeFlux = 1, #arbitrary as long as equsl litterFlux
                               litterFlux = 1, #arbitrary as long as equsl uptakeFlux
                               delta.bio = -1,
                               bioAccum = accFlux.all, #biomass grows!
                               bioLoss = lossFlux.all, #no biomass decline
                               event = "N",
                               runLength = length(accFlux.all)
                               )

#### plot results.
plot(out)
#####-----------
```

A2.3.2. R script for dynamic 2 box model of the terrestrial Ca cycle.

```
### Dynamic 2 box stable Ca isotope Model
### Created: 6/1/2015
### By: Ken Takagi
### Filename: CaIsoModel_2Box.R
### Notes: This model represents the terrestrial Ca cycle as 2 Ca reservoirs, a
### soil and biomass reservoir. Various fluxes move Ca into, out of and between
### the reservoirs. Each reservoir is assigned a d44Ca value, and the fluxes
### are assigned the d44Ca value of the reservoir the flux exits.
##########################################################################
### Inputs:
### soilCaMass <- Initial mass of soil pool (mol/ha).
### delSoil <- Initial d44Ca of the soil pool (permil, rel. to SW).
### vegCaMass <- Initial mass of biomass pool (mol/ha).
### delVeg <- Initial d44Ca of the biomass pool (permil, rel. to SW).
### atmFlux <- Flux of Ca from atmosphere into soil.
###     Assumed constant (mol/ha/yr).
### delAtm <- d44a of the atmospheric flux. Assumed constant
###     (permil, rel. to SW).
### wthFlux <- Flux of Ca from weathering of mineral soil. Assumed constant
###     (mol/ha/yr).
### delWth <- d44Ca of the weathering flux. Assumed constant
###     (permil, rel. to SW).
### lchSoilFlux <- Flux of Ca leached from soil (mol/ha/yr).
### decayFlux <- Flux of Ca from decay of organic matter into soil (mol/ha/yr).
### delDecay <- d44Ca of the belowground biomass decay flux
###     (permil, rel. to SW).
### inVegFlux <- Flux of Ca from nutrient uplift(mol/ha/yr).
### delInVeg <- d44Ca of the secondary weathering source to biomass
###     (permil, rel. to SW).
### lchVegFlux <- Flux of Ca out of vegetation that bypasses
###     soil and exits system (mol/ha/yr).
### uptakeFlux <- Flux of Ca removed from soil by vegetation (mol/ha/yr).
### litterFlux <- Flux of Ca returned from Vegetation back to soil (mol/ha/yr).
### delta.bio <- biomass fractionation factor (permil)
### bioAccum <- Flux of Ca returned from Vegetation back to soil (mol/ha/yr).
### bioLoss <- loss of Ca from the biomass pool (mol/ha/yr).
### event <- if, and what type of disturbance event takes place.
### runLength <- length of model run (years).

### Outputs:
### ModelResults <- dataframe with four variables. Change in soil pool mass
###   with time, change in veg pool mass with time, chnge in the d44Ca of
###   soil pool mass with time, and change in the d44Ca of the veg pool with time.

### Define function
dynamic_CaIsoModel_2Box <- function(soilCaMass,
                                    delSoil,
                                    vegCaMass,
                                    delVeg,
                                    atmFlux,
                                    delAtm,
                                    wthFlux,
                                    delWth,
                                    inVegFlux,
                                    delInVeg,
                                    lchSoilFlux,
                                    lchVegFlux,
                                    uptakeFlux,
                                    litterFlux,
                                    delta.bio,
                                    bioAccum,
                                    bioLoss,
                                    event,
                                    runLength){
```

```
#-------------------------------------------------------------------------------
library(deSolve)

# Parameter values for model
# Initial rate constants. Set proportional to mass of Ca pools (first-order).
parameters <- c(klf = litterFlux/vegCaMass,
                klV = lchVegFlux/vegCaMass,
                kuS = uptakeFlux/vegCaMass,
                klS = lchSoilFlux/soilCaMass,
                kiV = inVegFlux/vegCaMass,
                Fa = atmFlux,
                Fw = wthFlux,
                da = delAtm,
                dw = delWth,
                div = delInVeg,
                delta = delta.bio
)

# initial values for masses and dels.
state <- c(MVeg = vegCaMass,
           MSoil = soilCaMass,
           delVeg = delVeg,
           delSoil = delSoil
);

#Set timesteps and run length
tf = runLength; #final simulation time in years.
times = seq(1, tf, 1); #simulation time in years.

# Forcing fluxes
func_dyn_Fup <- function(t) bioAccum[t]
func_dyn_Fdown <- function(t) bioLoss[t]
func_dyn_FinVeg <- function(t) inVegFlux[t]
func_dyn_FoutVeg <- function(t) lchVegFlux[t]

#this is where the function uses the dynamic fluxes to calculate the
#incremental change in reservior sizes and isotope ratios

CaIsoSolver<-function(t, state, parameters) {
  with(as.list(c(state, parameters)),{

    #equations for dynamic fluxes
    FuS_dynamic = func_dyn_Fup(t) + kuS*MVeg
    Flf_dynamic = func_dyn_Fdown(t) + klf*MVeg
    FlV_dynamic = klV*MVeg
    FiV_dynamic = kiV*MVeg
    FlS_dynamic = klS*MSoil

    dMVeg = FuS_dynamic + FiV_dynamic - Flf_dynamic - FlV_dynamic;

    dMSoil = Fa + Fw + Flf_dynamic - FuS_dynamic - FlS_dynamic;

    ddelVeg = 1/MVeg*(FuS_dynamic*(delSoil + delta) + FiV_dynamic*(div + delta)
              - (Flf_dynamic + FlV_dynamic)*delVeg - (delVeg*(FuS_dynamic +
              FiV_dynamic - Flf_dynamic - FlV_dynamic)));

    ddelSoil = 1/MSoil*(Fa*da + Fw*dw + Flf_dynamic*delVeg -
              FuS_dynamic*(delSoil + delta) - FlS_dynamic*delSoil -
              (delSoil*(Fa + Fw + Flf_dynamic - FuS_dynamic -
              FlS_dynamic)));

    list(c(dMVeg, dMSoil, ddelVeg, ddelSoil))
  })
}

if(event == "N"){
  outCaEvent <- ode(func = CaIsoSolver, y = state, times = times,
```

```
                    parms = parameters)
}
return(outCaEvent)
}
```

A2.3.3. Tables

Table A2.1. 2 box model parameters for growing forest simulation

Variable	Units	Description	Value
M_V	$mol*ha^{-1}$	Mass of Vegetation	1
M_S	$mol*ha^{-1}$	Mass of Soil	5000
F_A	$mol*ha^{-1}*yr^{-1}$	Atm. deposition	75
F_W	$mol*ha^{-1}*yr^{-1}$	Weathering flux	75
F_U	$mol*ha^{-1}*yr^{-1}$	Uptake flux	1
F_R	$mol*ha^{-1}*yr^{-1}$	Litter flux	1
F_{NU}	$mol*ha^{-1}*yr^{-1}$	Nutrient uplift	0
F_{POM}	$mol*ha^{-1}*yr^{-1}$	Particulate organic matter flux	0
F_{Lch}	$mol*ha^{-1}*yr^{-1}$	Soil leaching flux	150
$\delta^{44}Ca_{Soil}$	‰	δ^{44}Ca of Soil reservoir	-1
$\delta^{44}Ca_{Veg}$	‰	δ^{44}Ca of biomass reservoir	-2
$\delta^{44}Ca_{Ex}$	‰	δ^{44}Ca of external sources	-1
Δ_U	‰	Uptake fractionation factor	-1

A2.3.4. Figures

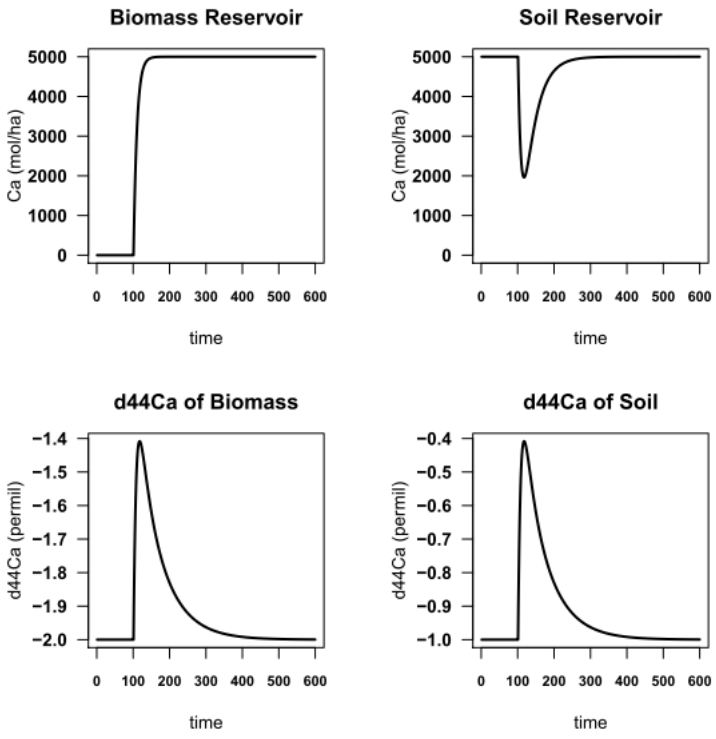

Figure A2.1. Results from the dynamic box model simulation of a growing forest presented in Section A2.2.

CURRICULUM VITAE